Prencipe, Michael

ISOTOPE EFFECTS INVOLVING LIQUID AND GASEOUS OXIDES OF NITROGEN UNDER PRESSURIZED CONDITIONS

City University of New York PH.D. 1984

ISOTOPE EFFECTS INVOLVING LIQUID AND GASEOUS OXIDES OF NITROGEN UNDER PRESSURIZED CONDITIONS

by

Michael Prencipe

A dissertation submitted to the Graduate Faculty in Chemistry in partial fulfillment of the requirements for the degree of Doctor of Philosophy, The City University of New York.

1984

This manuscript has been read and accepted for the Graduate Faculty in Chemistry in satisfaction of the dissertation requirement for the degree of Doctor of Philosophy.

September 12, 1984 — Takamaka Otto
date — Chairman of Examining Committee

9/12/84 — [signature]
date — Executive Officer

[signature]
[signature]
[signature]
Supervisory Committee

The City University of New York

Abstract

ISOTOPE EFFECTS INVOLVING LIQUID
AND GASEOUS OXIDES OF NITROGEN
UNDER PRESSURIZED CONDITIONS

by

Michael Prencipe

Advisor: Professor Takanobu Ishida

An isotope exchange apparatus that withstands elevated pressures and highly corrosive environments and is equipped with automatic level controls to facilitate its operation over a period of several days was designed and fabricated. This system was used to study N-15 production by means of a countercurrent isotope exchange between a gas and liquid phase composed of $NO-NO_2$ mixtures.

Results show that at near ambient temperatures the effective single stage separation factor, α, increases with partial pressure of nitric oxide. At 15°C, α increases from 1.006 at atmospheric pressure, to 1.030 at 4 atm. HETP studies indicate that at elevated pressures the overall exchange rate of nitrogen isotopes across the liquid-vapor interphase is relatively rapid (HETP = 1.07 cm at 4 atm, 15°C, and a liquid flow of 17.4 mmoles $N/cm^2 \cdot min$). Comparative data for the exchange system suggests a twenty-fold decrease in the volume of column needed to accomplish a given isotope separation task when pressure is

increased from 1 to 4 atm at 15°C. This is a direct consequence of the increase in α with pressure. Furthermore, the results indicate the volume of the column at elevated pressures (4 atm and 15°C) is approximately the same as that of much lower temperatures (1 atm and -9°C), thereby eliminating the need for refrigeration.

A force field calculation based on recent spectroscopic data for condensed and gaseous N_2O_3 and N_2O_4 in conjunction with a chemical composition study of the $NO-NO_2$ mixture predicts the single stage separation factor obtained from exchange column experiments reasonably well and significantly better than previous work. The results give a complete assignment for all fundamentals and support 160 cm^{-1} for ν_7 and 610∿630 cm^{-1} for ν_8 of N_2O_3 and 265∿270 cm^{-1} for ν_{10} of N_2O_4.

To my mother and father, the

dearest people in my life.

ACKNOWLEDGEMENTS

I wish to acknowledge with heartfelt appreciation my gratitude to:

- Professor Ishida for his invaluable assistance and guidance throughout the course of this research.

- Professors V. Fried and D. C. Locke for their help and guidance as thesis committee members during my association with The Graduate School of C.U.N.Y.

- Drs. A. Popowicz and J. Shulman for their assistance in construction of the apparatus used in this study and friendship.

- Miss A. Kanungo for reading this entire manuscript, friendship, and support.

- Mr. B. Bahavar for his assistance during the experiments and friendship.

- Mr. R. Schlott for his construction and repair of glass systems used in this study.

- Mr. E. Jordan for his help in setting up the laboratory.

- Miss Lillian Richardson for a very nice typing job.

- The Department of Energy for supporting this research.

TABLE OF CONTENTS

LIST OF FIGURES

LIST OF TABLES

I. INTRODUCTION

In the past, production of highly enriched nitrogen-15 from a natural abundance level of 0.365% has been of interest because of its use as a tracer in the chemical, biomedical, and environmental research. Recently, interest in more efficient methods for large scale production of this isotope has increased because of its possible application in nuclear energy.[1,2] For a number of years, N-15 has been concentrated with a variety of methods, including the nitrogen isotope exchange between nitric acid and nitric oxide[3] i.e., Nitrox process, distillation of liquid nitric oxide,[4] and exchange between liquid dinitrogen trioxide and nitric oxide.[5] The studies of isotope exchange processes and isotope effects are not only useful for finding new and improved methods of isotope enrichment, but are also a means to investigate the molecular and intermolecular forces of the condensed states.[6]

The isotope exchange between NO and N_2O_3, which is represented by Eq. (1):

$$^{14}N_2O_3(\ell) + 2\,^{15}NO(g) = {}^{15}N_2O_3(\ell) + 2\,^{14}NO(g), \qquad (1)$$

appeared promising because of the reasonably large single stage separation factor, α, which was found under atmospheric pressure to vary from 1.035 at -14°C to 1.016 at +14°C, and the relative rapidity of the exchange rate in comparison to that of the Nitrox process.[5] Although the system was described as being composed of only N_2O_3 and NO, a number of other chemical species are present in significant amounts: The liquid phase is composed of N_2O_3 and N_2O_4,[7] and the gas phase consists of NO, NO_2, N_2O_3, and N_2O_4.[8] For a mixture of oxides of nitrogen, the gas and liquid phase compositions depend markedly on

temperature and pressure. Since the isotope exchange occurs amongst all species, the dependence of the effective separation factor upon T and P is complex.

An experimental study of Monse et al.,[9] and a calculation performed by Ishida and Spindel[10] showed that the single stage separation factor could be enhanced at near ambient temperatures by increasing the partial pressure of nitric oxide. To further investigate the behavior of this system (hereafter known as the N_2O_3 system), and to study the feasibility of producing significant amounts of 99% N-15 efficiently at elevated pressures, an isotope exchange apparatus was designed, fabricated, and tested to 20 atm. This system consists of two parts: One is a packed column, in which the liquid mixture of N_2O_3 and N_2O_4 flows countercurrent to a mixture of gaseous oxides of nitrogen. The other is a product refluxer, where the enriched liquid draining from the bottom of the exchange column is chemically converted to a gas phase containing an equilibrium composition of NO_x determined by the conditions imposed on the exchange column. The chemical reduction is performed by means of SO_2 gas in a countercurrent stream of dilute H_2SO_4.

The exchange column was made of 316 SS, packed with stainless steel (SS) Helipack (No. 3013), and is equipped with O-rings molded out of special grade Viton, V-494, designed to withstand warm and concentrated nitric acid, and Pyrex windows, all designed for 20 atm service.

The product refluxer was initially constructed out of Pyrex according to the design of Monse et al.[5] in order to gain familiarity with its operation as well as to obtain data at atmospheric pressure. From the experience gained in these experiments a new refluxer, which is fabricated from a special SS known as Carpenter 20 (C-20) and is

equipped with viewports and automatic control devices, was constructed for operation at elevated pressures and temperatures up to 110°C. Automatic control of the reaction zone in the refluxer is accomplished with thermistors for sensing the heat evolved by the exothermic reduction of N_2O_3. The thermistors control a network of relays and solenoid valves to regulate the flow of reactant SO_2 gas to the refluxer. The liquid level of the sulfuric acid is controlled by a magnet inside a glass float which activates reed switches strategically placed around the H_2SO_4 drain tube at the bottom of the refluxer column (below the SO_2 inlet). The reed switches are part of an automatic circuit for pneumatically operating a ball valve to release the accumulating H_2SO_4.

Samples from the top and bottom (the product end) of the exchange column were reduced to N_2 at 800°C with copper turnings, and then analyzed for isotopic content using a dual collector isotope ratio mass spectrometer. The results were used to calculate the single stage separation factor, α, and the height of an equivalent theoretical plate, HETP, by using a method developed by Cohen,[11] which relates the overall separation of the exchange column as a function of product withdrawal.

The single stage separation factor was also evaluated from model calculations based on the Bigeleisen-Mayer algorithm[22] by determining the mole fractions and fundamental frequencies of the exchanging chemical species. The frequencies of NO and NO_2 were taken from previously reported force field calculations,[58] while the fundamentals for N_2O_3 and N_2O_4 were obtained from a vibrational analysis (cf: Chapter VIIB of this thesis) based on recent experimental data for these two molecules.[12-18] The chemical gas phase composition was determined from known equilibrium constants and spectrophotometric determinations using

a thermostatted cell able to withstand elevated pressures and highly corrosive environments. The components present in the liquid were computed by extrapolation of Beattie and Vosper's data.[27]

Comparative data obtained from the N_2O_3 column exchange experiments suggests a twenty fold decrease in the volume of column needed to accomplish a given isotope separation task when pressure is increased from 1 to 4 atm at 15°C. A vibrational analysis was performed on N_2O_3 and N_2O_4 in the gaseous and condensed phases using Wilson's[19] FG-matrix method. The force field calculations, in conjunction with a comparison of α calculated from the resultant frequencies and α obtained from the present experimental work produced a complete frequency assignment for the two molecules. This study also led to the conclusion that in order to reproduce the observed spectroscopic data and the experimental α's obtained from the exchange column experiments, there must be strong symmetry-allowed internal-external interactions.

In Chapter II, a survey of isotope separation methods will be given, with an indepth review of chemical exchange processes. The isotope exchange apparatus and its associated equipment will be described in Chapter III, and the experimental procedures will be detailed in Chapter IV. In Chapter V, the methodology for calculating α and HETP from exchange column experiments is dealt with, along with a procedure to calculate the mole fraction of the chemical components in the gas and liquid phases. A discussion of the results and implications of this experimental work and theoretical analysis will be contained in Chapters VI and VII, respectively. Chapter VIII will briefly summarize the significance of the results, and in Chapter IX recommendations for further studies on the oxides of nitrogen will be found.

II. REVIEW OF ISOTOPE SEPARATION PRACTICES

Separation of isotopes can be achieved by two general types of processes: 1) Irreversible processes, and 2) Equilibrium processes in which the separation is achieved on the basis of thermodynamic equilibria. Nonequilibrium processes include mass and thermal diffusions, centrifugation, electrolysis, and laser isotope separation methods. Examples of equilibrium processes are distillation and chemical exchange.

Some of the irreversible processes offer large unit stage separation factors but small throughput. In all the equilibrium processes the separation achieved in one equilibration step is small, although the throughput is large. It is, therefore, necessary to repeat the single stage separation operation many times before the desired degree of separation is attained. Another significant difference between reversible and irreversible processes is that, for the irreversible processes, substantial amounts of energy must be provided at every stage. The equilibrium processes, however, can be conducted almost reversibly, that is, with a minimum expenditure of energy, and, by using multistage countercurrent systems, energy or chemicals are needed only at the reflux ends.

IIA. Single Stage Separation Factor from the Partition Function

In the chemical exchange method, isotopes of an element exchange reversibly between two chemical species, as shown in a typical exchange reaction:

$$AX' + BX = AX + BX' , \qquad (2)$$

where X and X' are the isotopes, the prime referring to the lighter one. The possibility of calculating the equilibrium constants for such reactions from spectroscopic data alone was first pointed out by Urey and coworkers.[20-21] The equilibrium constant for Eq. (2) is given by:

$$K = (AX/AX')/(BX/BX') = (Q/Q')_{AX}/(Q/Q')_{BX} , \qquad (3)$$

where Q is the molecular partition function, which is related to K via the Gibbs free energy function. The single stage separation factor, α, is the ratio of the actual equilibrium constant to the value it would have if there were random distribution of isotopes among the chemical species involved, and is defined as:

$$\alpha = K/K_{cl} = [(Q/Q')_{qm}/(Q/Q')_{cl}]_{AX}/[(Q/Q')_{qm}/(Q/Q')_{cl}]_{BX} , \qquad (4)$$

where K_{cl} is the classical equilibrium constant, and Q_{qm} and Q_{cl} refer to the quantum mechanical and classical partition functions, respectively.

The separation factor can be conveniently expressed in terms of the Bigeleisen-Mayer's reduced partition function ratio for two isotopic species, (s/s')f:[22]

$$(s/s')f = (Q/Q')_{qm}/(Q/Q')_{cl} , \qquad (5)$$

and

$$\alpha = \{(s/s')f\}_{AX}/\{(s/s')f\}_{BX} , \qquad (6)$$

where s and s' are the symmetry numbers of the heavier and lighter molecules, respectively. Within the framework of the Born-Oppenheimer approximation, the assumptions of separability of internal and external

motions and negligible anharmonicity, the reduced partition function ratio becomes:[22]

$$(s/s')f = \prod_i (u_i/u_i')[\exp(-u_i/2)/\exp(-u_i'/2)] \{[1-\exp(-u_i')]/[1-\exp(-u_i)]\} , \quad (7)$$

where $u_i = hc\omega_i/kT$, ω_i is the wavenumber in cm^{-1} and c is the speed of light in cm/sec. The product is taken over all the degrees of freedom. For all isotopes except those of hydrogen, Δu_i (which is $u_i'-u_i$) is small, and $(s/s')f$ can be approximated by:[22]

$$(s/s')f = 1 + \Sigma G(u_i)\ \Delta u_i , \quad (8)$$

where

$$G(u_i) = 1/2 - 1/u_i + 1/(\exp(u_i)-1) . \quad (9)$$

The reduced partition function permits a correlation of the separation factor with molecular structure and chemical bonding. The value of $(s/s')f$ increases with strength and number of chemical bonds of the element X so that the heavy isotope will concentrate preferentially in the molecular species in which the overall forces acting on X are strongest. The separation factor is the ratio of the reduced partition function ratios of two chemical species, i.e., AX and BX, and α is largest for the exchange reactions in which the chemical bonding of the isotopic forms differ most widely between the two exchanging molecules.

IIB. Chemical Exchange Systems for Separation of Isotopes

The basic unit of the ideal separation process is the separating stage, which receives two feed streams of equal isotopic composition and produces two partially fractionated streams. The stage separation factor, α, is defined as:

$$\alpha = N'(1-N'')/N''(1-N') \quad , \tag{10}$$

where N' and N" are the atom fractions of the desired isotope in the enriched and depleted streams, respectively. When the desired degree of separation between the feed and product material is not obtained, it becomes necessary to connect stages in series. This is achieved by the countercurrent contacting between two chemical substances if one is liquid and the other gaseous, or if both are immiscible liquids, using conventional equipment such as bubble plate columns, and packed columns. A schematic for this type of system is shown in Figure 1. In this figure, the section of the cascade above the feed point (in the stripping section) is shown to indicate the possibility that the desired isotope X can be depleted below the natural abundance level in case the feed material is expensive. In the present study there is no stripping section: Natural abundance material is provided at the top of the column, and the gas phase which is in equilibrium with the feed is discharged as waste. The overall separation in a multistage fractionation column can be expressed as:[23-24]

$$S = [N_p(1-N_f)]/[N_f(1-N_p)] = \alpha^n \quad , \tag{11}$$

where S is the overall separation, N_p and N_f are the mole fractions of the desired component at the product and feed end, respectively, α is

$$AX' + BX \rightleftharpoons AX + BX'$$

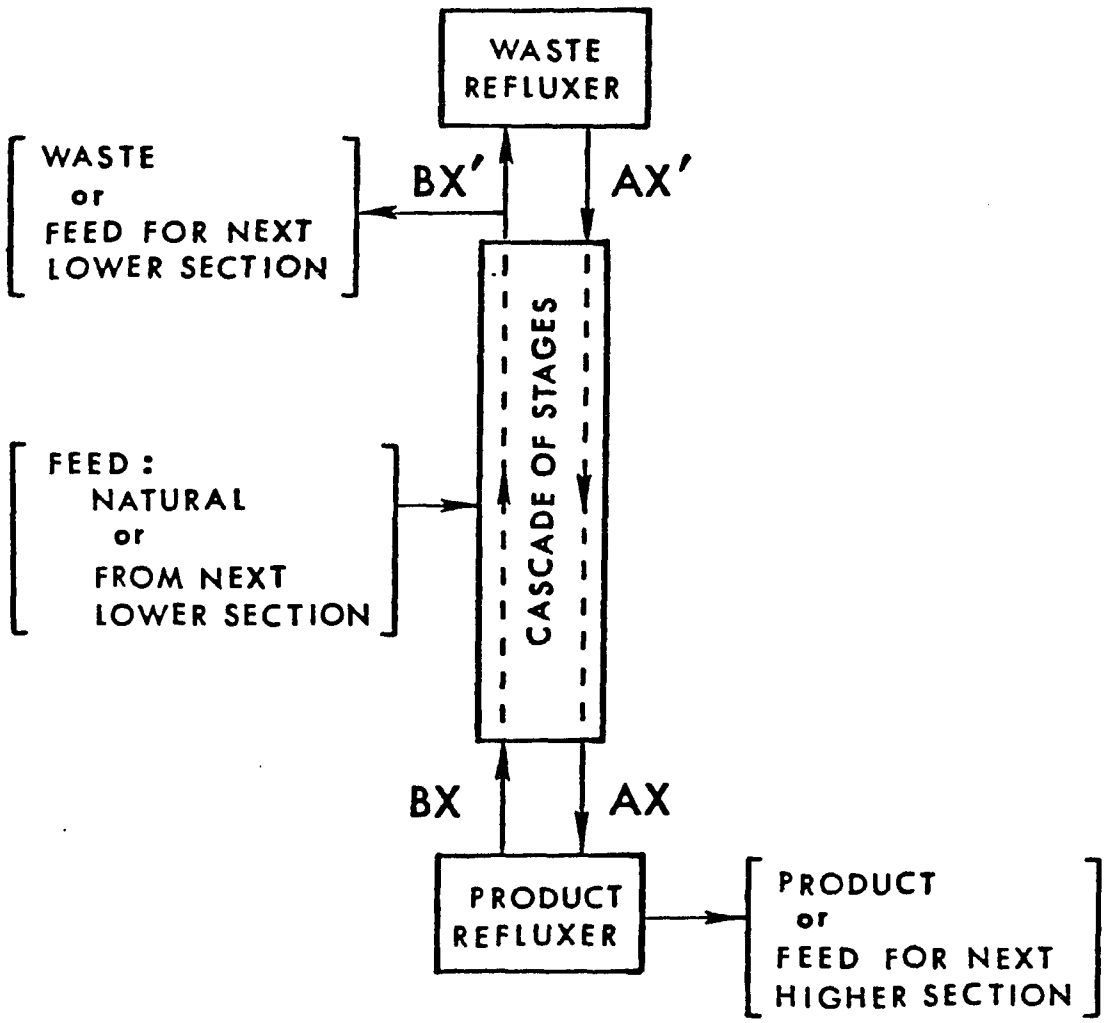

Figure 1: Schematic Flow Diagram of A Chemical Isotope Exchange Column Operation

the effective single stage enrichment factor, and n is the number of separating stages.

For a chemical reaction such as Eq. (1) to be utilized for separation of isotopes in this manner, it should have the following characteristics: 1) the separation factor must be other than unity, 2) an increase in the overall separation must be possible by countercurrent contacting of the two phases, 3) the overall exchange mechanism must permit rapid equilibration, and 4) a reflux process must be available for at least the product end (where the desired isotope is being enriched) of the system for quantitative conversion of one chemical species into another. In the N_2O_3 chemical exchange system (Eq. (1)), all of the above conditions are satisfied. The chemical reflux for conversion of N_2O_3 to NO in the product end is achieved by:

$$N_2O_3(\ell) \rightarrow NO(g) + NO_2(g) \ , \tag{12a}$$

$$3NO_2 + H_2O \rightarrow 2HNO_3 + NO \ , \tag{12b}$$

$$2HNO_3 + 3SO_2 + 2H_2O \rightarrow 3H_2SO_4 + 2NO \ . \tag{12c}$$

As pointed out earlier, the liquid phase is not "pure" N_2O_3 but is a mixture of N_2O_3 and N_2O_4. Similarly, the gaseous phase is composed mainly of NO, but also contains NO_2, N_2O_3, and N_2O_4, and their relative concentrations depend on T and P. The effective isotope fractionation factor for this gas liquid exchange system is given by:

$$\alpha = \{[\Sigma x_i(s/s')f_i]\}_{liq}/\{[\Sigma y_i(s/s')f_i]\}_{gas} \ , \tag{13}$$

where x_i and y_i are the mole fractions of exchangeable nitrogen atoms in the ith component of the liquid and gas phases, respectively. The

reduced partition function ratio (s/s')f of nitric oxide (+2 oxidation state of nitrogen) is smaller than those for all other oxides of nitrogen.[10] Lowering the temperature increases the mole fraction of +2 nitrogen in the gas phase at atmospheric pressure without a proportional increase in the liquid phase,[25-28] thus enhancing the single stage separation factor. This effect can also be achieved at ambient temperatures by increasing the partial pressure of nitric oxide.[9-10] The need for lower temperatures to achieve a larger separation factor can be avoided, thus circumventing the need for the refrigeration cost.

Since HETP for the N_2O_3 system is very favorable under atmospheric pressure and subambient temperature[5] and the possibility of avoiding refrigeration had been predicted,[10] a study to determine the feasibility of producing significant quantities of highly enriched N-15 using this system at higher pressures and ambient temperatures was undertaken. Short packed columns are usually used for conducting such studies since they give a good basis for estimating the characteristics of a cascade. In our laboratory a randomly packed exchange column and associated apparatus that can withstand pressures up to 20 atm and is not affected by the highly corrosive sulfuric and nitric acid environments was constructed for studying the behavior of the N_2O_3 system at elevated pressures. A vibrational analysis based on recently reported spectroscopic data of N_2O_3 and N_2O_4 in conjunction with an in situ spectrophotometric determination of the gas phase composition was performed to calculate α, compare the theoretical and experimental values, and consequently investigate the nature of molecular and intermolecular forces.

III. EXPERIMENTAL APPARATUS

Exchange apparati to fractionate nitrogen isotopes using the NO/N_2O_3 system have been reported by T.I. Taylor and associates,[3,5] who have employed packed and bubble plate Pyrex columns to separate nitrogen isotopes under a wide variety of operating conditions. However, the apparatus built in this study required major modifications from the earlier ones to be able to withstand the elevated pressures and highly corrosive environments.

A schematic assembly drawing for the exchange system is illustrated in Figure 2. It is shown to consist of two main sections: 1) The column, E, where the actual isotope exchange occurs, and 2) The product refluxer, P, for quantitative chemical conversion of the liquid phase to the gas phase.

The refluxer is the most difficult part of the exchange system to construct and operate properly because the chemical conversion of liquid N_2O_3 to gaseous NO must occur with no loss of nitrogen by any means, such as leaks, corrosion, side reactions, or incomplete chemical conversion. Even the loss of micromole quantities of enriched nitrogen for each mole processed would affect the overall separation.[29] Hence, the refluxer was first built from Pyrex according to the design of Monse et al.,[5] and was subsequently operated at atmospheric pressure to obtain data as well as to gain operating experience of its complex controls. From the experience gained in these experiments, an all SS product refluxer was constructed to withstand the pressures and corrosive environments required by this study, and to be operated for several days with no significant loss of enriched nitrogen using two types of automatic level controllers.

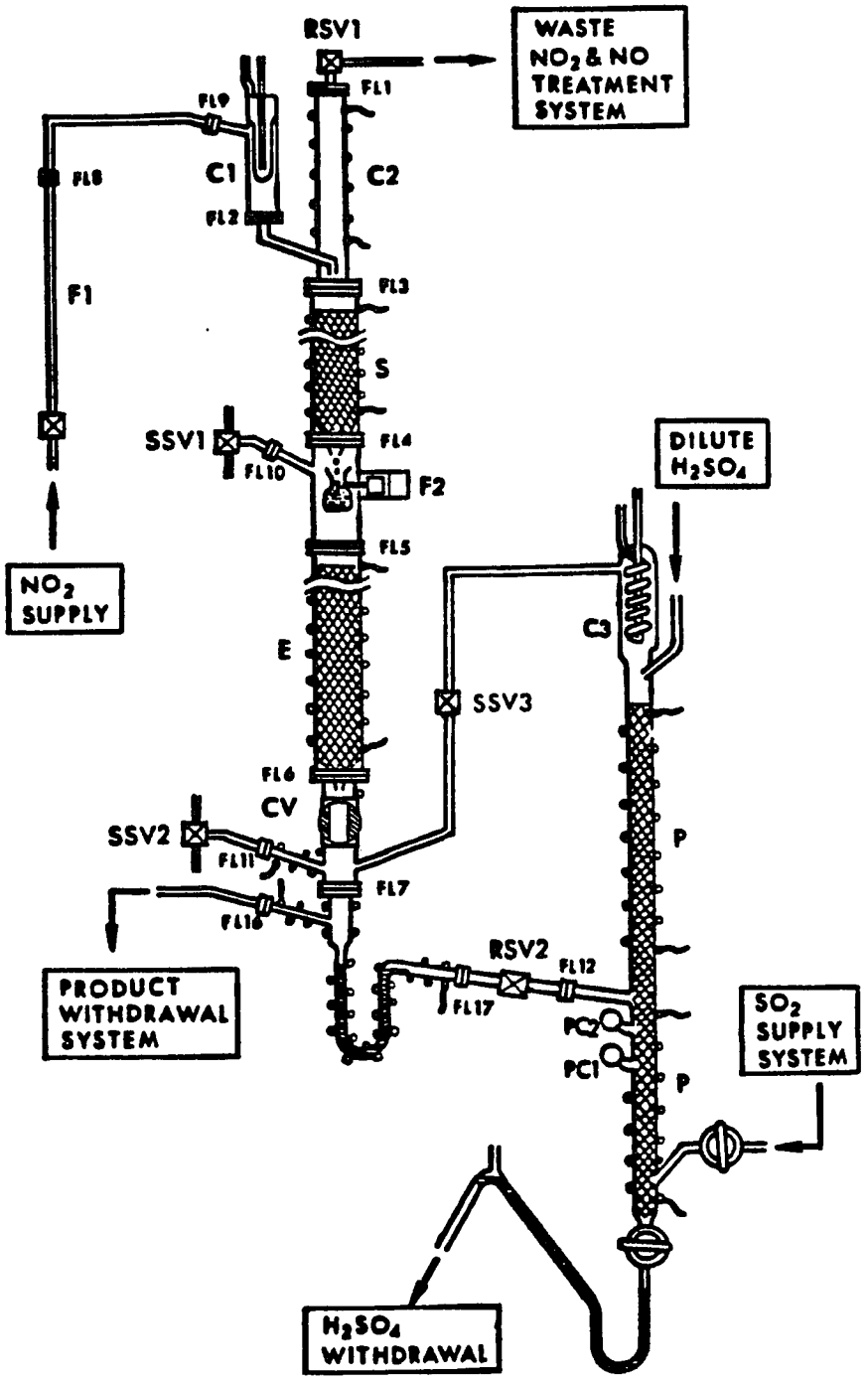

Figure 2: Isotope Exchange System

Legends for Figure 2:

CV: Ball valve (Type 316 SS)

C1: NO_2 condenser (Type 316 SS)

C2: Waste-end condenser (Type 316 SS)

C3: Product reflux condenser (Pyrex/SS)

E: Exchange column (Type 316 SS)

FL: Flanges or vacuum/pressure couplings (Type 316 SS)

F1: Gas NO_2 rotameter (Guarded Pyrex)

F2: Liquid drop flowmeter (magnetically operated, with a view port)

P: Product refluxer

PC1: Photocell and/or thermistor for SO_2 control

PC2: " " " " "

RSV1: Regulating throttle valve for waste gases

RSV3: Regulating throttle valve for refluxed NO

S: Packed equilibrator for liquid phase (Type 316 SS)

SSV1: Gas-sampling valve

SSV2: Gas-sampling valve

IIIA. The Exchange Column

This part of the system consists of a 316 SS exchange column, E, 50 cm. long and 1.55 cm. I.D., which is filled with Podbielniak's stainless steel Helipack No. 3013, and is provided with 316 SS bellows sealed Nupro valves SSV1 and SSV2 for sampling of the gas from the two ends of the packed section. The valve SSV2 also permits controlled withdrawal of the enriched product (See Section IIID for details of the enriched sample withdrawal system.)

The system is also equipped with a small packed column S (20 cm. long and 1.55 cm. I.D.) where the ascending gas phase (which is mostly NO) reacts with a descending stream of N_2O_4 to form an equilibrium mixture of N_2O_3/N_2O_4 before entering the exchange column. The flow rate of the liquid N_2O_3/N_2O_4 mixture is determined by directly measuring the time required to fill a Pyrex cup (1.61 ml. ±0.01) in a flowmeter, F2, shown in Figure 3. The flowmeter is equipped with a viewport to visually determine when the calibrated cup is filled. The measuring cup is rotated by means of a magnetic coupler, thereby eliminating the need for stempacking. Precision of the volume measurement is increased by reducing the diameter of the upper neck of the cup, where a graduation mark was etched.

After passing through the exchange column, the liquid mixture drains into the product refluxer through a small U-tube, which prevents gases in the refluxer from flowing back to the exchange column through that path.

The exchange column, E, the equilibrator, S, the condensers, C1 and C2, and the U-tube are jacketted and thermostatted to within ±0.5°C (usually at temperatures lower than ambient) by circulating a

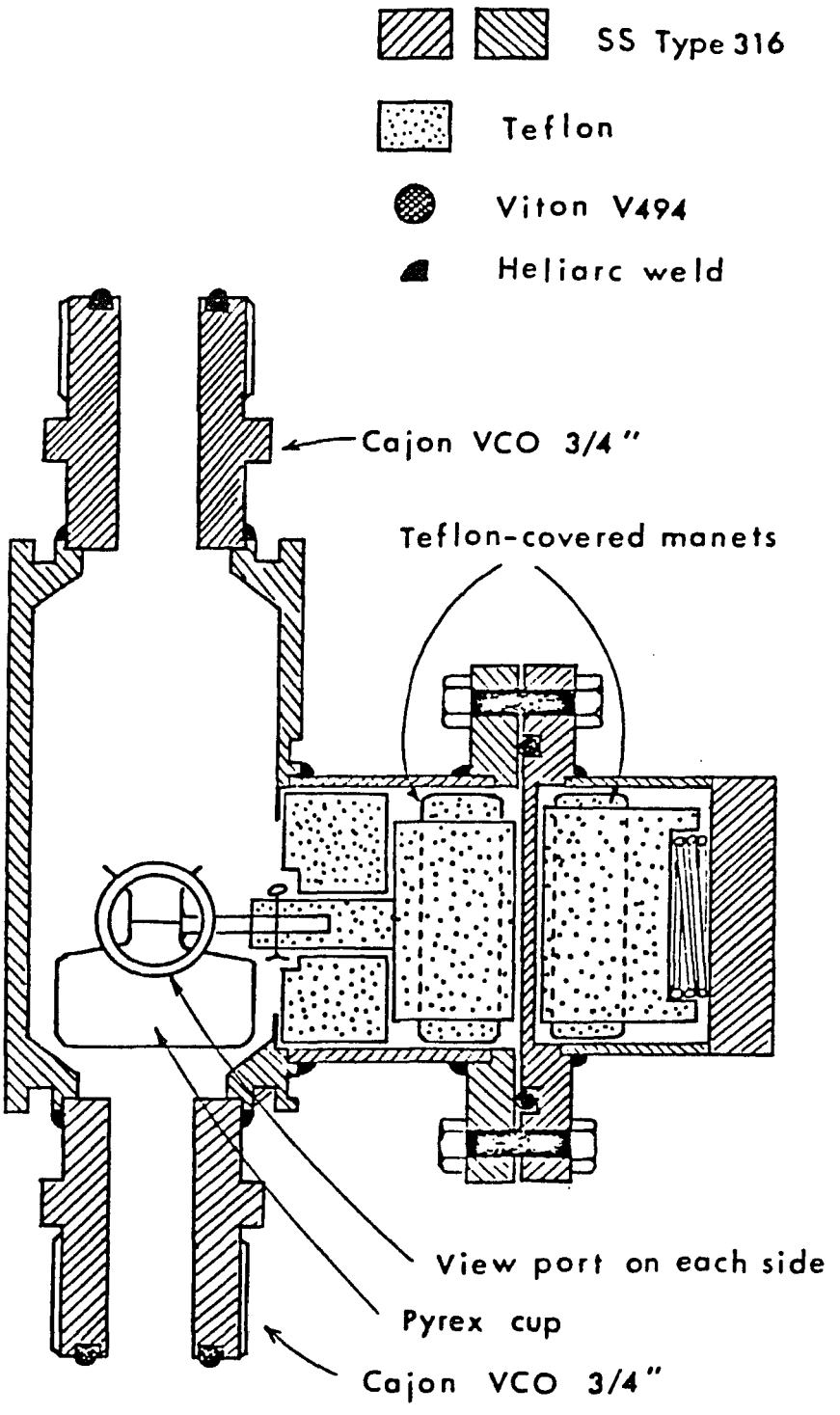

Figure 3: Cut-away view of the Liquid Drop Flowmeter

thermostatted fluid from a Revco refrigerating unit. The temperature is monitored at several points of the column and equilibrator using copper-constantan thermocouples with a digital indicator (Consolidated Controls Corp., precision ±0.1°C) for easy and rapid determinations.

The waste gas from the exchange column is passed through the condenser, C2, to remove excess NO_2 and is sent to a scrubbing tower, shown in Figure 4, where NO_x is converted to nitric acid by passing the waste and excess oxygen through the packed tower countercurrent to a downward stream of water. The oxides of nitrogen are allowed to mix with O_2 after being released by a backpressure regulator (Fairchild-Hiller Industries, type 316 SS, 2-150 psig) installed to maintain and control the pressure of the entire system. The backpressure regulator is equipped with a Bourdon tube Gauge (Type 316 SS, 6" diameter face, 0-150 psig, precision = ±0.75 psi) on the inlet side of the regulator for pressure determination.

IIIB. Pyrex Product Refluxer

IIIB1. Refluxer Column

The Pyrex refluxer with its essential features is illustrated in Figure 5. The column is filled with glass helices, 3/16" I.D., and is equipped with various condensers for temperature control. This was found necessary for condensing excess NO_2 from the NO_x returning to the exchange column to maintain an equilibrium amount of oxides of nitrogen. Dilute sulfuric acid rather than water was used in the reduction of liquid N_2O_3 because the increased acidity catalyzes the reflux reaction,[5] as evidenced by a sharper and darker reaction zone. The

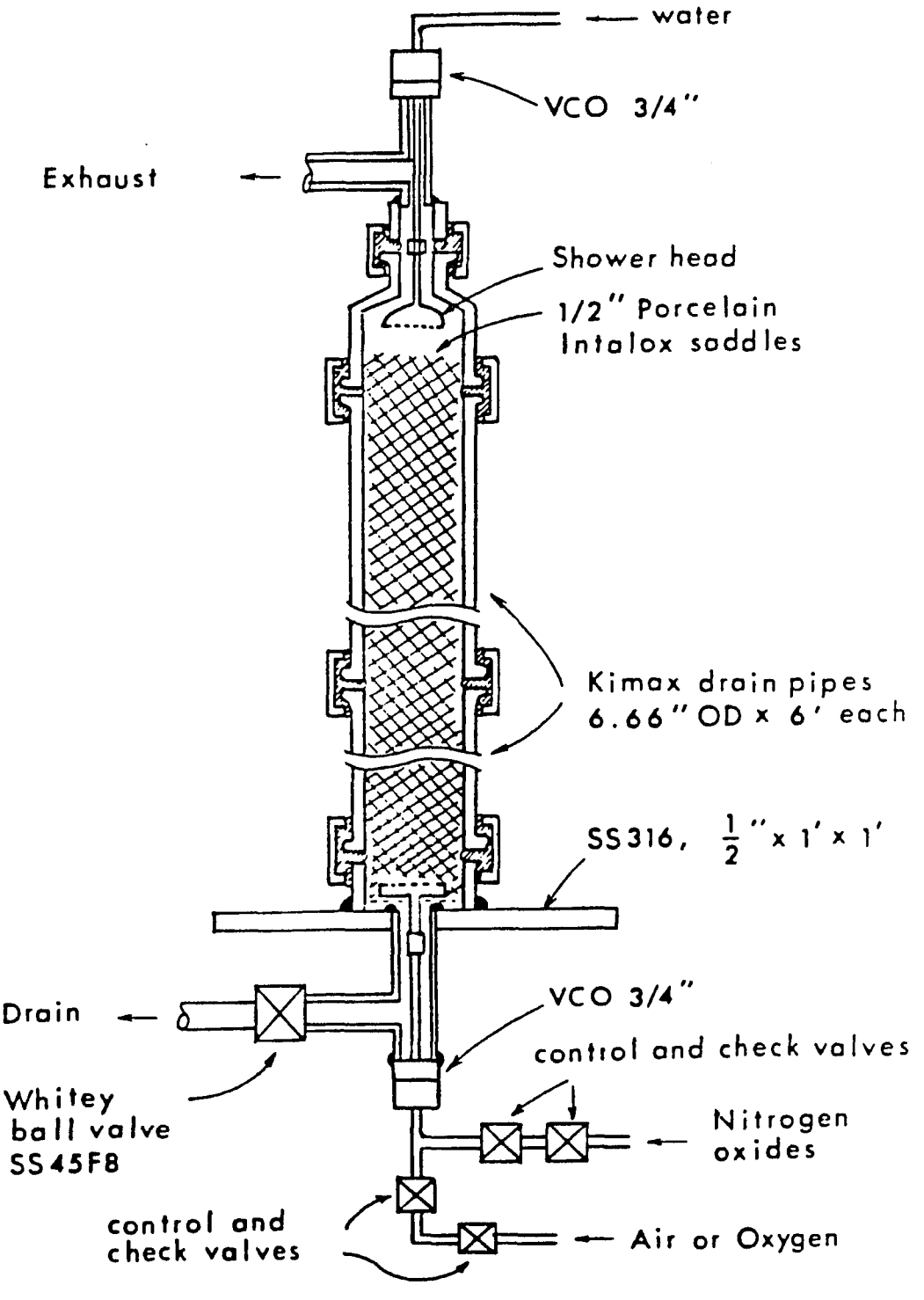

Figure 4: Scrubbing Tower for Nitrogen Oxides

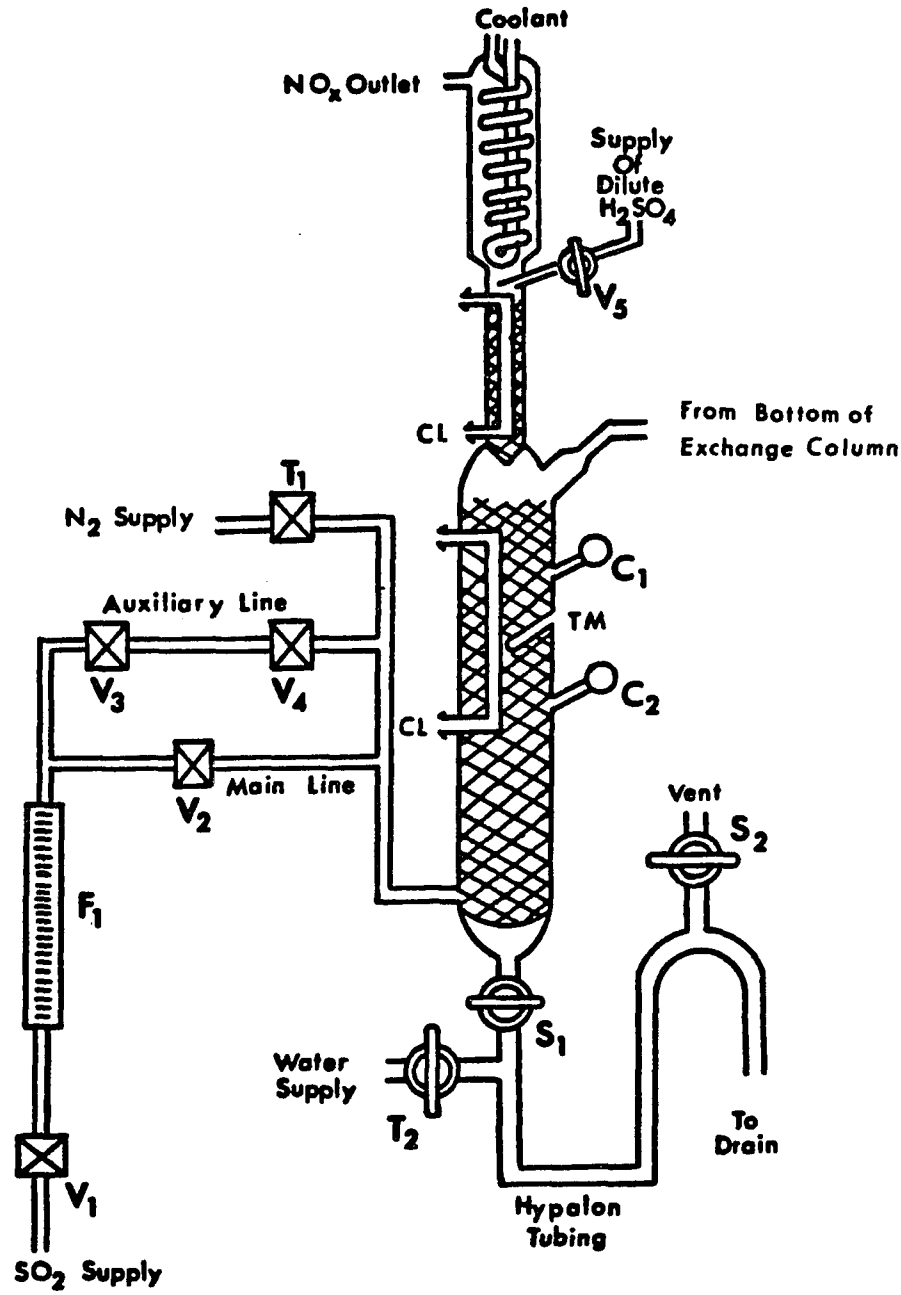

Figure 5: Pyrex Refluxer System with SO_2-Feed System

Legends for Figure 5:

C_1 and C_2:	Photocell detectors
CL:	Coolant
F_1:	Flowmeter
S_1, S_2, T_2:	Teflon-plug stopcocks
T_M:	Thermistor well
V_1, T_1:	Stainless-steel shut-off valve
V_2:	Stainless-steel regulating/shut-off valve
V_3:	Stainless-steel, bellows-sealed, pneumatic valve, actuated by air pressure controlled by a solenoid valve.
V_4:	Stainless-steel needle valve

flow of sulfuric acid pumped into the system is regulated to control the amount of tetravalent nitrogen in the gas phase. Failure to achieve the proper chemical composition of the gas phase entering the bottom of the exchange column would cause a loss of effective length of exchange column or affect the interstage flow rates.

IIIB-2. Automatic Control of SO_2 Flowrate

The SO_2 flow rate to the Pyrex refluxer was controlled automatically to facilitate its operation over several days by pneumatically opening and closing V_3 in the auxiliary line (Figure 5), thereby allowing more or less SO_2 inside the column, depending on whether the reaction zone was too low or too high.

The method of detection of the reaction zone employed by earlier workers consisted of a pair of photocells used as sensors and it was tested in the present study before the final design utilizing the thermistors (see below) was adopted. The photocells were mounted on short side arms, which were located on the packed column at an elevation near the reaction zone where the reduction took place and received light transmitted through a green filter. When the elevation of the reaction zone was too low, the brown NO_2 gas generated would cause the photocell current to decrease below a prefixed threshold, thus activating the solenoid valve to open V_3 and allow more SO_2 gas to flow in the product refluxer.

This method of detection was not found to be very reliable because of the delay caused by diffusion of NO_2 and SO_2 gases in the side arms. The level of the reaction zone (the boundary between the brown NO_2 gas and the colorless SO_2 gas) could not be controlled better than ±7-8 cm.

and, too frequently, the automatic control failed. Furthermore, to operate the refluxer at higher pressures using the photocell detection system would have necessitated a relatively complex design and construction.

To circumvent the need for a photocell type set-up, a new system was designed for detecting the heat evolved by the exothermic reaction. It used thermistors as the sensing elements. This method of controlling the reaction zone proved to have a perfect record of performance: it has never failed throughout our present study. The thermistor method was subsequently used for all the experimental runs, and was found to be more suitable for adoption to the elevated pressure operation of the refluxer.

The electronic circuitry that operates the automatic control is shown in Figure 6, and consists of a 741 operational amplifier connected as a Schmidt trigger with positive feedback. By properly choosing a reference voltage, the amplitude of the oscillations of the reaction zone could be controlled to better than ±1 cm. The electronic circuit operates the solenoid valve that pneumatically controls V_3 to regulate the SO_2 flow.

IIIC. Design and Construction of the Reflux System for Elevated Pressures

Major modifications from the Pyrex version were found necessary in order to operate the refluxer at elevated pressures.

Type 316 SS has a fairly high tensile strength and can easily handle the pressure range imposed in this experiment. However, it cannot be used for handling sulfuric acid, which is a by-product of

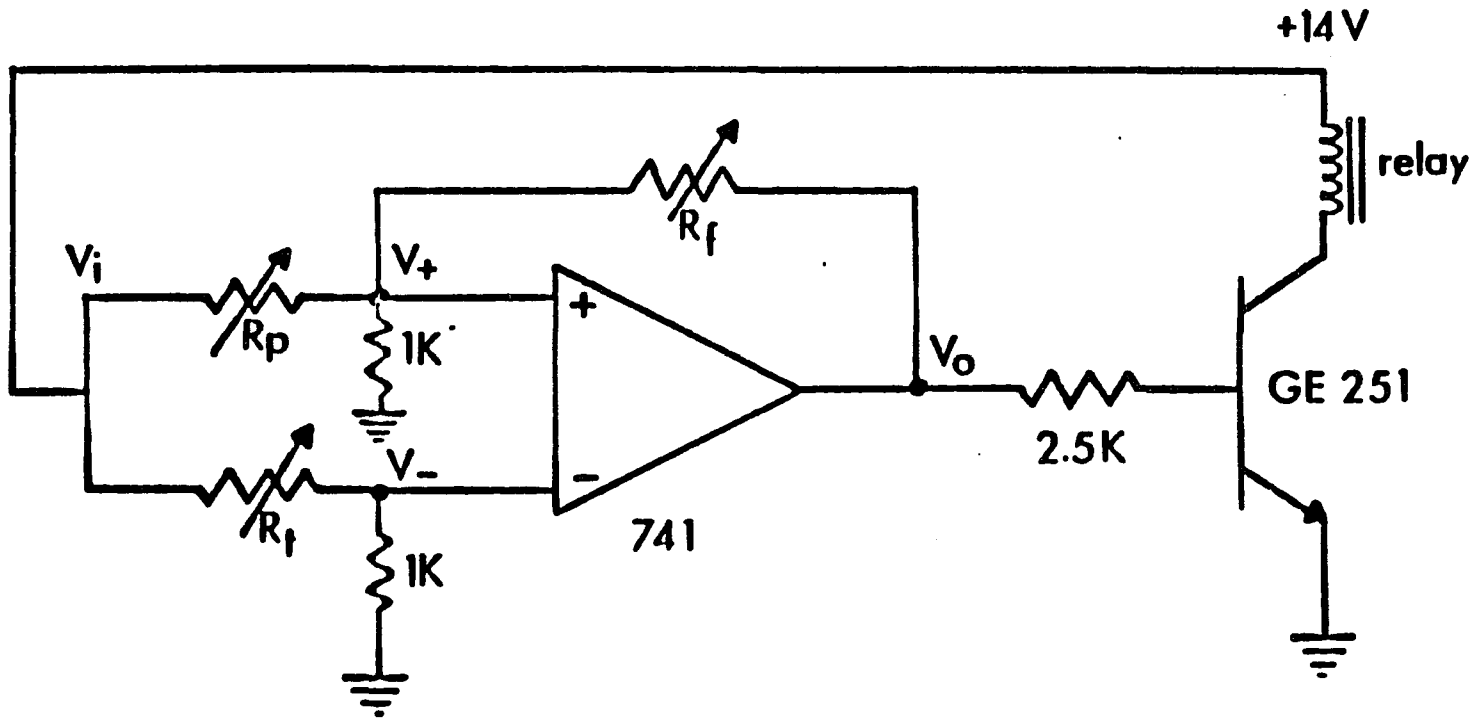

Figure 6: Sulfur Dioxide Flow Control Circuit Using Thermistor as Reaction Zone Sensor

Legends for Figure 6:

R_p: 1K ohm potentiometer

R_t: 10K ohm thermistor

R_f: 50K ohm potentiometer

741: Operational amplifier LM741

GE251: NPN silicon, general purpose switching (20W), transistor

the reduction of NO_2 by SO_2, because the corrosion rate of this alloy is too high when exposed to 8-9 M-H_2SO_4, even at ambient temperatures.

Consequently, a special kind of SS, known as Carpenter-20 (C-20) was purchased for the construction of the product refluxer as well as the auxiliary parts wetted by H_2SO_4. C-20 was especially developed for handling hot and cold, dilute and concentrated sulfuric acid. Its tensile strength is about the same as other austenitic steels, and the presence of niobium in the alloy minimizes precipitation of carbides during welding, hence it does not lose its corrosion resistant properties at or near the welds.[30]

Corrosion tests performed in our laboratory showed that C-20 satisfactorily withstands 8-9 M sulfuric acid at temperatures below 100°C, but the corrosion rate increases markedly as the temperature is increased beyond 120°C. Nitric acid at any concentration and NO_x apparently have no effect on C-20. Accordingly, the refluxer column, flanges, view ports, and other associated parts that are wetted by H_2SO_4 were constructed from C-20. The column packing used was 3/16" I.D. Pyrex helices which was supported at the bottom of the column with a teflon mesh.

The elevated pressure of the refluxer system presented another problem. That is, the vapor pressure of SO_2 at ambient temperature is only 3.34 atm. Therefore, the part of the refluxer system where SO_2 gas is present has to be heated to a sufficiently high temperature to ensure that SO_2 does not liquify. However, the inner walls of the C-20 must be kept at temperatures lower than 100°C to minimize the corrosion rate.

To prevent condensation of SO_2 and excessive corrosion

simultaneously it was necessary to control the temperature of various parts of the reflux system independently, and sometimes in a manner which would make the two thermostatting systems work against each other. For instance, heat had to be continuously removed from the walls surrounding the reaction zone where the exothermic reaction took place, while the lower parts of the refluxer where SO_2 feed entered the column had to be heated to eliminate condensation.

The operation of the refluxer for long periods of time at elevated pressures also required a liquid level control system for the safe and proper release of the waste sulfuric acid.

IIIC-1. Mechanical Structure

A schematic assembly drawing for the mechanical parts of the elevated pressure refluxer system is illustrated in Figure 7. No regard was given to actual relative dimensions so that all essential parts of the system could be shown. Figure 7 consists of five main sections. In the gas-conditioning and condenser/heat-exchanger sections, Type 316 SS was used since no sulfuric acid is present in these sections under normal operating conditions. All other wetted parts are Pyrex, Teflon, and special HNO_3-resistant Viton O-rings. The refluxer reaction column, the liquid level control section and the waste sulfuric acid temperature control sections are made of Carpenter 20, Teflon and Pyrex. All connections are heli-arc welded unless otherwise stated.

(i) Reflux Reaction Column

A 4:1 scale drawing of the reflux reaction column has been reproduced in Figure 8. The legends are found in the next page. All outside

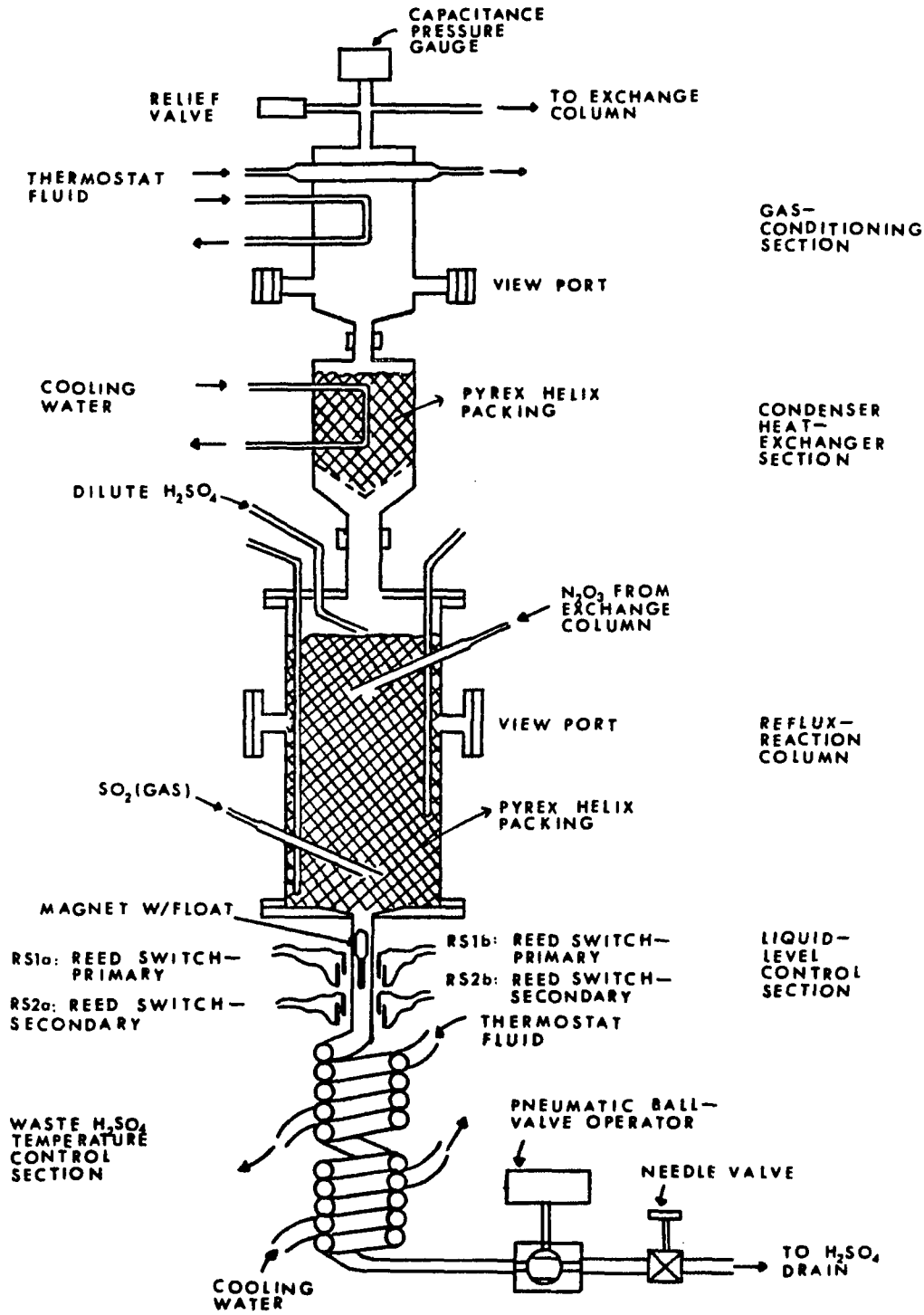

Figure 7: Schematic Assembly Drawing of the Pressurized Product Refluxer System

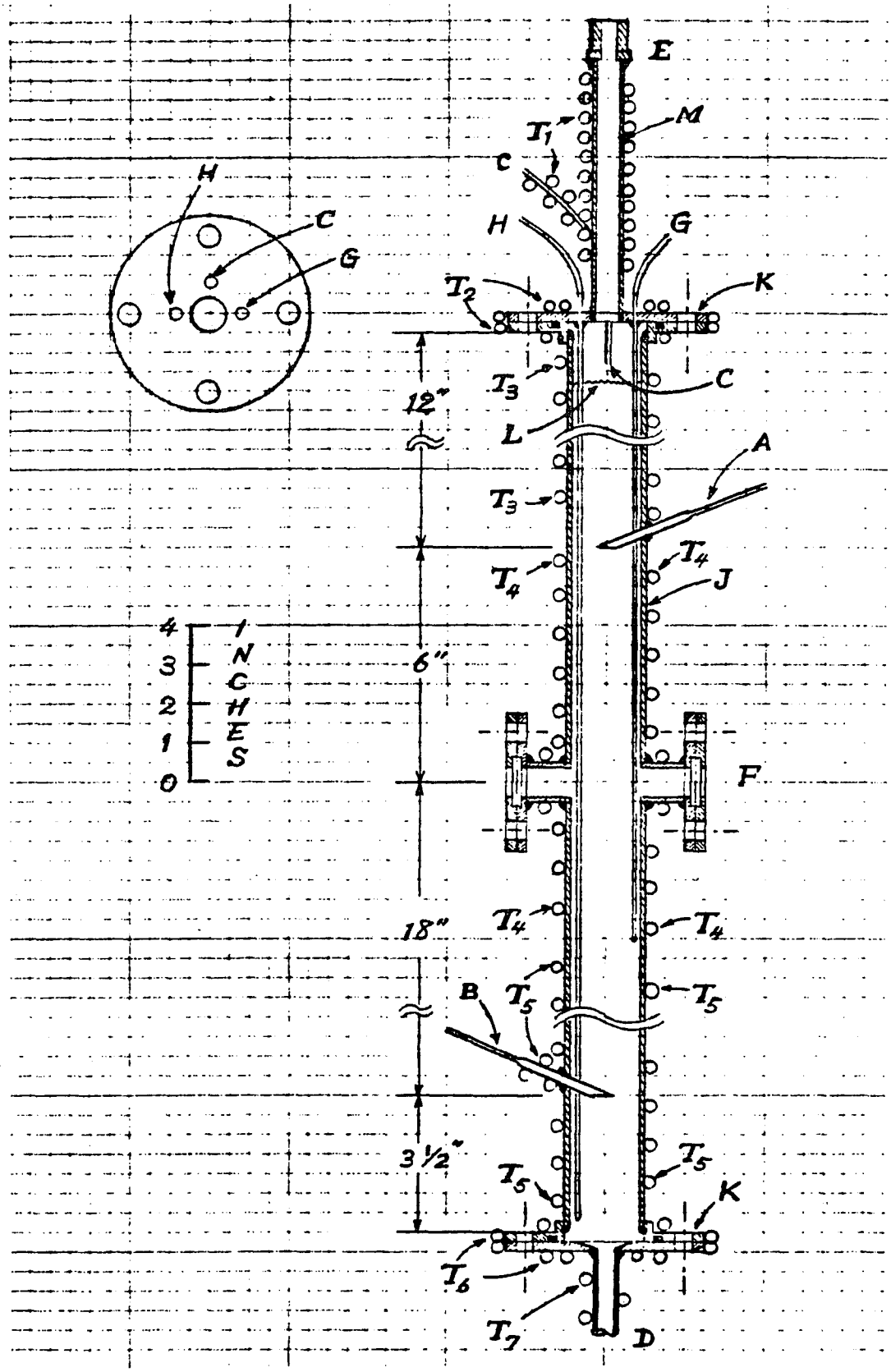

Figure 8: Reflux Reaction Column

Legends for Figure 8: [4:1 Scale]

A: N_2O_3-feed from exchange column's product end. 1/4" Pipe plus 1/4" O.D. tubing, Carpenter 20 (C-20), Heliark-welded (H-welded) through the wall of J at 30° from the horizontal line.

B: SO_2-feed from heated supply tank. Same construction as A.

C: Dilute H_2SO_4-feed. 1/4" O.D. tubing, reinforced by a 3/8" O.D. collar feedthrough on the flange K. All in C-20, H-welded.

D: Liquid level control section, in C-20, H-welded to the bottom flange K.

E: Cajon VCO fitting, 3/4" male, with special HNO_3-NO resistant Viton O-ring, in Type 316 SS, H-welded to M.

F: Two parallel viewing windows. Each window is an annealed disk of Pyrex, 1 1/4" O.D. x 3/8" thick, sandwiched by a Teflon ring washer on both sides and clamped between two 1/2" (nominal) C-20 flanges. All metal parts are C-20, H-welded together.

G: 1/4" O.D. tubing with a weld-sealed end, used to house reaction-zone detecting thermistor(s). Made in C-20 and reinforced at the flange feedthrough point in the same manner as for C.

H: 1/4" O.D. tubing, in C-20, constructed in the same manner as for G, but longer to reach the bottom of the column. Used to house several thermistors to monitor temperatures at various levels along the column.

J: 1 1/2" (nominal) pipe, schedule 40, 38 1/2" long, in C-20, welded on each end to a flange K.

K: 1 1/2" (nominal) flanges, in C-20, with a tongue-and-groove, Teflon washer, seal.

L: Top level of Pyrex helix column packing.

M: Connector tube, in C-20, H-welded to the top flange K at the bottom and to E on the top.

T_1-T_7: Type 304 SS tubing for carrying thermostatted fluid, and welded to ensure maximum area of contact and heat transfer.

parts are made of C-20 stainless steel. Pyrex glass was used for the viewing windows and for the helical packing material, and Teflon was employed as gasket material. Type 304 SS tubing was wound and welded on the outside of the column for thermostatting purposes. The main column is a 1 1/2" pipe (schedule 40), 38 1/2" in length, and welded at each end to a 1 1/2" flange (150 lbs rating). The flanges have tongue and groove faces with a Teflon gasket seal. Three 1/4" tubings (all C-20) penetrate the top flange: Tubing H runs the length of the column, is sealed at the bottom end, and houses several thermistors to monitor the temperatures at various levels of the column. Tubing G is also sealed at its lower end and is used to house the reaction zone controlling thermistor.

The feed streams for the refluxer are N_2O_3 liquid from the exchange column, SO_2 gas, and dilute sulfuric acid, shown in Figure 8 as A, B, and C, respectively. If the product refluxer is to be operated at elevated pressures, the feed streams must be pressurized as well. The N_2O_3 feed presents no problem because it is coming from the exchange column, which is already at the operating pressure. The dilute H_2SO_4 feed is pressurized using the diaphragm metering pump, purchased from the Crane Company. Its pumping capacity is 4 gph and the maximum head it can pump against is 800 psig. The wetted parts of the pump are made of C-20, Teflon, and Hastelloy C.

However, the SO_2 feed line, its supply tank, and the entire refluxer column have to be heated to avoid liquefaction of SO_2. The SO_2 feed and refluxer column may be heated by circulating a thermostatted fluid through tubings T1-T7, which have been welded on for maximum heat transfer, or with heat tapes. The latter method was found

to be sufficient for the operating pressures below 5 atmospheres, for which the reflux column temperatures are not much above ambient temperature. The reaction zone was provided with a separate coil, T4, through which cooling water was circulated to prevent the temperature from rising above 100°C.

The reaction zone was controlled within ±1 cm of a set level by using a thermistor as the probe and by automatically regulating the amount of SO_2 input into the refluxer and can be visually confirmed through viewport F. Two viewport windows were placed on opposite sides of the column, and each consisted of an annealed optical Pyrex glass disk, 1 1/4" O.D. and 3/8" thick, sandwiched between a pair of Teflon gaskets and clamped between two 1/2" C-20 flanges. The distance between the bottom of the reaction zone (about the level of the viewport) and the SO_2 feed point was chosen to be 18", which is more than sufficient to allow ample contact between the rising SO_2 and small fraction of HNO_3 which might escape the main reaction zone.

(ii) Condenser/Heat Exchanger

A condenser/heat exchanger was added as part of the product refluxer to prevent water vapor of the heated reflux reaction column from entering the exchange column. This section is shown in Figure 9. It consists of a 316 stainless steel tubing, 1 1/4" O.D. by 1/16" wall and 13" in length, which is filled with glass helices (3/16" I.D.). The packing is supported by a stainless steel wire mesh (E) shaped into a narrow-angled cone.

The packing offers increased surface area for condensation of water vapor and for more effective heat exchange between the hot water vapor and the descending liquid. If the amount of water vaporized is

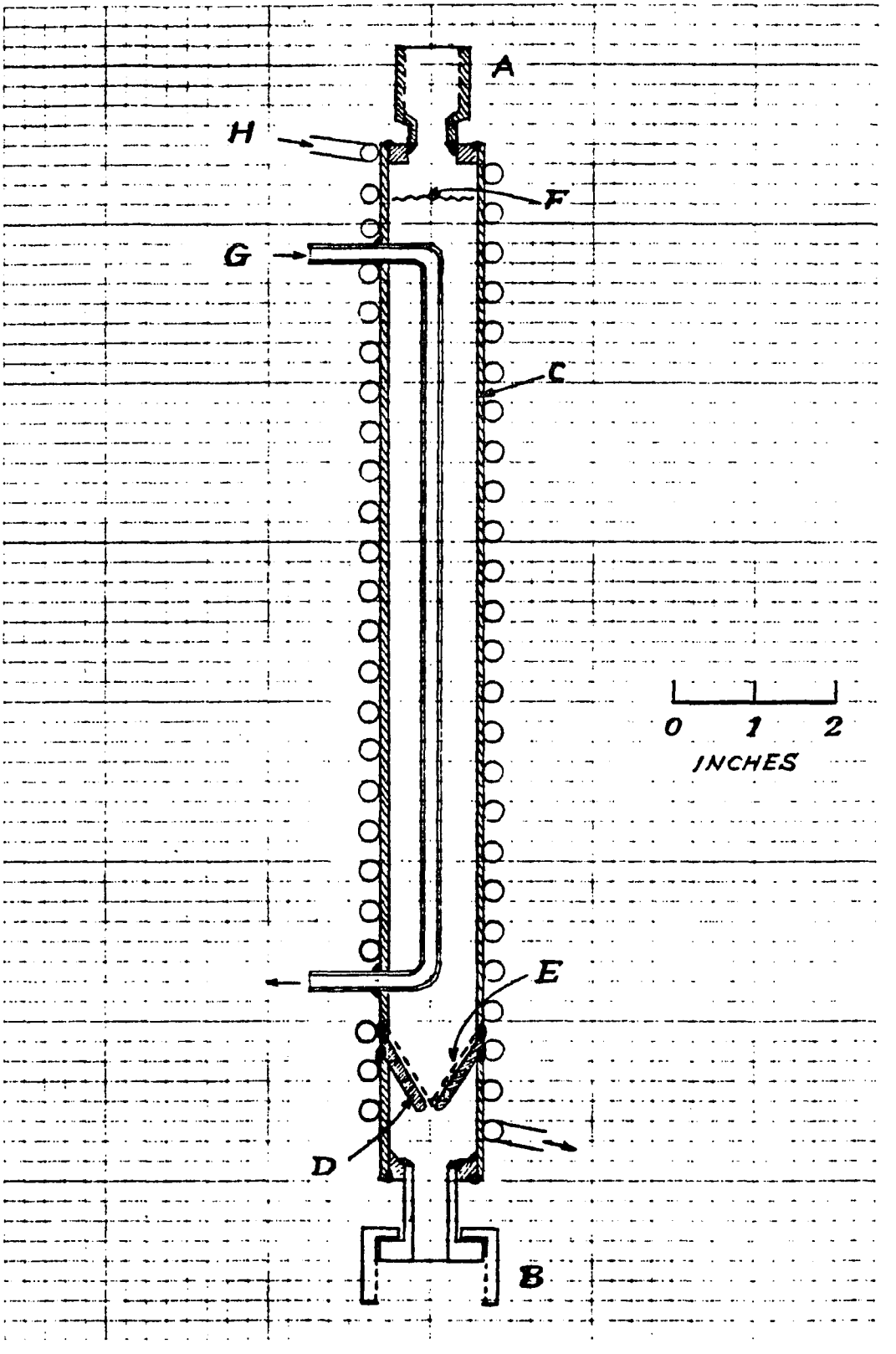

Figure 9: Condenser/Heat-Exchange [2:1 Scale]

Legends for Figure 9: [2:1 Scale]

A: 1/2" FPT, in Type 316 SS, Heliark-welded (H-welded) to C via an adaptor.

B: Cajon VCO fitting, 3/4" female, in Type 316 SS, H-welded to C via an adaptor.

C: 1 1/4" O.D. x 1/16" wall x 13" long tubing, in Type 316 SS.

D: 1/8" diameter, Type 316 SS, rods H-welded to the wall of C at an angle of about 30° relative to the vertical line.

E: Type 316 SS wire mesh shaped into a cone.

F: Top level of Pyrex helix column packing.

G: 1/4" O.D. tubing, Type 316 SS, H-welded to C and used to carry cooling water. The vertical part of G is coaxial with C.

H: 1/4" O.D. Type 304 SS tubing, welded on C and used to carry cooling water.

large, an effective heat exchanger will prevent the temperature of the liquid draining into the product refluxer column from being too low, thus lowering the column temperature. The direction of cooling water flow through H and G are from top to bottom to ensure that the gas entering the next (gas-conditioning) section is cooled to ambient temperatures, and for most effective heat exchange.

(iii) Gas-Conditioning Section

The top-most section of the product refluxer structure consists of a gas conditioning system fabricated out of Type 316 SS. It is shown in Figure 10. Its purpose is to ensure that the effluent gas from the refluxer is at the same temperature as the exchange column. By controlling the temperature, an equilibrium gas phase composition is maintained.

The section consists of Type 316 SS tubing (F), 1 1/4" O.D. by 1/16" wall and 16" in length. Its walls are kept at the temperature of the exchange column by three cooling systems represented by J, H, and K. J actually consists of three vertical inner tubings, each of which is a 1/4" O.D. tubing. H is a radial baffle made out of 1/2" O.D. tubing, and K is a 1/4" O.D. Type 304 SS tubing welded on to F.

The viewport, E, consists of two annealed optical Pyrex windows, each being 3/4" O.D. and 1/4" thick, backed by Teflon gaskets and clamped with a 3/4" VCO fitting. The viewport is used for visual or photometric determination of the concentration of NO_2 in the gas phase returning to the exchange column. The cross at the top of the gas-conditioning section is for connecting the product refluxer system to the exchange column, for a capacitance gauge connection, and for a pressure relief valve in case of failure of the back-pressure regulator

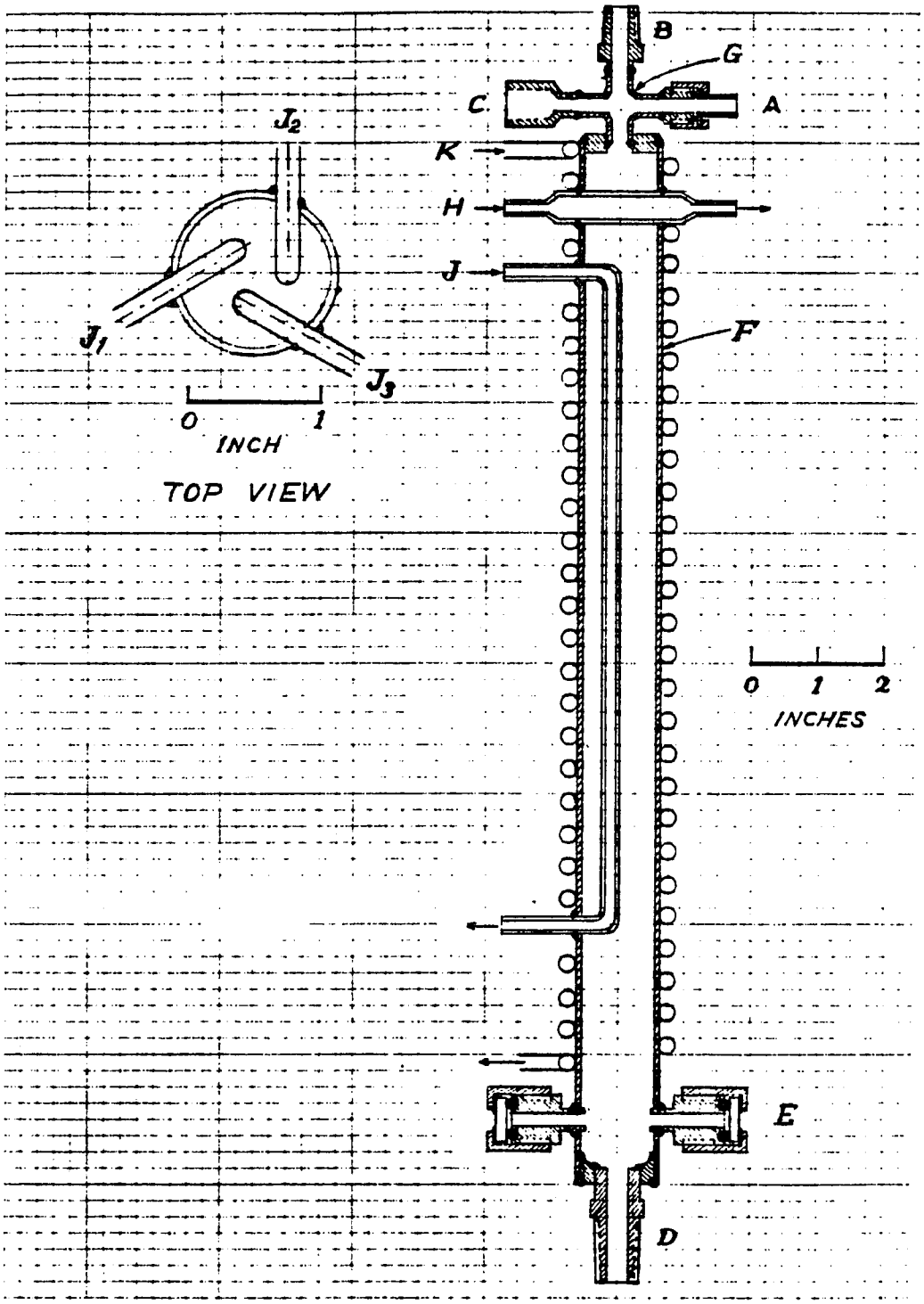

Figure 10: Gas-Conditioning Section

Legends for Figure 10: [2:1 Scale, except for the top cut-away view of the column, which is in 1:1 scale]

All parts are in Type 316 SS and Heliark-welded together, except K which is Type 304 SS.

A: 1/4" VCO connector for gas returning to the exchange column.

B: 1/4" MPT for connecting a capacitance pressure gauge.

C: 1/4" FPT for connecting a pressure relief valve.

D: 1/2" MPT for connection to Condenser/Heat-Exchanger section.

E: Two parallel view ports made of two 3/4" VCO, each used to clamp an annealed Pyrex window, 3/4" O.D. and 1/4" thick, which is backed up by a Teflon ring gasket.

F: Type 316 SS tubing, 1 1/4" O.D. x 1/16" wall x 16" long.

G: Cross used to butt-weld A, B, C, and F.

H: Radial (1/2" O.D.) thermostatting fluid path for baffling excess condensables.

J: Inner vertical thermostatting tubes (1/4" O.D.), one of which is shown in the side view. Relative positions of three J's are shown in the "top view".

K: 1/4" O.D. Type 304 SS tubing welded on F and used to carry the thermostatting fluid at the temperature of the exchange column.

that maintains a set system pressure. The capacitance gauge is Setra Model-204E (pressure range = 0-1000psia), which is used to monitor and record the system pressure during the experiments.

(iv) Liquid Level Control Section

This section, shown in Figure 11, consists of a vertically mounted piece of C-20 pipe, a magnet enclosed in a Pyrex capsule float, and four pairs of reed switches (all of which are of the normally-open type). Figure 11 shows only one switch from each pair.

The pipe is C-20, 1/2" pipe (schedule 40). The magnet is a Teflon-clad stirrer magnet (outside dimensions = 1" long x 3/8" O.D.), enclosed in a float made of a 3" long piece of medium wall 12 mm O.D. Pyrex tubing. This dimension is large enough to support the total weight of the magnet and the glass enclosure in water and in 10 $\underline{M}$-H_2SO_4, and this design withstood an external test pressure of more than 20 atm. The annular gap between the 12 mm O.D. tubing and the I.D. of the 1/2" pipe is sufficiently large to allow free flow of sulfuric acid.

During the normal operation only the pairs of switches marked RS1 and RS2 were used. Each pair, as well as the other two, marked RS3 and RS4 in Figure 11, consists of two identical switches (for instance, RS1a and RS1b) placed at radially opposite sides of the C-20 pipe. When the liquid H_2SO_4 accumulates sufficiently, the magnet activates RS1, which, through a control circuit described later, opens a ball valve to drain the accumulating liquid. The rate at which the liquid drains is controlled by the metering valve placed downstream of the ball valve (Figure 7). After sufficient sulfuric acid has been released the magnet closes RS2, resulting in the automatic shutoff of the ball valve. Thus, the gas-liquid interphase is maintained between

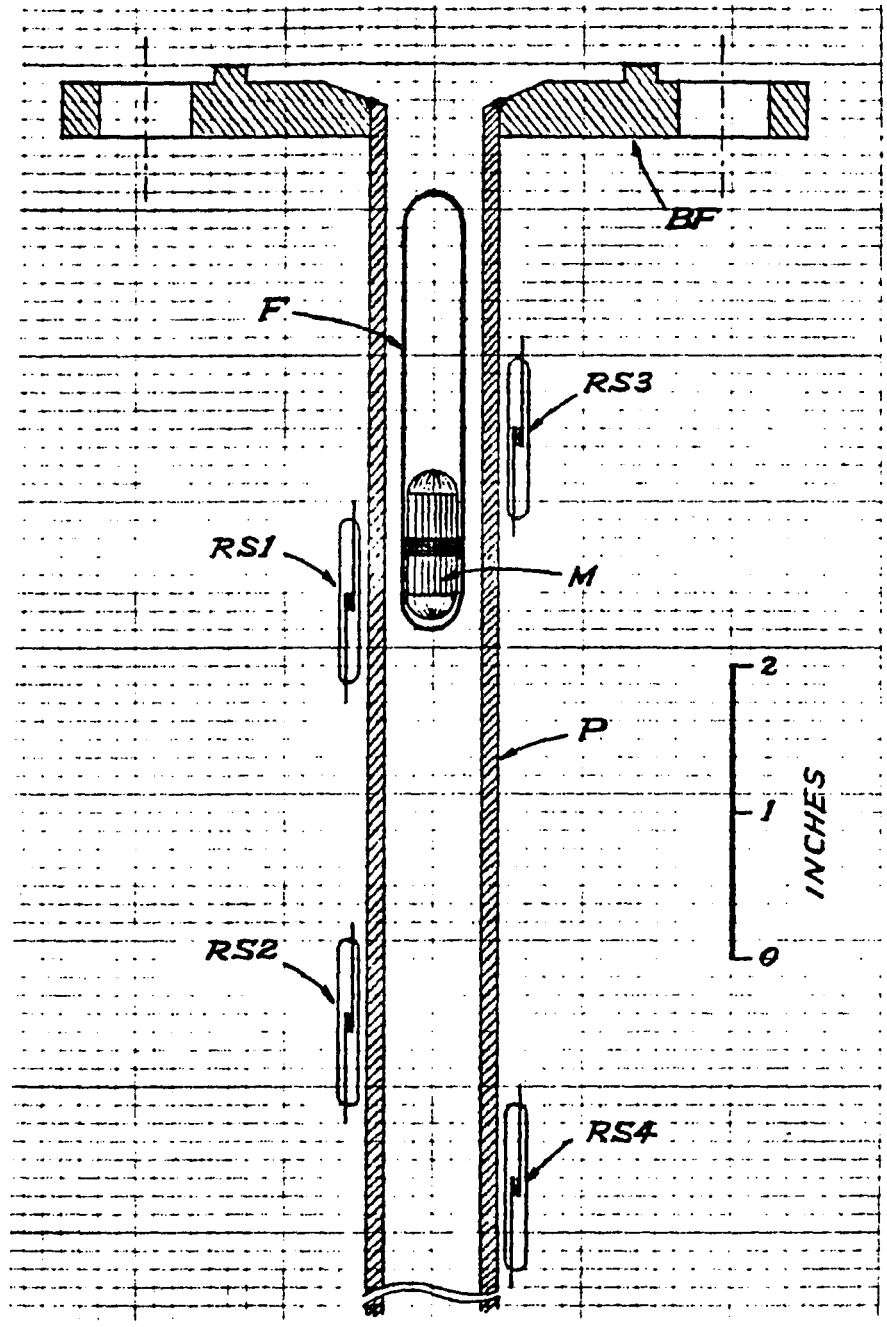

Figure 11: Liquid Level Control Section

Legends for Figure 11:

RS1: Reed Switch (high level detecting)

RS2: Reed Switch (low level detecting)

RS3: Reed Switch (high emergency)

RS4: Reed Switch (low emergency)

BF: Bottom flange of reflux reaction column

F: Float (medium-wall Pyrex tubing, 3/8" O.D.)

M: Magnet (stirrer, Teflon-clad)

P: C-20 1/2" pipe (Schedule 40)

RS1 and RS2. Two member switches are used as a precaution against the possibility that the magnet is so far away from the side of the pipe wall where a reed switch is mounted that it fails to activate the switch.

If, regardless of the twin switch arrangement, the magnet on its way downward fails to close the ball valve, the pair RS4 is activated and will immediately override all control logic to close the valve and sound an audio alarm. If the other case of malfunction occurs, where the magnet on its way upward goes past RS1 without opening the ball valve, then RS3 will be activated to sound the audio alarm. Color coded pilot lights on the control circuit would alert the operators as to which of the two situations is developing, so that they could act accordingly.

(v) Waste Sulfuric Acid Temperature Control Section

The hot sulfuric acid formed in the refluxer column must be cooled before it reaches the ball and metering valves since they are not available in C-20 and are made from Type 316 SS. However, H_2SO_4 cannot be simply cooled because the SO_2 gas will liquify at the gas-liquid interphase causing disastrous situations such as gas locks inside the coiled portion of the tubing and discharge of the SO_2 gas into the atmosphere of the laboratory.

To circumvent this problem, H_2SO_4 was thermostatted in two sections, as shown in Figure 7. The top section, where the interphase of the H_2SO_4 and gaseous SO_2 exists, is heated to the temperature of refluxer column, and the bottom section is cooled with running water. Copper tubing (3/8" O.D.) is coiled and brazed on to the 3/8" C-20 tubing coil, which is carrying the H_2SO_4 effluent, for maximum heat

transfer.

IIIC-2. Liquid Level Control Circuit

The level sensing devices have been described previously (IIIC-1-iv) and the arrangement of the sensors has been depicted in Figure 11 of that section. In this section, the circuitry for control of the liquid level of the sulfuric acid which, through a network of sensors, relays and solenoid valves, controls the pneumatic operations of the Whitey ball valve will be described.

The ball valve is operated by a pneumatic operator, which is positioned so that the valve is normally closed and can be opened when the operator is pressurized to 80 psig. When the pressure is released, a return spring rotates a gearing system to close the valve.

The control circuit is shown in Figure 12, and the associated electrical and mechanical connections are shown in Figure 13. In Figure 12 RS1 and RS2 are the reed switches that control the high and low liquid levels, respectively. The heart of the circuit is the operational amplifier (op amp) LM741 (A1) which is connected as a bistable multivibrator. When RS1 is activated by the magnet in the float, the bistable sends out a positive voltage that turns on the transistor (Q1) and consequently the coil of the relay K1. This action turns on two solenoid valves, SV1 (normally closed) and SV3 (normally opened), thereby supplying pressure to the pneumatic operator and opening the ball valve. The signal from the bistable also triggers the 555 timer which starts charging a capacitor, C1. The voltage across the capacitor increases as a function of time, and is compared to a reference voltage by another 741 op amp, A2. If RS2 is not

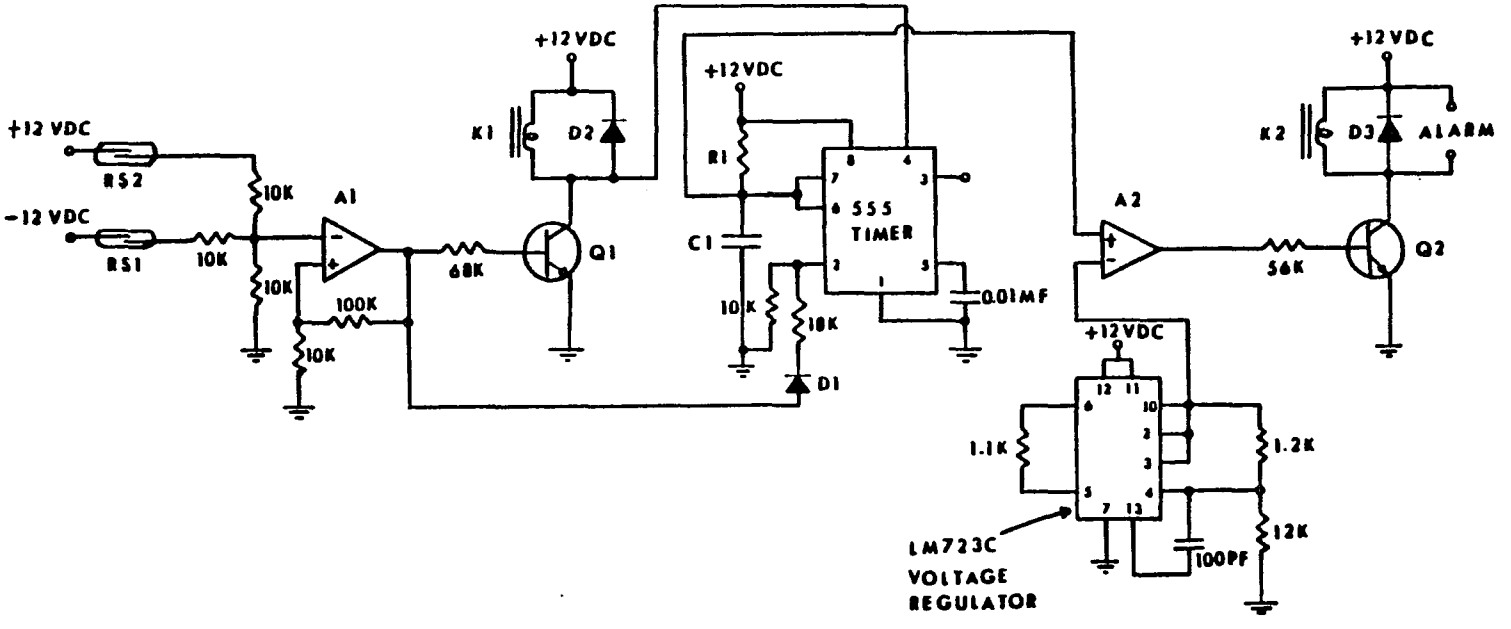

Figure 12: Circuit for Automatic Liquid Level Control

Legends for Figures 12 and 14:

A1-A4: Operational amplifiers, LM741

D1-D5: Silicon diodes, IN4004 (1A, 400 V)

K1-K4: DPDT relays (Coil resistance = 700 Ω, Power = 800 mW, Coil input voltage = 24 VDC, Max. Contact rating = 5A)

Q1-Q4: npn silicon transistors, 2N3569 (I_c = 500 mA, V_{CE} = 40 V, V_{BE} = 5 V)

RS1-RS4: Reed switches (500 mA, 200 V)

Resistors: 0.5 W, ±10% tolerance

[Pin identifications]

LM723C Voltage Regulator

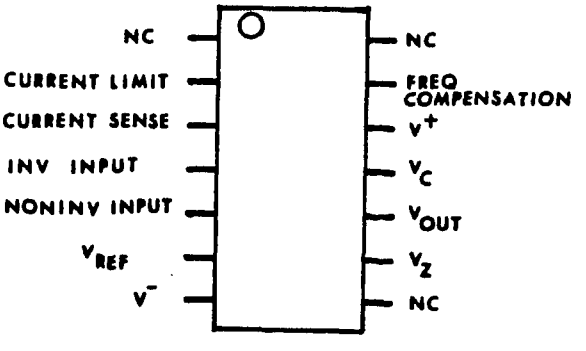

555 Timer

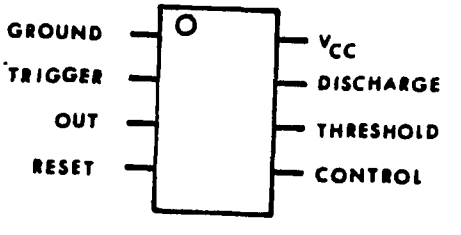

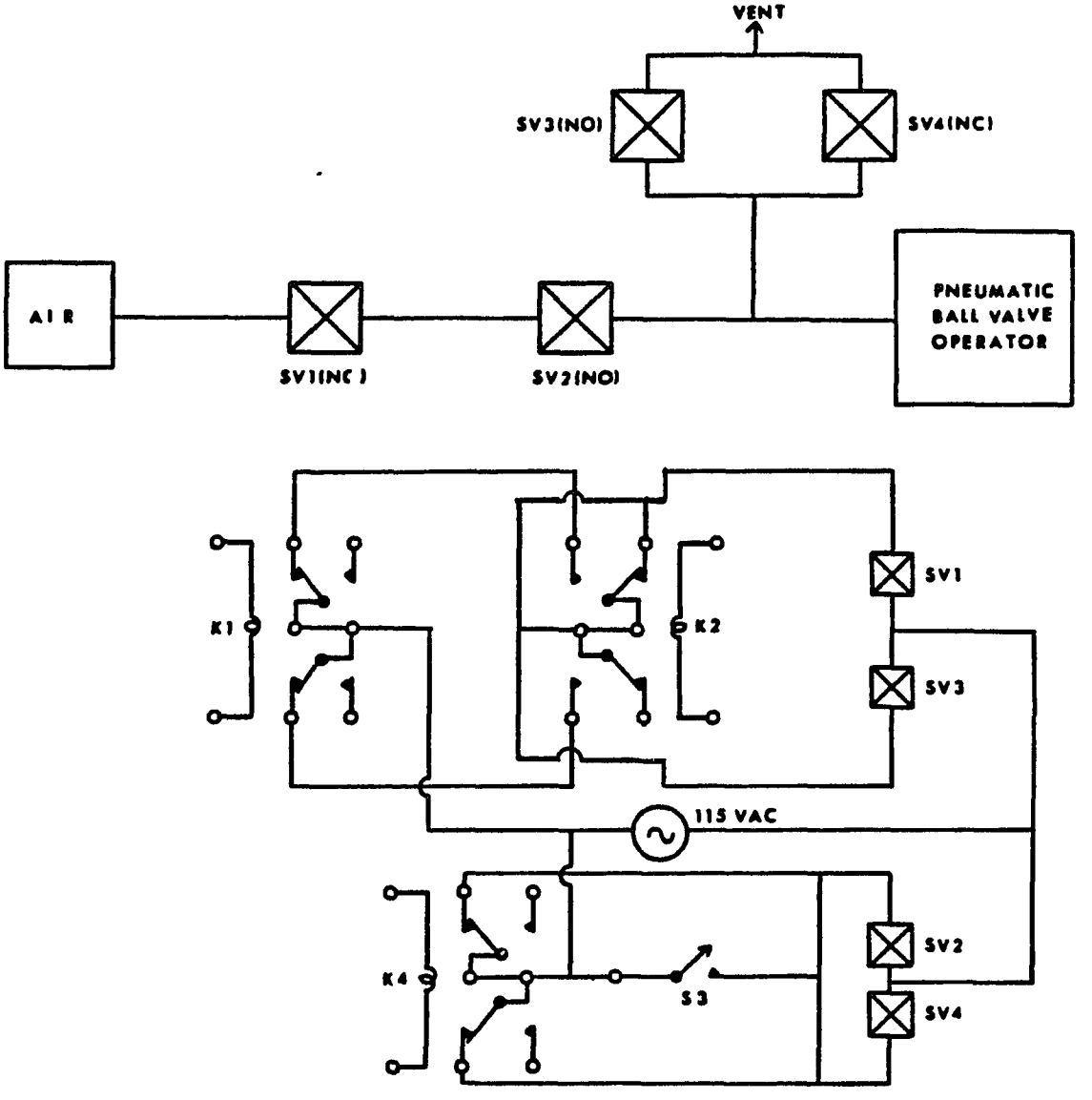

Figure 13: Electrical Connections for Relays and Solenoid Valves (Relay Contacts Shown in the On Position)

Legends for Figure 13:

K1, K2, and K4:	DPDT relays (24 VDC, 35 mA), all shown with the coil-ON position
S3:	SPST switch (1A)
SV2, SV3:	Solenoid valves, normally open (NO), 2-way, 115 VAC, 10 W, 150 psig
SV1, SV4:	Solenoid valves, normally closed (NC), 2-way, 115 VAC, 10 W, 450 psig

activated within a preset time determined by the R_1C_1 time constant, the timer will activate a warning alarm and relay K2, and the latter will cause the ball valve to close (Figure 13). This prevents the catastrophic possibility of SO_2 escaping through the ball valve. The delay time period is determined by the flow rates used in the experiment and is controlled by properly choosing R_1 and C_1. If RS2 is activated within the time limit, the ball valve will close, and the timer is reset (Figures 12 and 13).

The circuitry for the reed switches RS3 and RS4 is shown in Figure 14. The 741 op amps, A3 and A4, are again connected as bistable multivibrators. The function of the momentary switches S1 and S2 is simply to reset the multivibrators in case they have been triggered. If RS4 is activated, it would mean the automatic control system of Figure 12 has failed for some reason. In this case, the circuits have been wired to close the ball valve immediately. When RS3 is activated, a buzzer, connected in series with the then closed contacts of relay K3, will alert the personnel that the liquid level is too high. The ball valve can also be operated manually using switch S3 when the automatic circuitry is off. Table I is a truth table summarizing the states of the relays, solenoid valves, ball valve, and alarms for all possible situations that could arise during operation of the liquid level control.

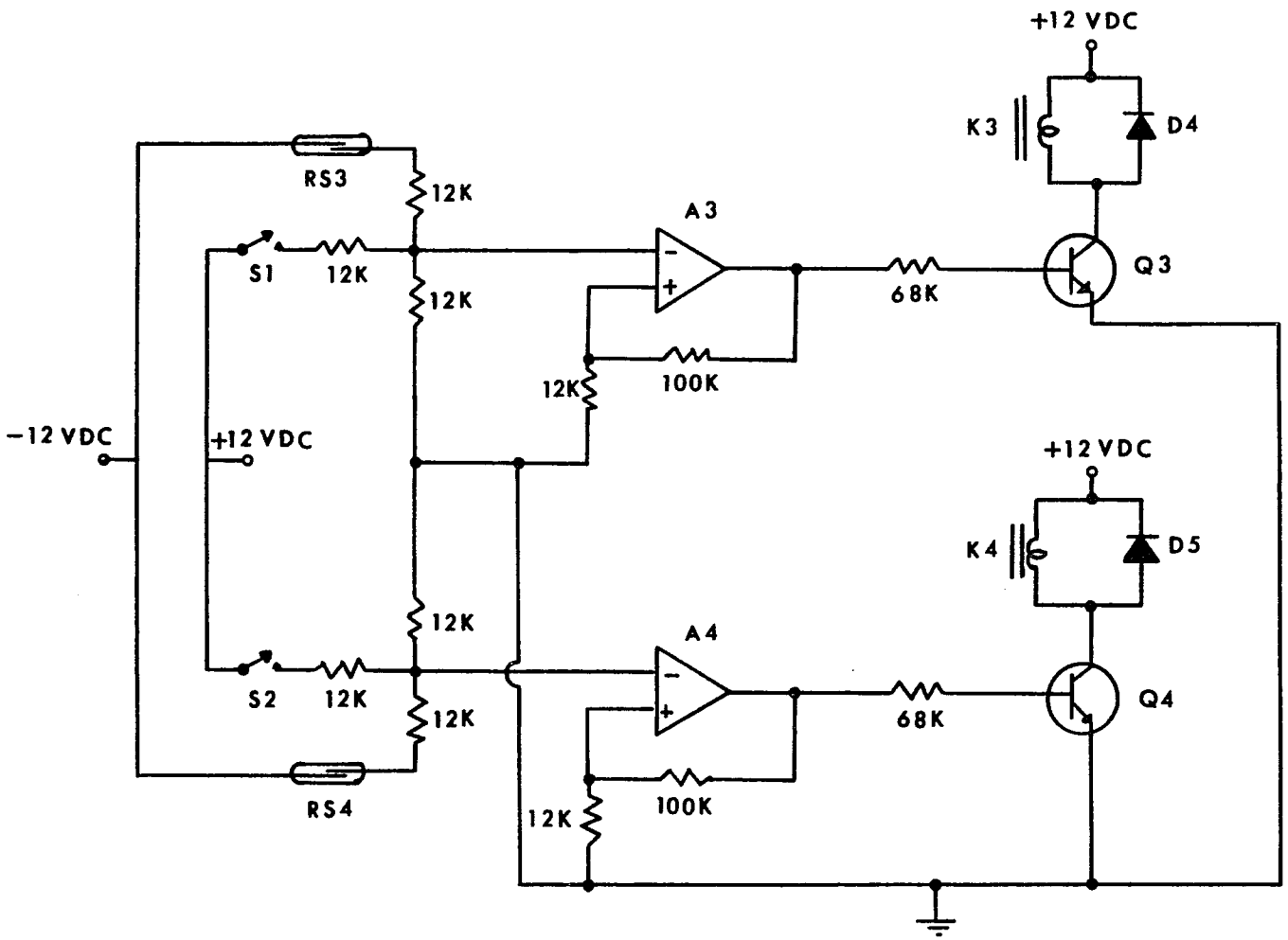

Figure 14: Circuit for Back-up System to the Automatic Liquid Level Control

Table I. State of Active Elements During Operation of Liquid Level Control

Situation	RS_1	RS_2	RS_3	RS_4	K_1	K_2	K_3	K_4	SV_1	SV_2	SV_3	SV_4	Ball Valve	Alarm
1	+	-	-	-	on	off	off	off	O	O	C	C	O	off
2	+	-	-	+	on	off	off	on	O	C	C	O	C	on
3	-	+	-	-	off	off	off	off	C	O	O	C	C	off
4	-	+	+	-	off	off	on	off	C	O	O	C	C	on
5	+	-	-	-	on^+	on	off	off	C	O	O	C	C	on
6	-	+	-	-	off^+	on	off	off	C	O	O	C	C	on

RS_1-RS_4, K_1-K_4, and SV_1-SV_4: See Figures 13 and 14.

+ = Switch activated

- = Switch deactivated

O = Opened

C = Closed

on^+, off^+ = element on or off longer than allowed for.

IIID. Product Withdrawal System

According to the theory of isotope separation, (see section VA), α and HETP can simultaneously be determined if the overall separation of a fractionating column is obtained as a function of the product withdrawal rate. A product withdrawal system was built from Pyrex after the design of Monse et al.,[5] except for the SS bellows-sealed shut-off and metering valves used in series for reduction of pressure from the exchange column, as shown in Figure 15.

The system consists of a Teflon microbellows metering pump (pumping rate = 0-26 ml/min) for withdrawing product as a gas from the bottom of the exchange column at a controlled rate, a 250 ml reaction chamber where the gas, which is a mixture of NO_x, is converted to NO_2 by reaction with an excess O_2 supplied through a capillary tubing, 1 mm I.D. The capillary tubing prevents back-diffusion of gaseous NO_2 to minimize product loss. The reaction chamber is cooled to about 0°C to ensure the completeness of the exothermic reaction. The buret is jacketted to circulate running water for condensing the NO_2 (B.P. = +21.5°C) and for obtaining the product withdrawal rate volumetrically. The mercury pressure regulator keeps the partial pressure of O_2 in the reaction chamber at about 80 torr.

IIIE. High Vacuum System for Reduction of NO_x

The progress of the overall separation, S, which is defined as the ratio of the atom ratio, N^{15}/N^{14}, at the enriched product end to that at the top of the exchange column, was followed as a function of time via the isotope ratio analysis of gas samples taken through SSV1 and SSV2

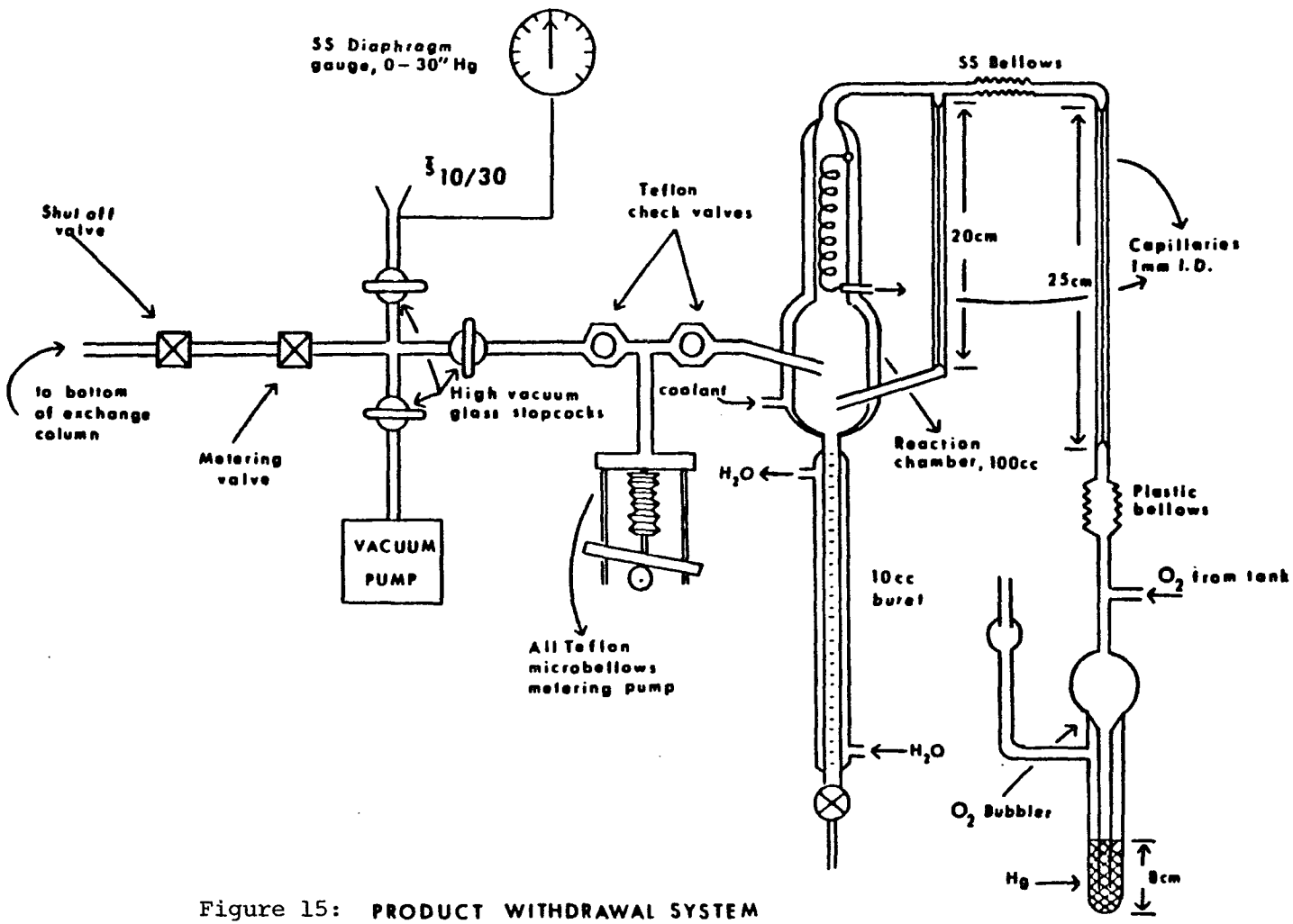

Figure 15: PRODUCT WITHDRAWAL SYSTEM

(Figure 2). However, the direct introduction of oxides of nitrogen into a mass spectrometer for sample analysis is unsatisfactory, mainly because of the erratic behavior of nitrogen dioxide stemming from its chemical reactivity. The NO_2 attacks traces of reactive materials which are always present in the high vacuum system of the mass spectrometer, such as water, carbon and polymerized hydrocarbons. These materials exist in the ionization chamber because of the standard procedure used for carbiding the ionization filament of the mass spectrometer with unsaturated hydrocarbons to obtain increased stability.[31]

It was, therefore, necessary to convert the NO_x samples to N_2 to simplify the isotopic analysis. The reduction was accomplished with a high vacuum system shown in Figure 16. It consists of a quartz chamber filled with copper turnings and copper(II) oxide and is kept at 800°C. Cupric oxide is used to remove carbon monoxide, in case it finds itself in the sample of N_2. The removal is necessary because its m = 28 peak interferes with the isotopic analysis of N_2. The temperature of the oven was continuously monitored with an iron-constantan thermocouple pair connected to a Fisher recorder (series 5000) for a direct readout of the voltage generated by the thermocouple. The Toepler pump is used for transport of noncondensible gases. The diffusion pump is filled with Dow Corning No. 704 silicone fluid, and the stopcocks are greased with Dow Corning high vacuum silicone grease. A carbon-based grease would have been attacked by the very reactive NO_2.

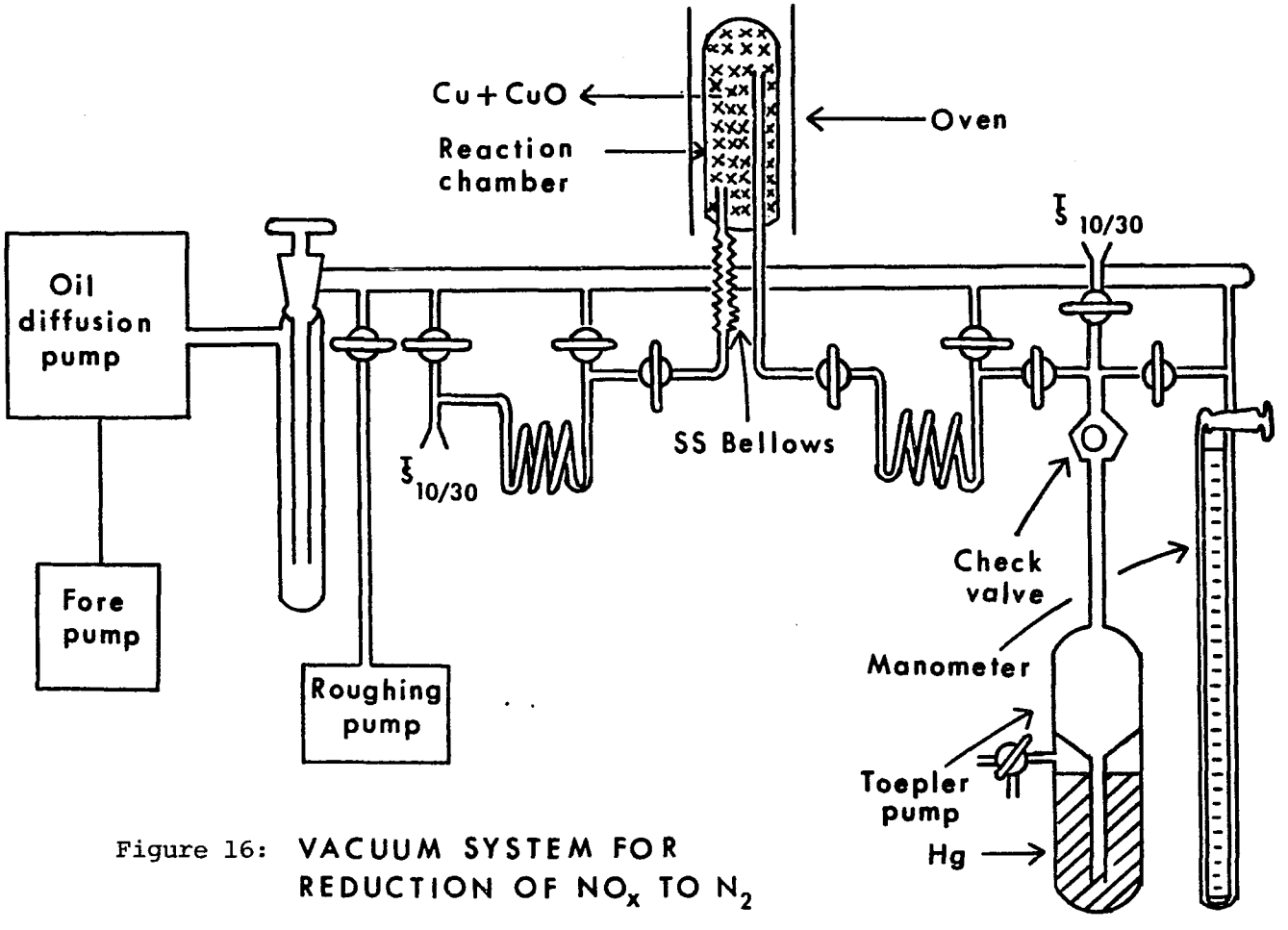

Figure 16: VACUUM SYSTEM FOR REDUCTION OF NO_x TO N_2

IIIF. Mass Spectroscopy

For isotopic analysis of the reduced nitrogen samples, a dual collector Consolidated-Nier isotope ratio mass spectrometer model 21-201 was used. Major modifications have been made on the mass spectrometer, which included modifying of the sample inlet system to make it a dual system, fabricated in Type 316 stainless steel. Each half of the dual system consists of four bellows-sealed Nupro valves, equipped with Kel-F stem tips and gaskets, and silver-soldered together. A schematic diagram of the inlet system is shown in Figure 17. It is connected to the MS ionization chamber via a VCR connector. Three additional bellows-sealed Nupro valves are provided for evacuating the sample inlet system.

Two viscous leaks, one on each half of the inlet system, consist of capillary tubings 0.005" I.D. x 7' in length. The two large non-Nupro valves CV1 and CV2, are home made compressors operated by manually compressing and or expanding the bellows silver soldered on to the valve. The design of these compressor valves is shown in Figure 18. The internal volume of the bellows and the rest of the inlet system were designed so that a ten fold increase in the pressure is obtained when the bellows is fully compressed from its expanded state.

The absolute and differential sample pressures are measured using a Setra differential pressure gauge, CG, model 236. The gauge has a pressure range of 0-20 psid, a proportional voltage output of 0-5 VDC, and can detect pressure differences of 0.2 torr. The sample holders used are glass-bodied, stainless steel bellows-sealed valves, and are connected to the inlet system via Cajon's ultra-torr adapters, thus making the entire inlet system free of grease and bakeable to 300°C.

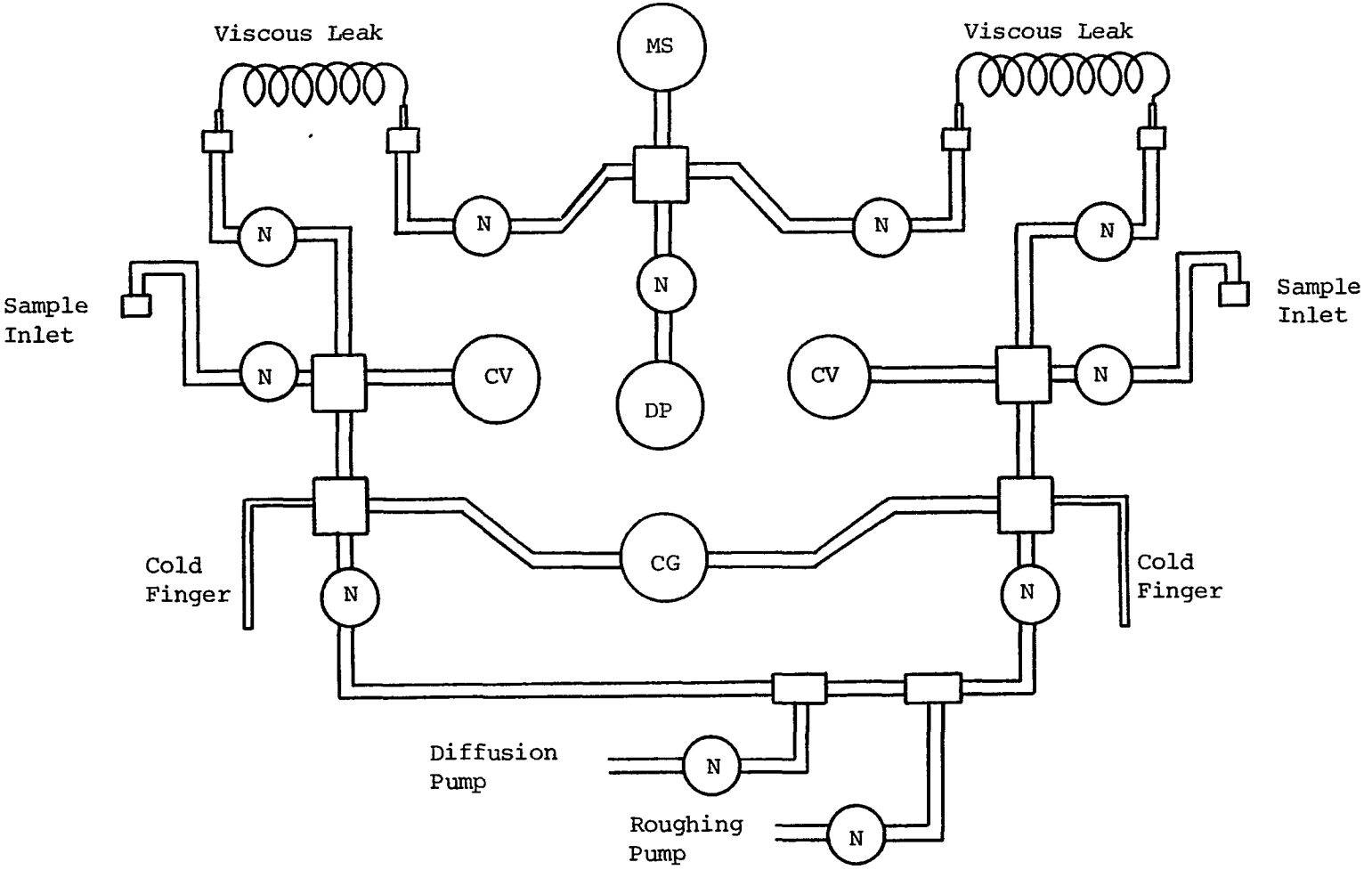

Figure 17: Dual Sample Inlet System

Legends for Figure 17:

MS: Mass Spectrometer

CV: Compression Valve

N: SS Bellows Sealed Nupro Valve

CG: Capacitance gauge (Differential)

DP: Diffusion Pump

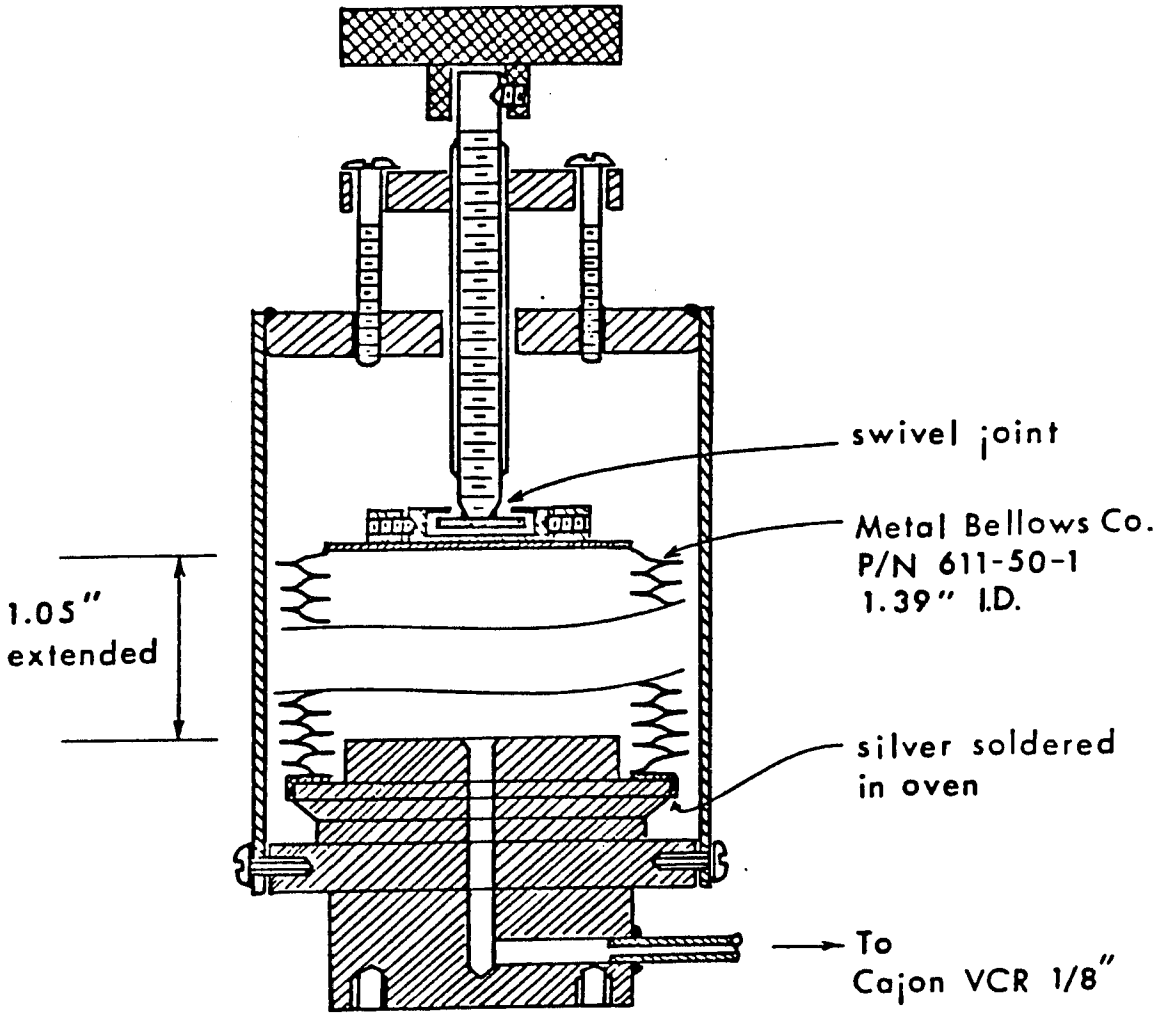

Figure 18: MS Sample Compressor Valve

The advantages of having such a dual inlet system are numerous. Top and bottom samples have separate inlet manifolds leading to the mass spectrometer. This is particularly useful in eliminating memory effects especially within the viscous leaks which, due to the capillary inner diameter and length, are difficult to evacuate.

The model 21-201 MS is equipped with a dual collector system that makes it particularly suitable for the kind of isotopic analysis needed in the present work. Ions with higher mass are focussed on the second collector, at which time ions of the immediately lower mass focus on the first collector. This allows simultaneous recording of the number of ions impinging on each collector. The current produced by the ions is amplified by an impedance transformer which has an input resistance of 40,000 MΩ and an output impedance of 1Ω. Each collector has its own current amplifier, and the voltages subsequently produced are read as a ratio using a 4 1/2 digit DVOM model 3400, purchased from the Data Precision Corporation.

The double collector technique eliminates any errors due to changes in the sample pressure as a function of time, and fluctuations that occur in the ionizing current and accelerating voltage. Also, since the overall separation is taken as the ratio of isotopic ratios, corrections that would be necessary for determination of absolute values of the isotopic ratios are not needed. One such correction has to do with the ion beam of the heavier isotope being wider than the slit width of the second collector, which would make it necessary to compensate for part of this beam being registered on collector one. Another correction that does not have to be applied is due to differences in the input resistances of the two amplifiers, since

such differences are cancelled out between two samples when the ratio is taken.

IIIG. Gas Cell for Spectrophotometric Determination of Gas Phase Composition

The gas cell used for the spectrophotometric measurements, which is shown in Figure 19, was constructed for operation at elevated pressures and subambient temperatures. The absorbance path is 3.2 cm., and all parts wetted by NO_x are 316 SS, Pyrex glass, and special NO_x-resistant Viton V-494. The viewing windows are two annealed Pyrex disks, each being 1 1/4" O.D. and 3/8" thick, and backed with Teflon gaskets. The required temperature was maintained by circulating a thermostatically regulated coolant, and the temperature was monitored with a copper-constantan thermocouple.

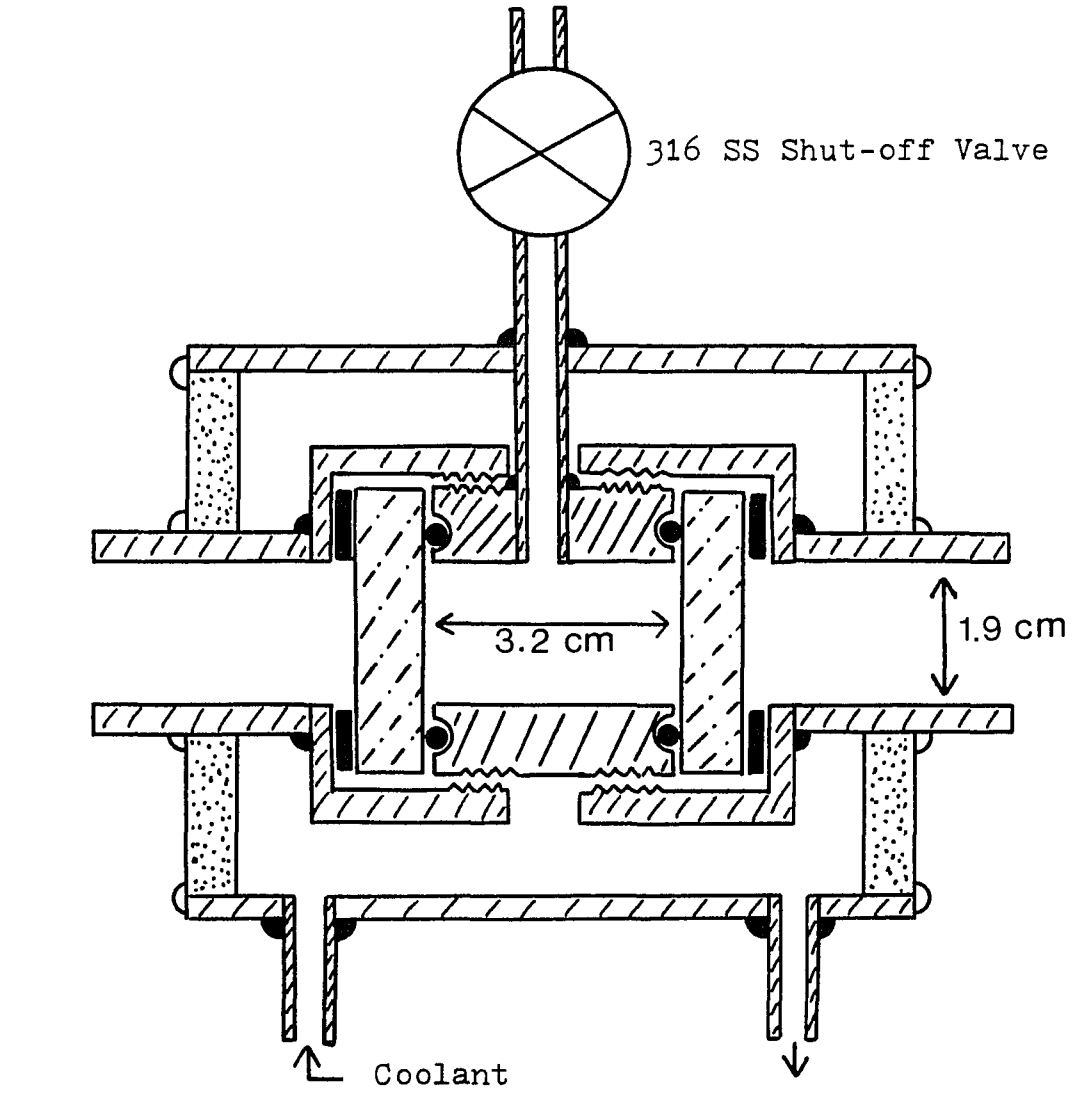

Figure 19. Gas Cell used for Spectrophotometric Determination of Gas Phase Composition

IV. EXPERIMENTAL PROCEDURE

The apparatus for studying nitrogen-15 fractionation using the N_2O_3 system was described in Chapter III. In this Chapter, the operation of the exchange column is discussed, followed by a section on processing and isotopic analysis of the samples. Procedures for determining the total amount of nitrogen in the waste sulfuric acid of the product refluxer, and the chemical analysis of the gaseous components which exist in the column are also outlined.

IVA. Exchange System

IVA-1. Start-up Procedure

Before commencing the experiments, the exchange column is filled with liquid N_2O_4 to wet the packing material. Gaseous nitrogen dioxide is introduced through a rotameter type flowmeter (F_1), (cf: Figure 2) and is liquified in the condenser, C_1, which is cooled by a thermostatted fluid circulated from a Revco refrigerating unit. By keeping the ball valve, CV, closed at the bottom of the exchange column, liquid N_2O_4 is allowed to wet the column packing. When the liquid becomes visible through the viewport of the flowmeter, F_2, the flow of gaseous NO_2 is decreased to a minimum, and the ball valve CV is opened while SSV3, on the return path of NO from the refluxer, is kept closed. The liquid is allowed to drain into the refluxer until a buildup of NO_x gases prevents further drainage from the exchange column. The ball valve is then closed, and dilute sulfuric acid is used to flush out the oxides of nitrogen from the refluxer column. The valve CV is reopened

to allow further drainage, and the cycle is repeated several times until most of the liquid is eliminated from the exchange column. This procedure was found necessary in order to avoid a flooding condition being created within the exchange column due to large inflow of gas.

IVA-2. Operation of the Exchange System

After this initial procedure, both valves CV and SSV3 are opened, and the flow rate of feed NO_2 is increased to a value L_f chosen for the run. The liquid from the exchange column enters the product refluxer and is reduced to NO according to equations 12a, 12b, and 12c. The flow of SO_2 gas is controlled with valves V_2, V_3 and V_4 (Figure 5). With valve V_3 closed, V_2 is adjusted so that SO_2 flows into the refluxer at a rate required to maintain the boundary of the reaction zone at the level of the sensing element. This flow is reduced 15% by partially closing V_2, and is then increased 30% by adjusting the needle valve, V_4, with V_3 opened. The 30% difference in the flow of SO_2 gas ensures that the rate at which the reaction zone rises and falls is not too fast or too slow. During the run, the level of the reaction zone did not usually fluctuate more than 1 cm.

The exchange column is equipped with Nupro valves SSV1 and SSV2 for sampling of the gas from the top and bottom of the exchange column. Bottom samples (4 cc at NTP) are taken every three to four hours, while sampling at the top of the column is less frequent.

Progress of the overall separation is followed until a steady state at total reflux is achieved, whereupon product withdrawal is started and another steady state condition is achieved.

The product withdrawal system is flushed with O_2 for approximately

1/2 hour prior to product withdrawal, and the Teflon microbellows metering pump is activated to start withdrawing gas from the bottom of the exchange column at a controlled rate. Typically, fluctuations of the product withdrawal rate were less than 4% of the magnitude of the withdrawal rate over a period of a few days.

IVB. Sample Processing

IVB-1. Reduction of Samples

The gas samples taken from the top and bottom of the exchange column are first degassed by repeating the liquid nitrogen freeze-pump-melt-freeze cycle using the high vacuum system described earlier (Figure 16). The sample is then passed through the quartz chamber and a liquid nitrogen trap at a flow rate of 30-40 ml/min by means of a Toepler pump. The LN_2 trap is used to condense CO_2 and unreacted NO_x. The nitrogen gas produced is compressed into a small sample holder for isotopic analysis.

To ensure that no significant amount of carbon monoxide exists in the MS samples, the N_2 gas obtained was occasionally analyzed using gas chromatography. A 20 ft column, 1/4" O.D. and filled with Molecular Sieve 5A (60-80 mesh) at 100°C separates O_2, N_2 and CO very well. The retention times relative to N_2 are: $R(O_2) = 0.72$, $R(N_2) = 1.00$, $R(CO) = 2.02$. No carbon monoxide was detected in any of the samples tested (detection limit 50 ppm for a 0.7 cm^3 sample at NTP).

To test for completeness of the reaction in the quartz chamber, the products of the reduction are collected without the LN_2 trap between the quartz chamber and Toepler pump. Mass spectrometer scans are

subsequently obtained, showing that, typically, the peak at mass 30 is significantly above background, and corresponds to the presence of about 0.2% nitric oxide. A 99.8% conversion at 800°C is considered to be sufficiently high so that isotope fractionation, if any, is negligible.

IVB-2. Isotope Analysis

Prior to analysis of the samples, a natural abundance N_2 sample is introduced in the inlet system. The gas is admitted to the ion source at low pressure (10^{-6} torr) where it is ionized by electron bombardment. The ion accelerating voltage is set at 1200 VDC and the magnetic field is varied to place the 29 peak on the number two collector. The peak is placed directly on the collector by using the ion accelerating voltage as a fine adjust. With the 29 peak being focussed on the number two collector, the 28 peak is automatically focussed on the number one. For all subsequent samples, only slight adjustments in the ion accelerating voltage were necessary to refocus the peaks. Amplifiers were zeroed and checked periodically for electronic drifts.

IVB-3. Total Nitrogen Content in the Effluent Sulfuric Acid

The effluent sulfuric acid was checked periodically for nitrogen content using a colorimetric procedure developed by G. Norwitz,[32] which is based on the determination of the pink color of $FeNO^{+2}$. The procedure is as follows: A ferrous sulfate solution is prepared by dissolving 2 gms of ACS grade $FeSO_4 \cdot 7H_2O$ in 30 ml of water containing a few drops of concentrated sulfuric acid. This sulfuric acid is necessary to prevent air oxidation and hydrolysis of the ferrous ion.

Concentrated sulfuric (100 ml) is added, and the solution is allowed to cool to room temperature.

For analysis, 3 ml of sample solution are added to 10 ml of concentrated H_2SO_4 and 10 ml of the $FeSO_4$ solution. The mixture is allowed to develop the color fully, and the concentration of the $FeNO^{+2}$ is determined colorimetrically at the wavelength of 520 nm. Actual samples from the column experiments are bubbled with He prior to analysis to liberate the dissolved SO_2. The calibration curve for this method is illustrated in Figure 20, and obeys the Beer-Lambert law within the concentration used. This method allows for rapid analysis of the samples and is able to determine the nitrogen concentration to ±3 ppm.

Usually, samples contained less than 10 μgms N/ml of H_2SO_4 acid. This corresponds to an average loss of 20 ppm of the nitrogen entering the product refluxer at a flow rate of 30 mmoles N/min in the exchange column and a sulfuric acid flow of 2 ml/min in the refluxer. This loss is considered sufficiently low for production of highly enriched N-15.[33]

IVC. Spectrophotometric Analysis

The absorbance of NO_2 in the visible region was used to determine the equilibrium gas phase composition. Details of equations and data needed for computing gas and liquid phase compositions will be found in Chapter VB.

For the calibration curves of absorbance vs P_{NO_2} nitrogen dioxide obtained from the Matheson Co. at 99% purity was purified by mixing it with O_2 in a 1:1 volume ratio at room temperature, and later removing

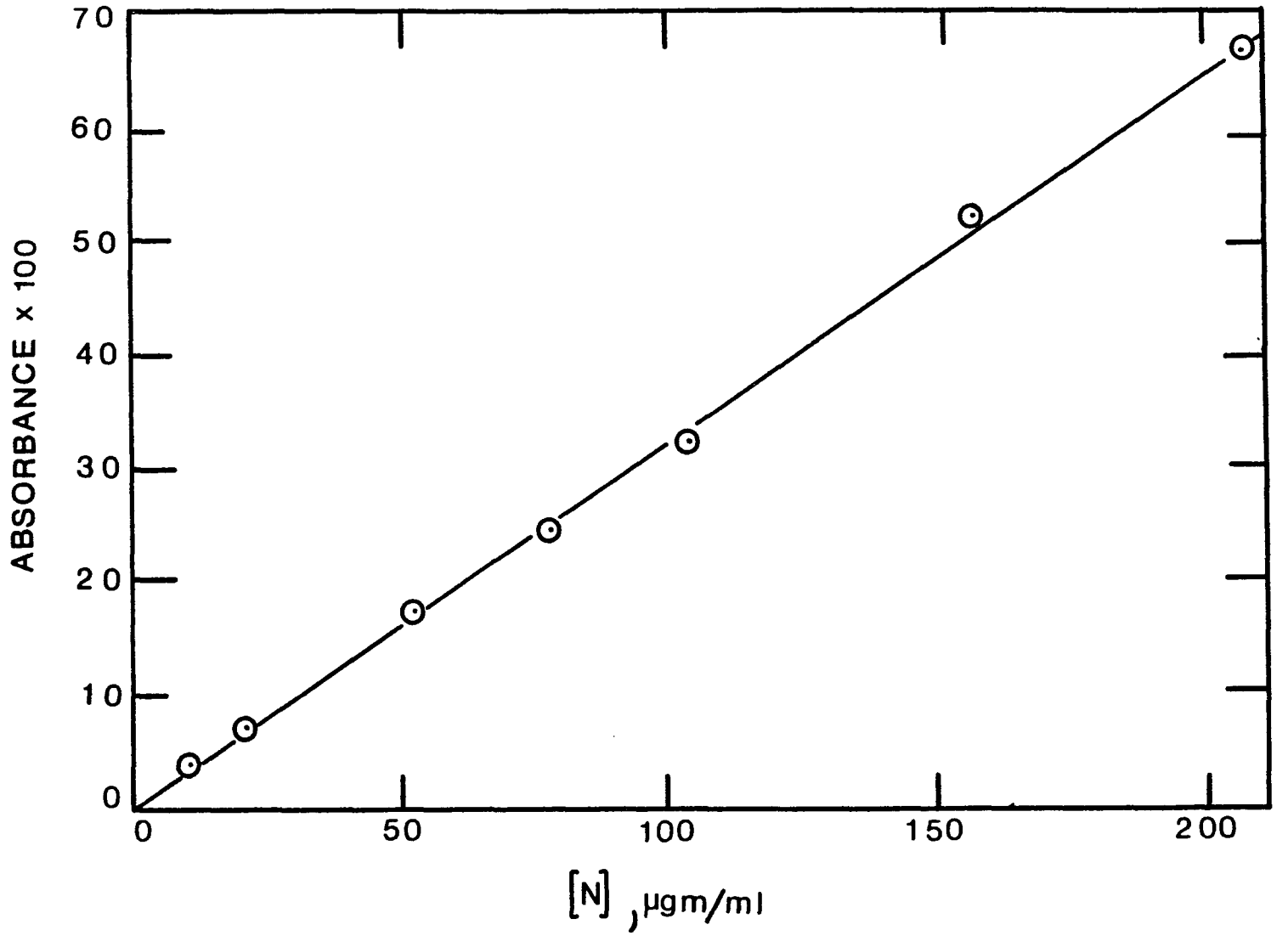

Figure 20: Calibration Curve for the Norwitz Procedure

the excess oxygen by repeatedly performing the freeze-pump-melt cycle with a dry-ice acetone bath. The purification procedure was repeated until a pure white solid was obtained on cooling the sample to -78°C. The N_2O_3 impurity, if present, could have been detected by the blue color which it imparted on the solid.

The pressure measurements were obtained with a mercury manometer which was protected from the oxides of nitrogen with a layer of silicone oil. High vacuum silicone grease was used on all ground joints and stopcocks. A Cary spectrophotometer, Model 14, was used throughout the work.

A preliminary scan in the region of interest (400-500 nm) showed two peaks, one at 436 nm and the other at 477 nm which were suitable for the NO_2 analysis with the particular cell length available (3.2 cm). Air was used as a reference, and absorbance of the samples was corrected for absorption of the evacuated cell. Tables II and III and Figure 21 offer the calibration data of A vs P_{NO_2} at 25°C and at two different wavelengths. The linearity of the plots (Figure 21) shows that Beer's law is obeyed. The calibration curve at λ = 477.0 nm was used in all the calculations of gas phase composition because of the expanded range of P_{NO_2}.

Table II. Absorption Coefficient ε' for NO_2 at λ = 453.9 nm, Length of cell = 3.2 cm[a]

	P_t Torr	P_{NO_2} Torr	A —	ε' $(Torr)^{-1}\ cm^{-1}$	$K_1^{25°C}$ atm
1	20.5	10.1	0.265	0.00825	0.1400
2	11.0	17.6	0.457	0.00817	0.1399
3	37.5	29.4	0.779	0.00833	0.1398
4	46.0	34.7	0.938	0.00850	0.1397
5	57.5	41.4	1.143	0.00868	0.1396
6	67.5	46.8	1.282	0.00861	0.1394
7	80.0	52.2	1.422	0.00857	0.1394
8	90.5	58.3	1.585	0.00855	0.1392
9	92.0	63.7	1.743	0.00860	0.1392
10	110.0	67.2	1.849	0.00865	0.1390
11	121.5	72.2	1.992	0.00867	0.1390

ε'_{avr} = 0.00851 $Torr^{-1}\ cm^{-1}$, σ = 0.00018.

[a] P_t is the sum of the partial pressures of NO_2 (P_{NO_2}) and N_2O_4 ($P_{N_2O_4}$). K_1 is the dissociation constant of N_2O_4 and is calculated using a method outlined in Chapter VB. ε' is the absorption coefficient of NO_2 at the given wavelength.

Table III. Absorption Coefficient ε' for NO_2 at λ = 477.0 nm, Length of cell = 3.2 cm[a]

	P_t Torr	P_{NO_2} Torr	A —	ε' $(Torr)^{-1}$ cm^{-1}	$K_1^{25°C}$ atm
1	11.5	10.4	0.154	0.00421	0.1399
2	21.5	18.3	0.266	0.00457	0.1399
3	38.0	29.7	0.431	0.00456	0.1397
4	52.5	38.5	0.547	0.00373	0.1396
5	71.0	48.6	0.695	0.00450	0.1394
6	97.0	61.4	0.884	0.00453	0.1392
7	113.5	68.7	0.990	0.00453	0.1390
8	131.0	76.1	1.120	0.00463	0.1387
9	161.0	87.7	1.293	0.00464	0.1383
10	189.5	98.0	1.460	0.00468	0.1380
11	220.0	108.1	1.583	0.00460	0.1374
12	248.0	116.9	1.725	0.00464	0.1370
13	268.0	122.8	1.806	0.00462	0.1367
14	304.0	133.0	1.971	0.00466	0.1360

ε'_{avr} = 0.00451 $Torr^{-1}$ cm^{-1}, σ = 0.00025.

[a]See footnote of Table II.

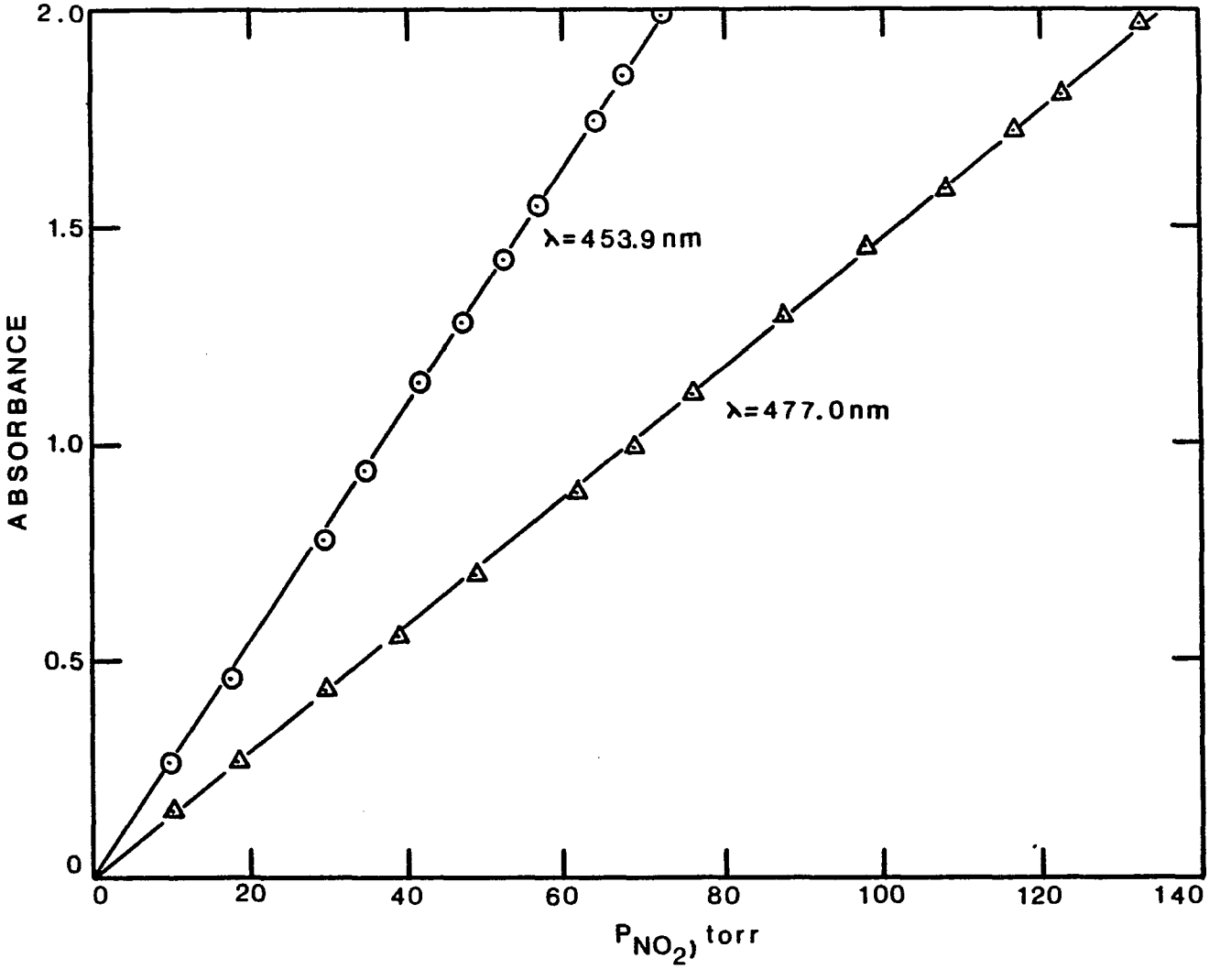

Figure 21: Absorbance vs P_{NO_2} at 25°C

V. METHOD OF DATA REDUCTION

In this Chapter, the methodology for obtaining the single stage separation factor, α, and the number of theoretical plates, n, from the overall separation of a fractionating column will be described in Section VA. Section VB contains details of the method by which the components present in the gas phase are obtained from an experimental study of the absorbance of NO_2 in the visible region and the stoichiometric and equilibrium relationships which exist amongst them. The determination of the liquid phase composition, which is obtained from an extrapolation of Beattie and Vosper's results,[27] is contained in this section as well. These quantities are needed for theoretical evaluation of α using Eq. (13).

VA. Determination of α and n

VA-1. Application of Isotope Separation Theory to Column Experiments

The single stage separation factor and the number of theoretical plates were determined by measuring the overall separation as a function of product withdrawal rate P (mmoles N/min). According to Cohen's theory,[11] which is valid for close separations, i.e., $|\varepsilon| = |\alpha - 1| \ll 1$, n is given by:

$$n = [(1-P/L)/(\varepsilon+P/L)]\ln[(1+P/L\varepsilon)S_p^{-1}-P/L\varepsilon]^{-1} , \qquad (14)$$

or

$$S_o^{-\frac{1+\theta}{1-P/L}} = (1+\theta)/S_p - \theta , \qquad (15)$$

where $\theta = P/L\varepsilon$, P is the product withdrawal rate, in mmoles N/min, and L is the liquid interstage flow, in mmoles N/min. S_o and S_p are the overall separations of the exchange column at total reflux i.e., P = 0, and at a finite product rate P, respectively. The effective separation factor is obtained from Eq. (15) as follows. Given the experimental values P, L, S_o, and S_p, each side of Eq. (15) is a function of θ. Let the left-hand side of Eq. (15) be $F(\theta)$, and the right-hand side $G(\theta)$. Then, the value of θ that satisfies Eq. (15) is obtained as the intersection of the plots of $F(\theta)$ vs θ and $G(\theta)$ vs θ. The corresponding ε is equal to $P/\theta L$, and n is obtained by solving $S_o = \alpha^n$. S_o and S_p were determined directly from mass spectrometry measurements of the samples taken from top and bottom of the exchange column:

$$S = (^{15}N/^{14}N)_{bottom}/(^{15}N/^{14}N)_{top} \quad . \tag{16}$$

P was evaluated volumetrically from the rate of accumulation of liquid N_2O_4 in a thermostatted buret (cf: Figure 15), and L was obtained from the direct measurement of the time required to fill a small calibrated Pyrex cup (cf: Figures 2 and 3).

VA-2. Determination of the Liquid Flow Rates for Different Phase Compositions

As discussed in the previous section of this Chapter, the liquid flow rate, L, is a quantity needed to simultaneously calculate α and n, and can be obtained using both direct and indirect methods. The direct measurements of the liquid flow λ, (ml/min) can be transformed to L in mmoles N/min with the following relationship:[5]

$$L = 1000\ \lambda\ d/[G_2+x(G_1-G_2)]\ , \qquad (17)$$

where x is the mole fraction of nitrogen with a +4 oxidation state in the liquid phase (the remainder, 1-x, being the mole fraction of nitrogen in the +2 oxidation state), d is the density of the liquid (g/ml), G_1 is the molecular weight of NO_2, and G_2 is the molecular weight of NO.

The density of liquid nitrogen dioxide (x=1) between -10°C and 20°C is well documented;[34] however reliable data on the density of the system dinitrogen tetroxide/dinitrogen trioxide is not available in the temperature range of interest. Results have been reported by Geuther for "pure" N_2O_3 boiling at about +3.5°C.[35] Judging from this boiling point, the mole fractions of N_2O_3 (x_3) and N_2O_4 (x_4) in the liquid are 0.46 and 0.54, respectively (Eqs. (23)-(25), cf: Section VB). The density of N_2O_3/N_2O_4 mixtures was then determined using the following procedure. Addison et al.[34] reported that the density of N_2O_4 from -10°C to +20°C was well represented by:

$$d^T(N_2O_4) = 1.4927-2.235\text{x}10^{-3}T-2.75\text{x}10^{-6}T^2\ . \qquad (18)$$

The densities reported by Geuther[35] were fitted to a curve using the method of least squares and is given by:

$$d^T(\text{mixt}) = 1.4494-1.2809\text{x}10^{-3}T+5.3146\text{x}10^{-5}T^2-1.7875\text{x}10^{-6}T^3\ , \qquad (19)$$

where for an ideal mixture,

$$d^T(\text{mixt}) = x_3 \cdot d^T(N_2O_3) + x_4 \cdot d^T(N_2O_4)\ . \qquad (20)$$

The validity of Eq. (20) has been tested by Shaw et al.[37] who found that mixtures of liquid N_2O_3/N_2O_4 behave in a nearly ideal manner. The density of pure N_2O_3 as a function of T can be evaluated by solving Eqs. (18)-(20) for $d^T(N_2O_3)$ under the assumption that $x_3 = 0.46$ and $x_4 = 0.54$ for Geuther's mixture. This procedure yields:

$$d^T(N_2O_3) = [d^T(mixt) - x_4 \cdot d^T(N_2O_4)]/x_3 \ . \qquad (20a)$$

This method was tested by using density data reported by Pascal and Garnier[36] for a liquid mixture of N_2O_3 and N_2O_4 which boils at -3.8°C ($x_3 = 0.64$, $x_4 = 0.36$) and with data obtained by extrapolating the values from a recent investigation of Shaw and Vosper[37] who measured the N_2O_3 density from -67°C to -37°C. Table IV contains a summary of reported and calculated values for the density of a mixture of N_2O_3 and N_2O_4. All presently calculated values are within 1% of the experimental results: An error of this magnitude would not have any significant effect on the present values of α and n.

Since the procedure for determining the liquid density d was found to be reasonably reliable, L was obtained from Eq. (17) for all runs, including those at the elevated pressures.

Two other methods for determining L are conceivable and can be derived from material balance considerations in the isotope exchange system. Figure 22 schematically shows the flow scheme of liquid and gaseous oxides of nitrogen. Here x and y are the mole fractions of +4 nitrogen in the liquid and gas phase, respectively.

At total reflux and steady state conditions, the amount of nitrogen fed per unit time as gaseous NO_2, L_f (mmoles N/min), is equal to the amount of nitrogen leaving the system as NO and NO_2 in the waste stream.

Table IV. Comparison of Densities of Liquid N_2O_3, N_2O_4, and Their Mixture Having a Composition ($x_3 = 0.64$, $x_4 = 0.36$).

T(°C)	[a] $d_{N_2O_3}$	[b] $d_{N_2O_3}$	[c] $d_{N_2O_4}$	[d] d_{mix}	[e] d_{mix}	[f] d_{mix}
-10	1.4276	1.4174	1.5147	1.4590	1.4524	1.4530
-5	1.4213	1.4045	1.5037	1.4510	1.4401	1.4440
+5	1.4097	1.4002	1.4815	1.4356	1.4295	-
+15	1.3988	1.4097	1.4586	1.4203	1.4273	-

[a] Extrapolation from Ref. 37.

[b] Present calculation from Eq. (20a).

[c] From Eq. (18).

[d] From Eq. (20), using $d^{a}_{N_2O_3}$ and $d^{c}_{N_2O_4}$.

[e] Present calculation from Eq. (20), using the data obtained from Eqs. (18) and (20a).

[f] Reported in Ref. 36.

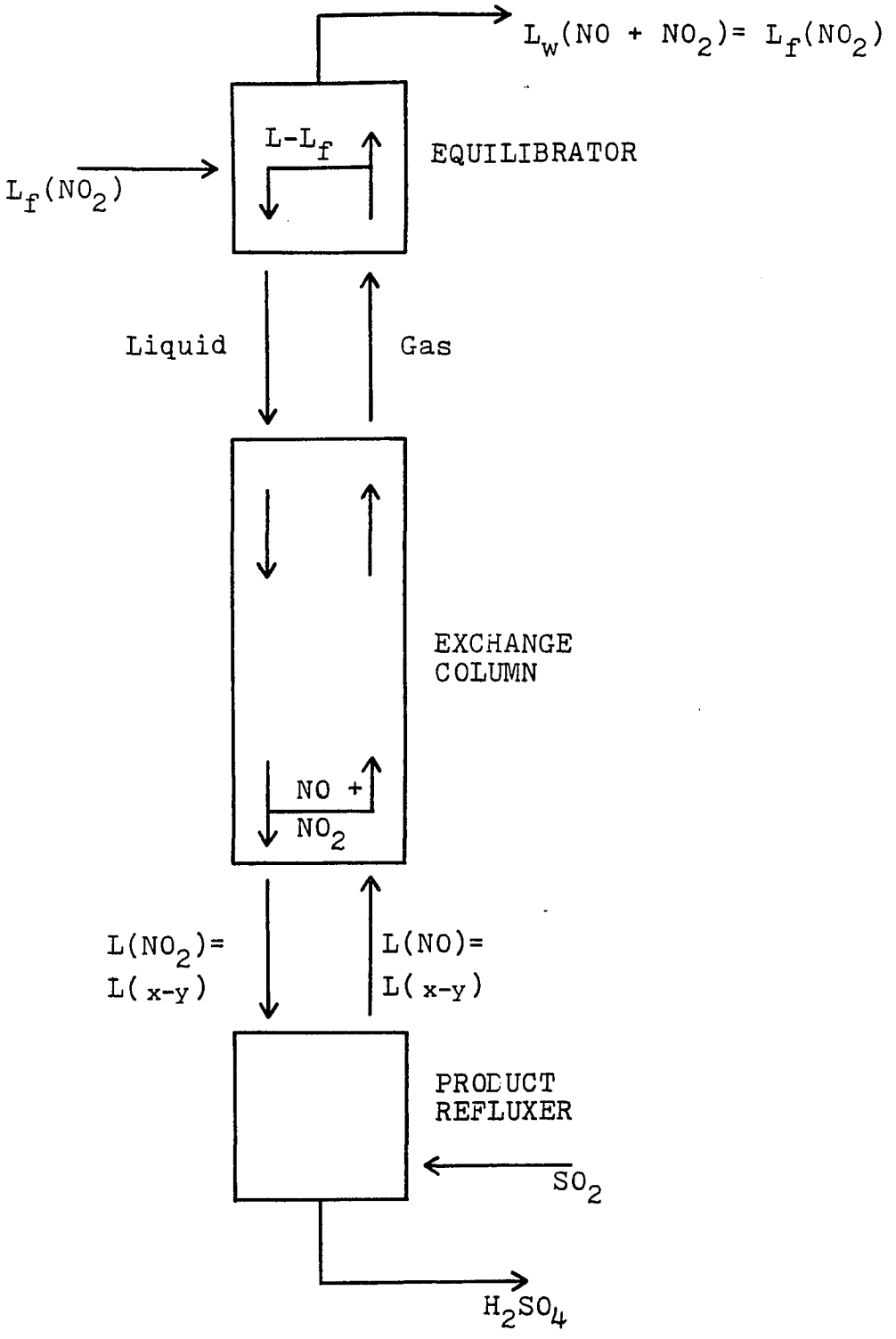

Figure 22: Schematic Diagram for Flows in the N_2O_3 Exchange System

The amount of +4 nitrogen that enters the refluxer and is reduced to NO (Lx-Ly) must equal the amount of nitric oxide escaping the waste stream, L_f (1-y), as shown in Eq. (21):

$$L = [(1-y)/(x-y)] \cdot L_f \quad . \tag{21}$$

It should be noted that if the column were operated at low temperature and/or high pressure, the liquid phase would essentially consist of pure N_2O_3 (x = 0.5), and the gas phase would be pure NO (y = 0). The liquid interstage flow, L, under these conditions would obviously be twice the feed flow L_f.

This method of calculating L, however, is very cumbersome since the feed flow is measured using a calibrated rotameter type flowmeter. The calibration must be accomplished for exactly the same conditions under which the flowmeter is to be used since the flow rate of any fluid will vary with density and viscosity, and both are functions of T and P. Thus the flowmeter would have to be calibrated for each of the runs performed. It is also worth noting that Eq. (21) only holds at total reflux, and would be incorrect to apply it to runs with finite production. Hence, the flowmeter was only employed as a rough guide for the feed flow of NO_2 during the experiments, and was not used for any of the calculations reported in this study.

The liquid interstage flow rate can also be determined from the amount of +4 nitrogen reduced to NO in the refluxer column per unit time, (Lx-Ly), which is equal to the amount of sulfuric acid formed:

$$L = \Delta L(SO_4^{=})/(x-y) \quad . \tag{22}$$

Here, $\Delta L(SO_4^{=})$ is the number of mmoles of sulfuric acid formed in the

refluxer per unit time. From the molarity and flow rates of the feed and waste H_2SO_4, L can be determined. However, this method also suffers from the problems of calibrating flowmeters under different experimental conditions. In addition, a flowmeter fabricated from C-20 to withstand H_2SO_4 acid and the pressures imposed in the experiment is not available commercially. Thus the measurement of the H_2SO_4 flow did not lend itself to be a practical one for the experiments at elevated pressures.

VB. Chemical Composition of Mixtures of Oxides of Nitrogen

VB-1. Liquid Phase

The two phase equilibria of $NO-NO_2$ mixtures has been studied by several authors,[25-28] who found that the relative amounts of +4 nitrogen in the two phases is determined by the temperature and pressure of the system. Purcell and Cheeseman[25] conducted a series of P-T determinations for gaseous mixtures of NO and NO_2 of known compositions using glass spiral manometers, and interpolated the results, along with vapor pressure data of the liquid, to determine the composition of the two phases at various temperatures and atmospheric pressure. They found their results to be in good agreement with those of Baume and Roberts.[26] Beattie and Vosper[27-28] measured the vapor pressure of the $NO-NO_2$ liquid mixtures from -60°C to 0°C, and have been able to express their results in the following form:

$$\log_{10}P(\text{mm Hg}) = 8.95-f(x)/T \ , \qquad (23)$$

where f(x) is a tabulated function of the mole fraction, x, of +4 nitrogen in the liquid phase, T is the absolute temperature, and P is

the total pressure. Their results further indicated that liquid $NO-NO_2$ mixtures consist mainly of N_2O_3 and N_2O_4, with almost no physically dissolved NO. This finding has been substantiated by a more recent investigation of Vosper.[7]

Whittaker et al.[38-39] studied the equilibrium between nitrogen dioxide and its dimer in the liquid phase and found that the concentration of NO_2 in pure N_2O_4 is only 2×10^{-4} g/cc at -10°C, increasing to 1×10^{-3} g/cc at +20°C. The electrical conductivities of dinitrogen trioxide[40] and dinitrogen tetroxide[41] are very small, of the order of 10^{-12} mhos/cm, so that self-ionization can only produce negligible quantities of the ionic species. Therefore, to a very good approximation, the liquid may be considered to consist of only N_2O_3 and N_2O_4, and its composition can be calculated from Eq. (23). The mole fractions of N_2O_3 (x_3) and N_2O_4 (x_4) would then be:

$$x_3 = 2(1-x) \ , \tag{24}$$

and

$$x_4 = 2x-1 \ . \tag{25}$$

Monse et al.[5] measured the content of +4 nitrogen in the liquid phase at pressures ranging from 3 to 9.5 atm at 23°C and found their results agreed satisfactorily with the extrapolated values of Eq. (23). Although Eq. (23) was originally obtained at low temperatures for which the vapor pressure was well below one atmosphere, Monse's results render justification for using this equation at the higher temperatures.

VB-2. Gas Phase

The equilibrium composition of the gas phase is obtained experimentally by determining the partial pressure of NO_2 from its absorbance spectrum in the visible region, and computing the partial pressures of each of the other gases by stoichiometry and data on dissociation constants of N_2O_3 and N_2O_4. The analysis of a mixture of gaseous oxides of nitrogen is simplified by the fact that nitric oxide is transparent at wavelengths longer than 230 nm at normal pressures,[42] while N_2O_4 does not absorb above 400 nm.[43] The spectrum of dinitrogen trioxide in several solvents and low temperatures[44] (where it should be almost completely undissociated) has shown the presence of a weak absorption maximum at approximately 700 nm, and an intense absorption, similar to that of the gas phase, below 350 nm. Hence, in the wavelength range of 400 to 500 nm, the only absorbing species is NO_2, which is free of interferences from the other oxides of nitrogen. The visible absorption spectrum of NO_2 has been studied by Dixon,[45] Hall and Blacet,[43] and Holmes and Daniels,[46] who have reported measurements on the extinction coefficients of the oxides of nitrogen over a wide range of wavelengths.

Assuming that the gaseous phase is composed of only NO, NO_2, N_2O_3, and N_2O_4,[8] the following relations hold true among the partial pressures of the nitrogeneous gases:

$$K_1(\text{atm}) = (P_{NO_2})^2/P_{N_2O_4} , \tag{26}$$

$$K_2(\text{atm}) = P_{NO} \cdot P_{NO_2}/P_{N_2O_3} , \tag{27}$$

and, for the ideal case:

$$y = (P_{NO}+P_{N_2O_3}+2.0\cdot P_{N_2O_4})/(P_{NO}+P_{NO_2}+2.0\cdot P_{N_2O_3}+2.0\cdot P_{N_2O_4}) \ , \quad (28)$$

and

$$P_t = P_{NO}+P_{NO_2}+P_{N_2O_3}+P_{N_2O_4} \ . \quad (29)$$

Here K_1 and K_2 are the equilibrium constants for the dissociation of N_2O_4 and N_2O_3 respectively; P_t is the total measured pressure, and y is the mole fraction of +4 nitrogen in the gas phase. From Eqs. (27) and (29),

$$P_{N_2O_3} = [P_t-(P_{NO_2}+P_{N_2O_4})]/(1+K_2/P_{NO_2}) \ . \quad (30)$$

Hence, the partial pressures of all the oxides of nitrogen are computable from the above relationships.

For the present study, the equilibrium constant for the dissociation of N_2O_4 at infinitesimal pressures was determined from the equation:

$$\log_{10}K^o_1 = -2891/T+1.75\log_{10}T+0.0046T-8.92\times10^{-6}T^2+3.934 \ , \quad (31)$$

given by Bodenstein and Boes.[47] K^o_1 was then corrected for gas imperfections due to nonidealities in the system using a procedure suggested by Giauque and Kemp.[48] In this procedure, K_1 is calculated from:

$$K_1 = [4.0P_1(\alpha_o+B\cdot P_1)^2]/[1-(\alpha_o+B\cdot P_1)^2] \ . \quad (32)$$

Here P_1 and B are given by:

$$P_1 = P_{NO_2}+P_{N_2O_4} \ , \quad (33)$$

$$B = -0.01(294.0/T)^3 \quad , \tag{34}$$

where B is the virial coefficient, and α_o is evaluated from:

$$K^o_1 = 4.0P_1 \alpha_o^2/(1-\alpha_o^2) \quad . \tag{35}$$

Beattie and Bell[49] have reported the dissociation constant for N_2O_3 at temperatures ranging from 5°C to 45°C, with K_2 at a given temperature showing a strong, linear dependence on P_{NO_2}. In the present study, their values were extrapolated using the following procedure. Assuming the vapor phase constant has the form:

$$K_2 = K^o_2 - m \cdot P_{NO_2} \quad , \tag{36}$$

where K^o_2 is the equilibrium constant extrapolated to zero pressure. The constants K^o_2 and m for the various temperatures are fitted to the forms:

$$\log_{10} K^o_2 = -A_1/T+B_1 \quad , \tag{37}$$

$$\log_{10} m = -A_2/T+B_2 \quad , \tag{38}$$

using the method of least squares, and are extrapolated into the temperature of interest. Hence the values of K_1 and K_2 for computing the gas phase composition from spectrophotometric absorbance measurements of NO_2 include a correction for deviation from ideal gas laws, and the only ideal relationship assumed for the calculations of the gas phase composition is Dalton's law, Eq. (29).

VI. RESULTS

VIA. Experimental Results of α and HETP at Various Temperatures and Pressures

Figures 23-28 are plots of the overall separation as a function of time for runs at -9.0°C, -4.0°C, +5.0°C, +14.0°C, and +15.5°C, all under atmospheric pressure. The overall separation, S, was obtained directly from the mass spectrometer readings as the ratio of atom ratios, $^{15}N/^{14}N$, between the two ends of the column (Eq. (16)). Each of the curves, except for Run 8 (Figure 24) has two steady states, the higher one corresponding to the overall separation under total reflux, and the lower one corresponding to separation with a finite production. For Run 8 no product was withdrawn due to its termination because of power failure. In Run 5 (Figure 26) a different size column was used (0.95 cm I.D., and 100 cm long). This column, however, was too long and narrow. It provided more than 100 theoretical plates to produce a high separation, and consequently the time required to reach steady state was too long. Also, due to its small diameter, flooding occurred during the runs unless the liquid flow rates were reduced to unrealistically low levels. Hence, the column design was changed to 50 cm long and 1.55 cm I.D. Both columns were packed with the same size packing material (Helipack No. 3013 SS helices).

Figure 27 (Run 7B) shows the overall separation decreasing as a function of time because it was a continuation of Run 7A, in which the final steady state was higher than the ones for 7B. In Run 10A (Figure 28), the separation at total reflux was obtained twice, i.e., before and after the product withdrawal experiment. This was done to check the consistency of the values for the column separation at equilibrium, the

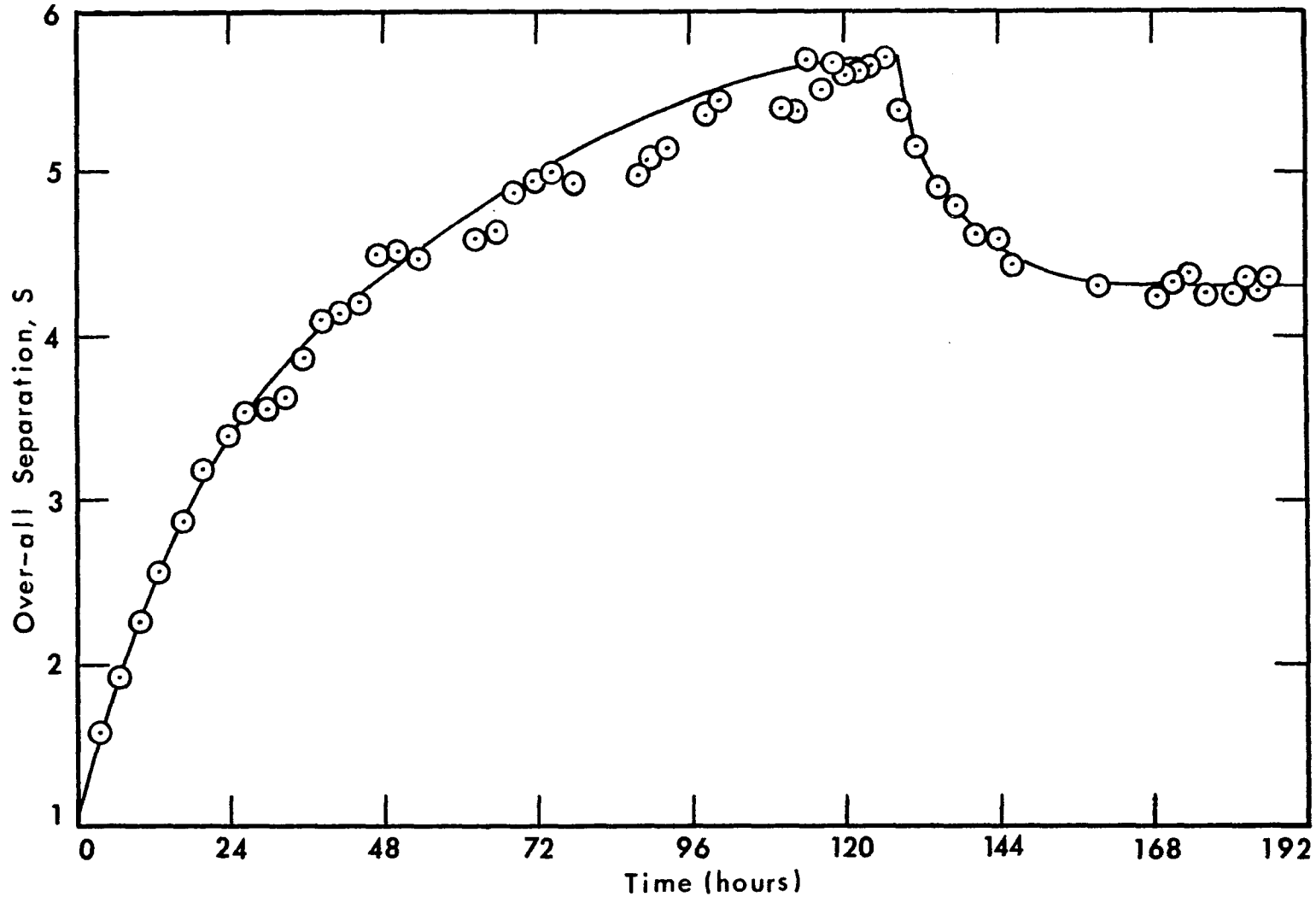

Figure 23: Overall Separation as a Function of Time: T = -9.0°C, P = 1 atm [Run 7A]

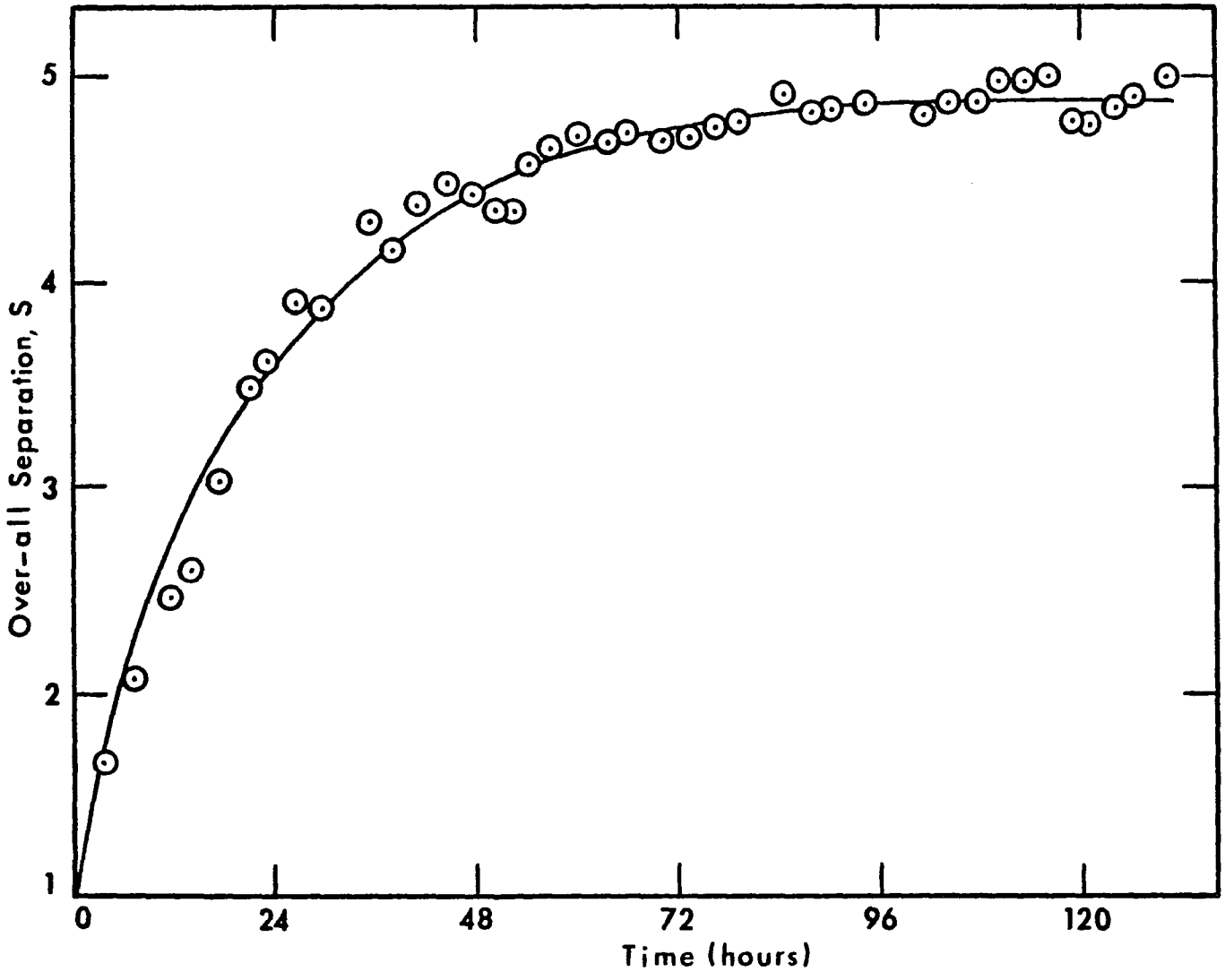

Figure 24: Overall Separation as a Function of Time: T = -4.0°C, P = 1 atm [Run 8]

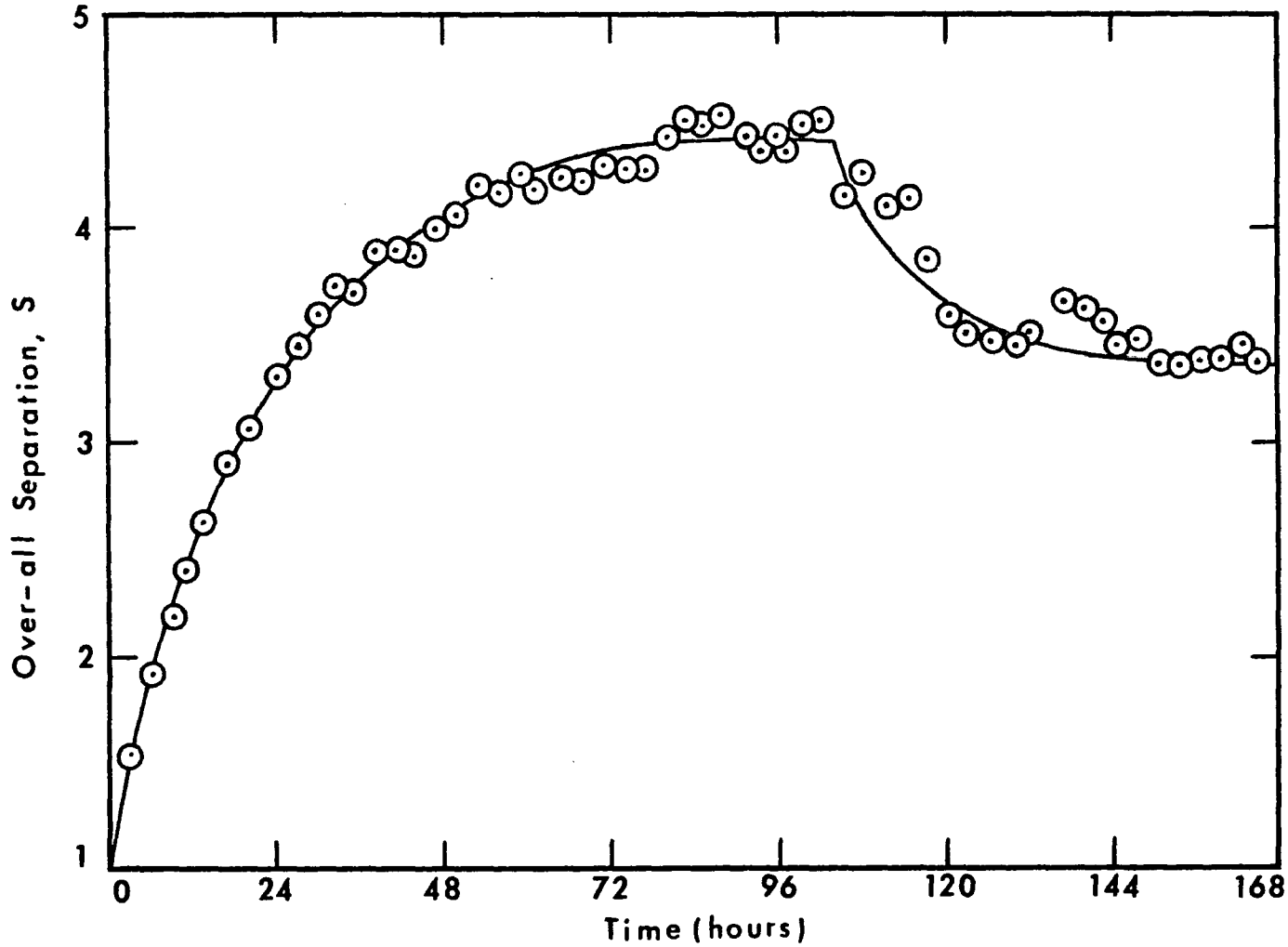

Figure 25: Overall Separation as a Function of Time: T = -4.0°C, P = 1 atm [Run 9]

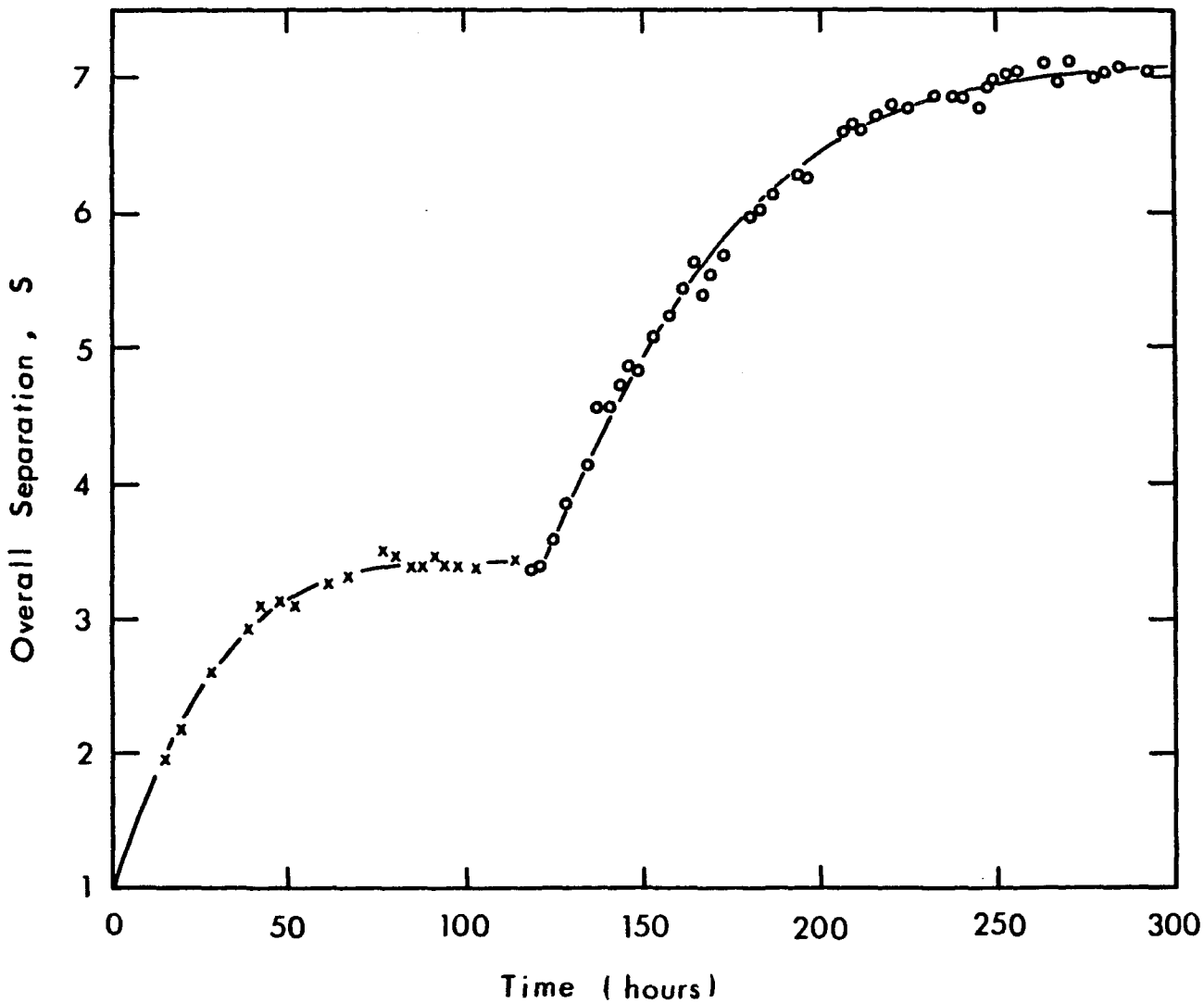

Figure 26: Overall Separation as a Function of Time: T = +5.0°C, P = 1 atm
[Run 5, Performed with the 100 cm long column, 0.95 cm I.D.]

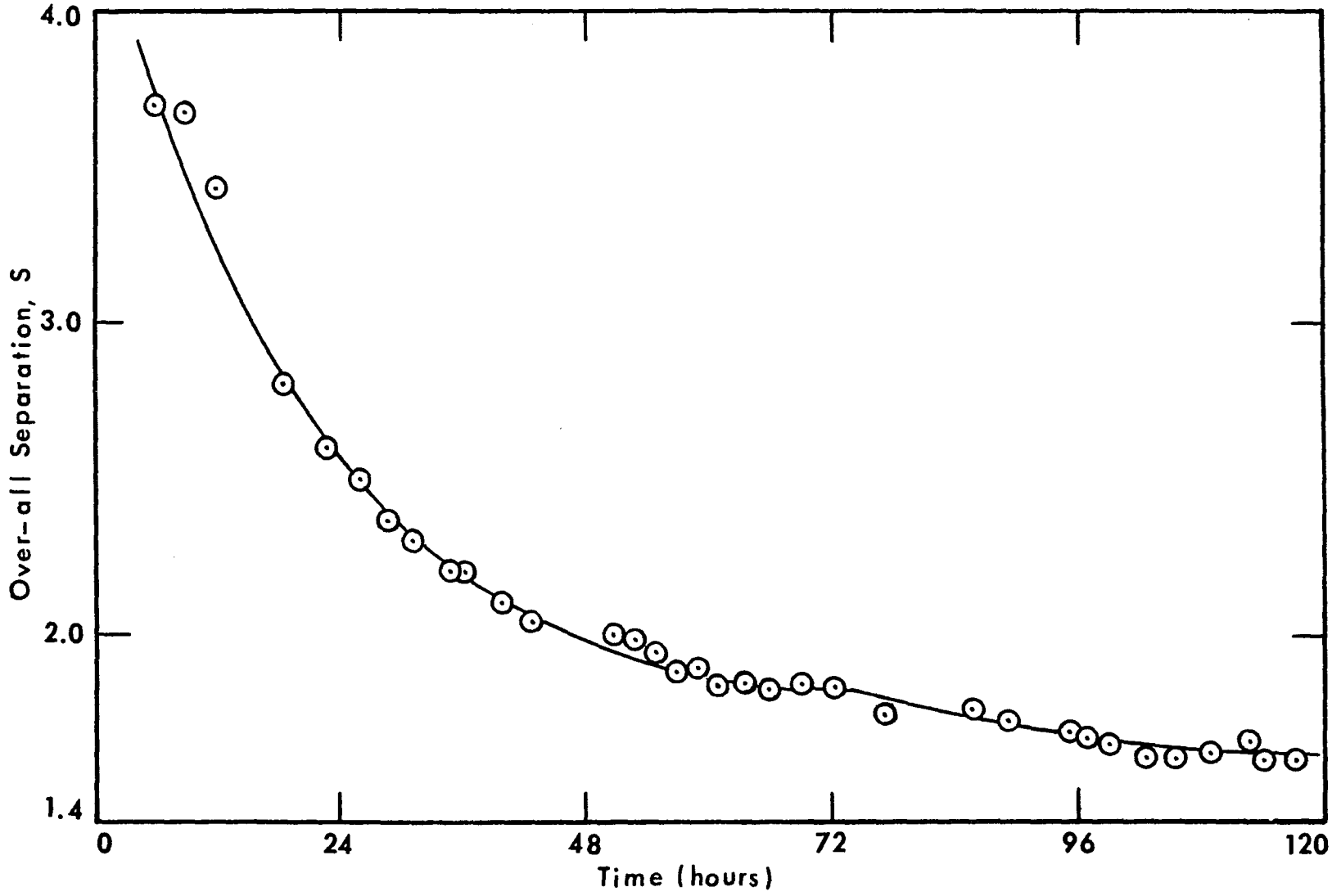

Figure 27: Overall Separation as a Function of Time: T = +14.0°C, P = 1 atm [Run 7B, a Continuation of Run 7A (cf: Figure 23)]

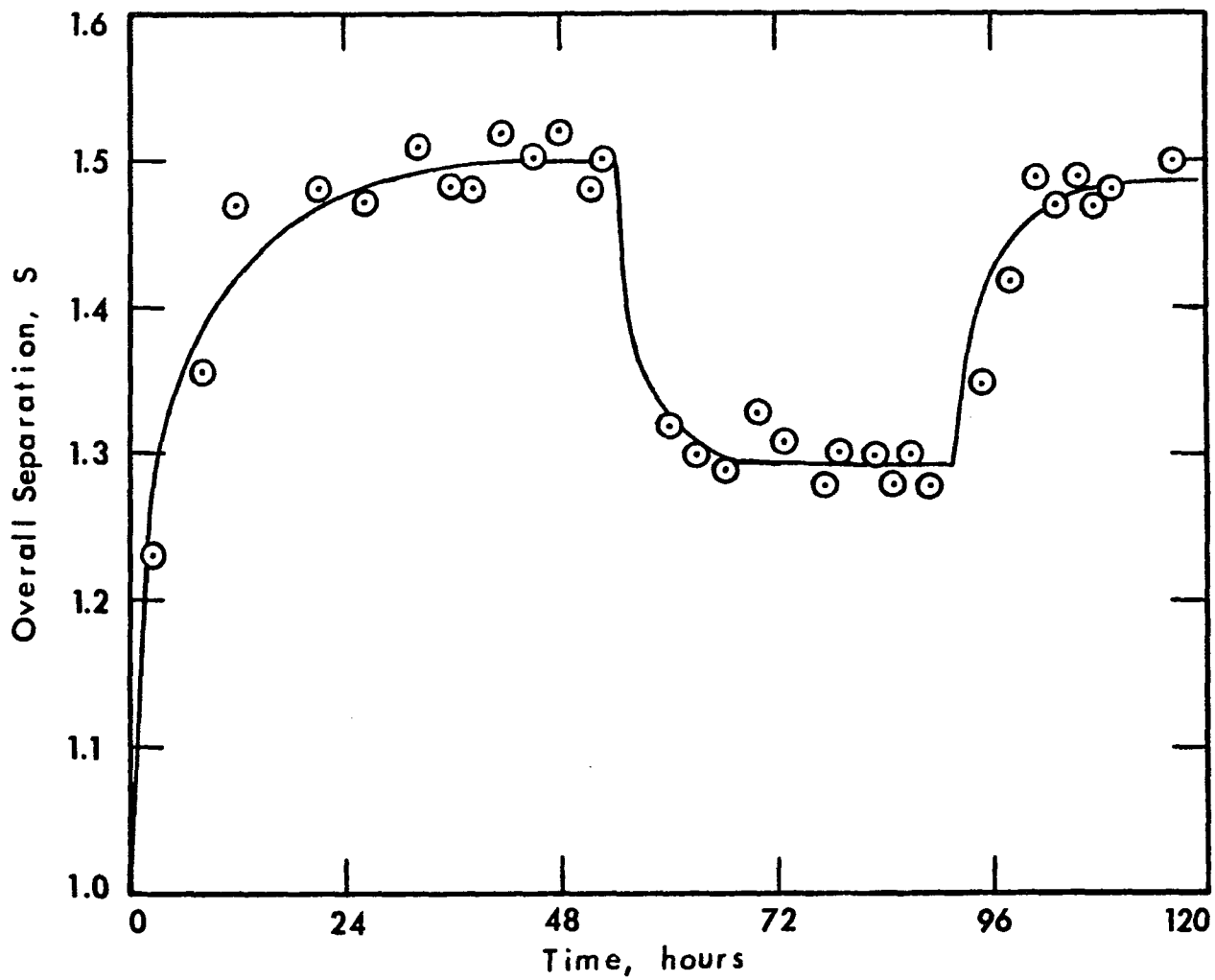

Figure 28: Overall Separation as a Function of Time: T = +15.5°C, P = 1 atm [Run 10A]

quantity upon which α is most strongly dependent. The two values for S_o in Run 10A are within 1.4% of each other.

Figures 29-36 show the overall separation as a function of time for the pressurized Runs 10B, 10C, 11, 12A, 12B, 14, 15, and 16, respectively. Runs 10B (1.5 atm, 15.5°C), 10C (2.0 atm, 15.5°C), and 12B (2.0 atm, 20.0°C) do not begin at S=1 because they are continuations of other runs. A run was attempted at 1 atm and 20.0°C, but was unsuccessful because the amount of NO in the gas phase under these conditions was almost nonexistent, causing difficulties in the operation of the refluxer system as well as obtaining meaningful data from such low values of S_o and S_p.

Table V contains the summary of the data obtained from the exchange column experiments using the methodology outlined in Chapter V.

VIB. Results of Phase Composition Analysis

Table VI contains the summary of results obtained from the spectrophotometric determination of the gas phase composition. The mole fraction of +4 nitrogen in the liquid phase was calculated using Eq. (23). In Figure 37, a comparison of the results in Table VI is shown with extrapolated values of Purcell and Cheeseman,[25] and Beattie and Vosper[27] as a function of temperature at one atm. Figure 38 shows the comparison as a function of pressure at T = 15°C. It should be noted that at low temperatures and high pressures (below -5°C at 1 atm, or above 3 atm at 15°C) x and y become relatively insensitive to changes in these two parameters.

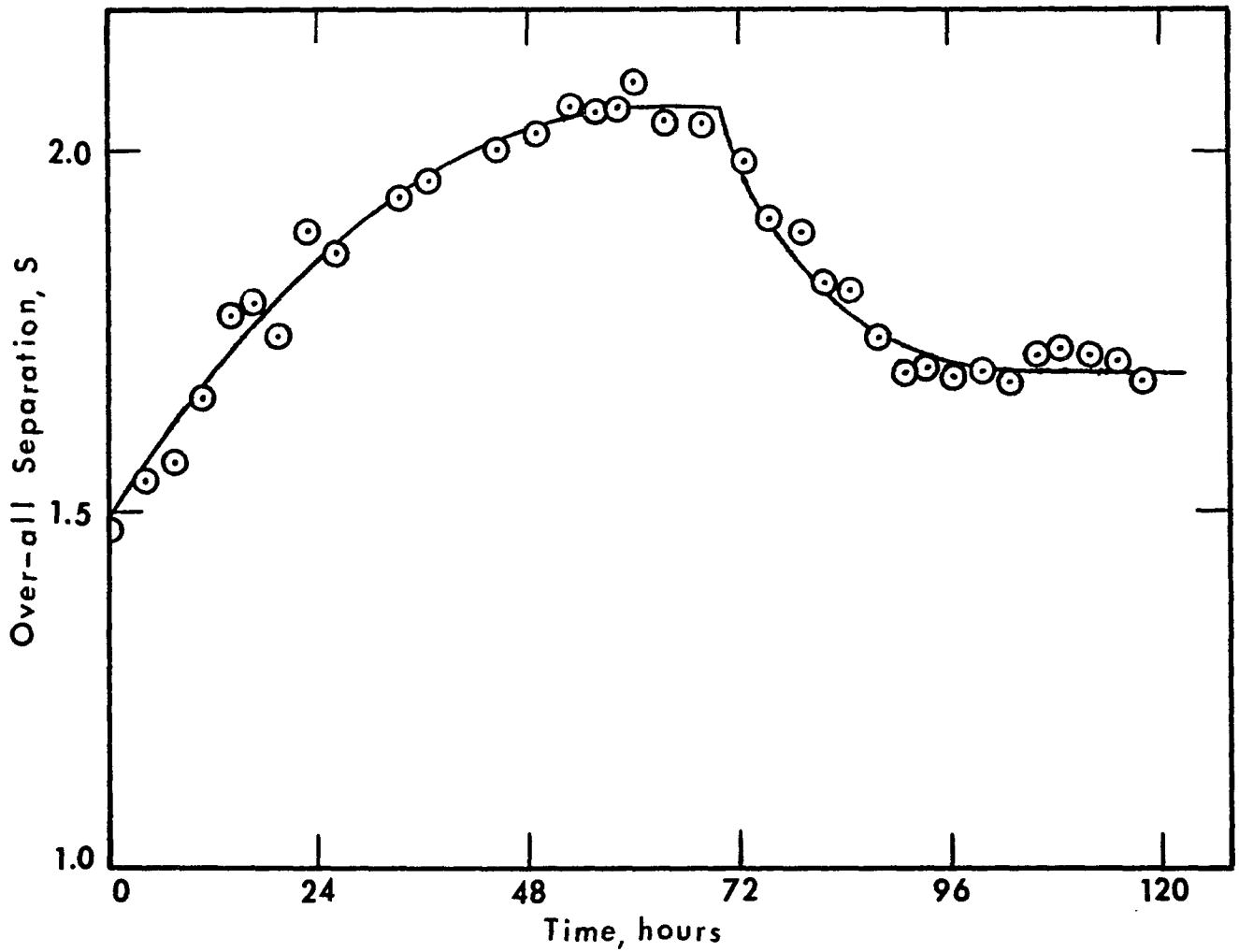

Figure 29: Overall Separation as a Function of Time: T = 15.5°C, P = 1.5 atm
[Run 10B, a Continuation of Run 10A (cf: Figure 28)]

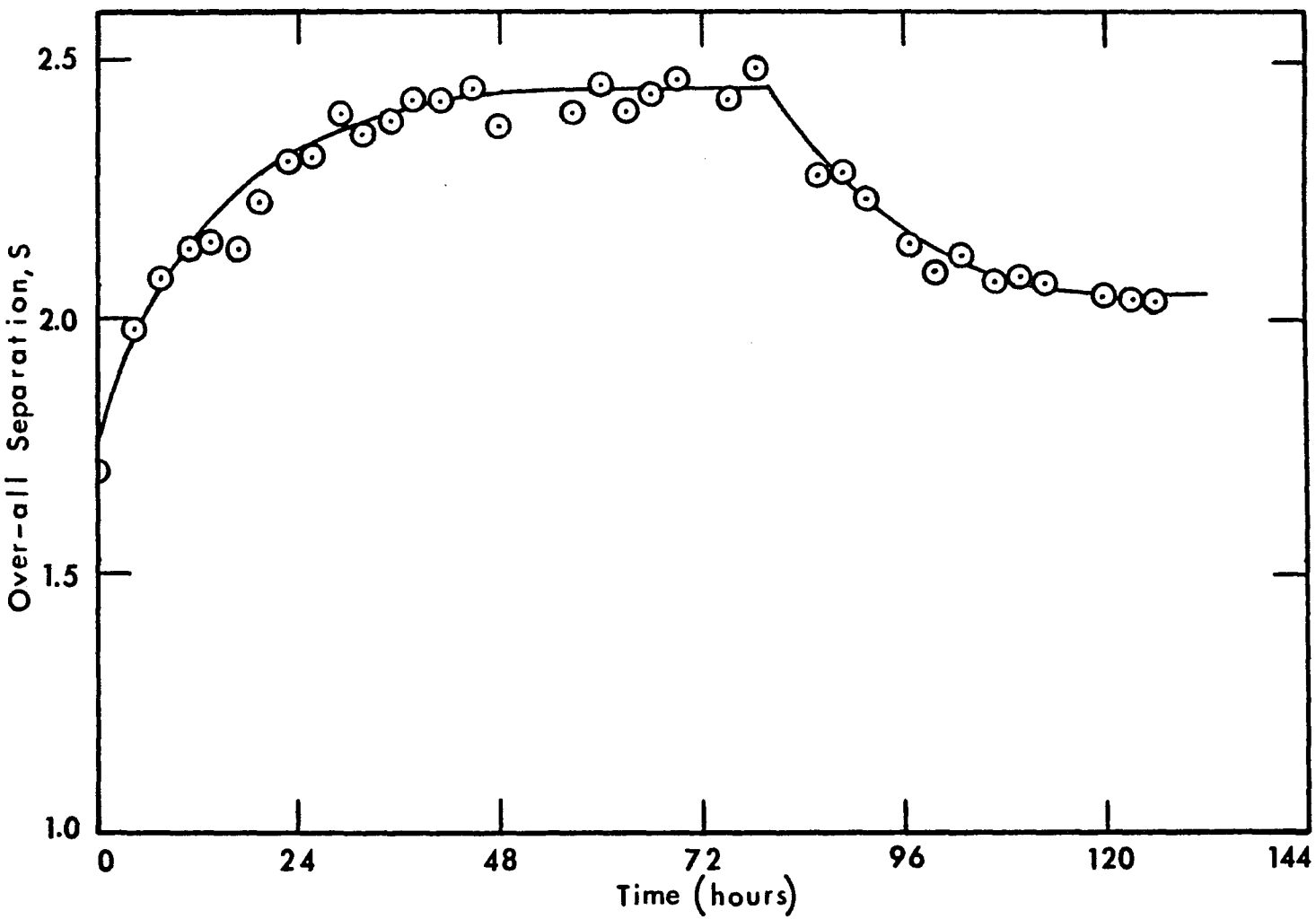

Figure 30: Overall Separation as a Function of Time: T = +15.5°C, P = 2.0 atm
[Run 10C, a Continuation of Run 10B (cf: Figure 29)]

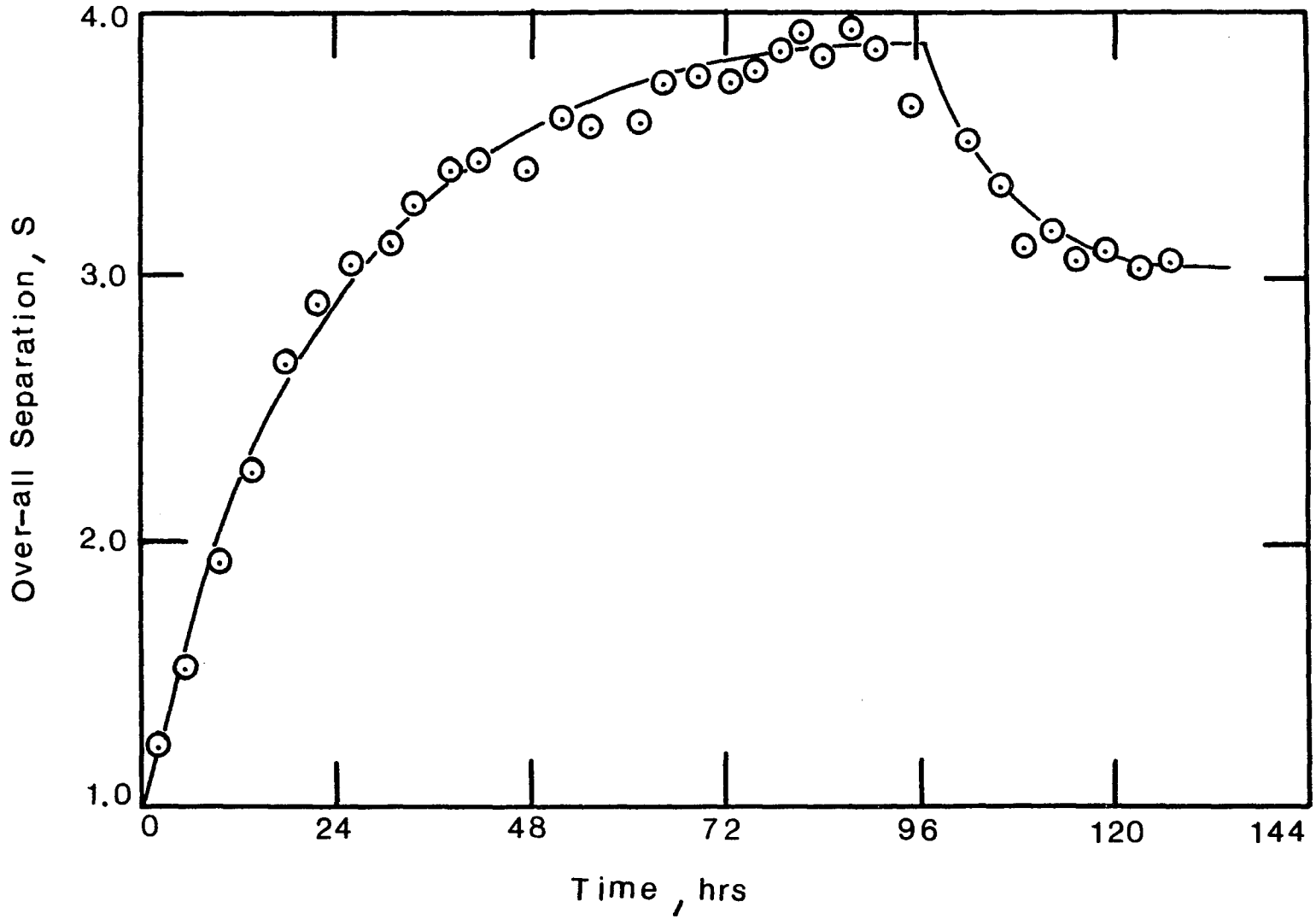

Figure 31: Overall Separation as a Function of Time: T = -4.0°C, P = 1.6 atm [Run 11]

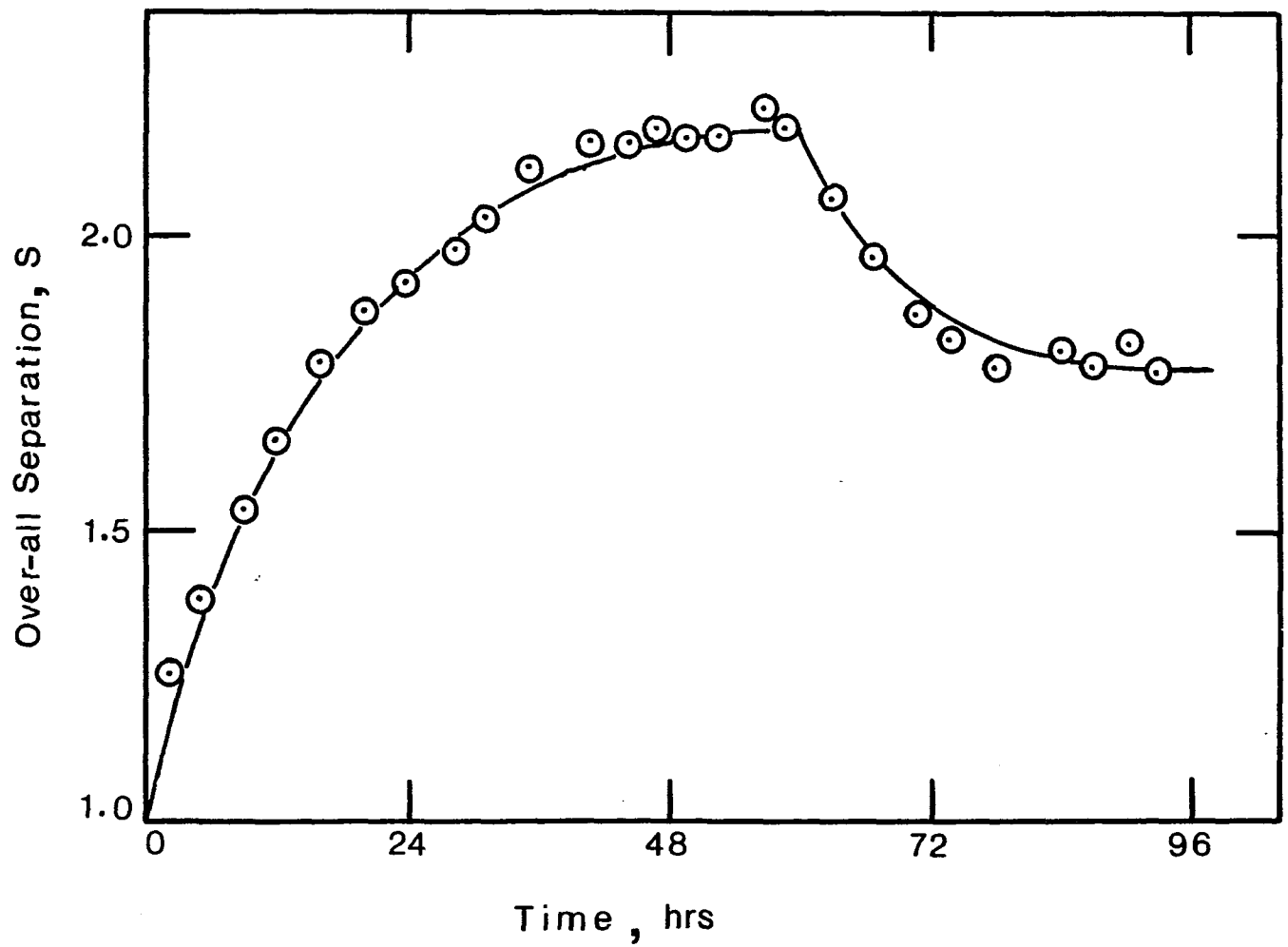

Figure 32: Overall Separation as a Function of Time: T = 20.0°C, P = 1.5 atm [Run 12A]

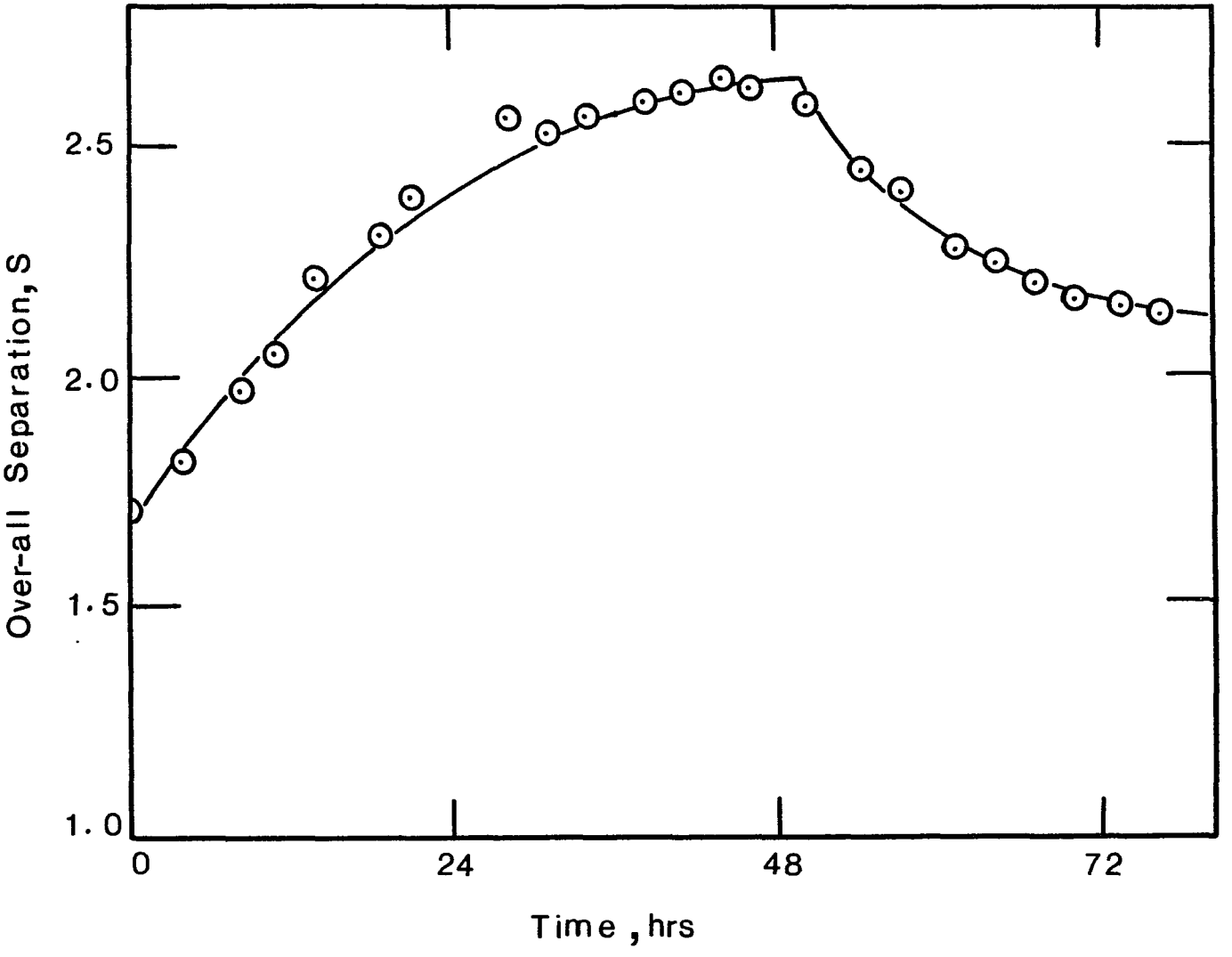

Figure 33: Overall Separation as a Function of Time: T = 20.0°C, P = 2.0 atm
[Run 12B, a Continuation of Run 12A (cf: Figure 33)]

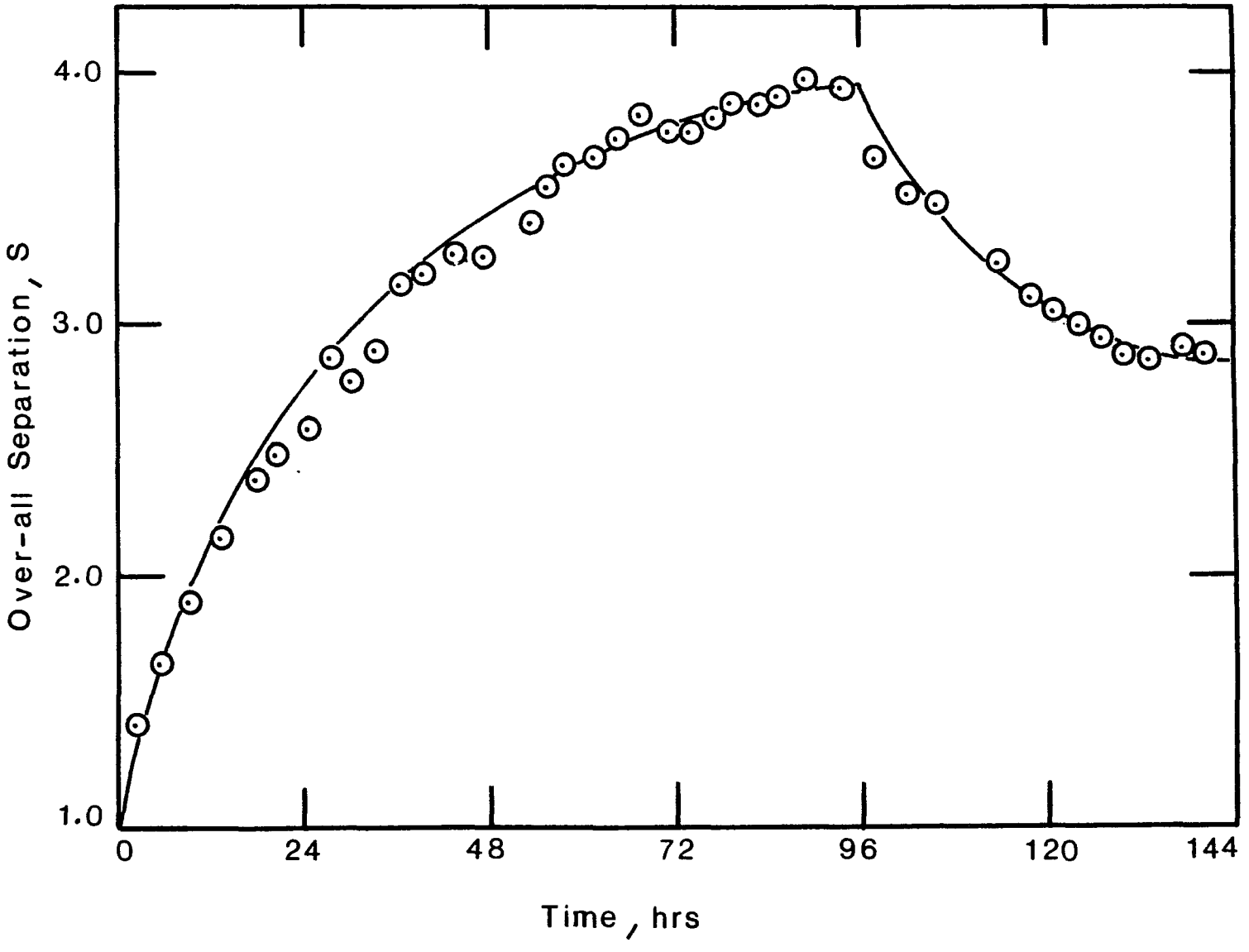

Figure 34: Overall Separation as a Function of Time: T = 15.0°C, P = 2.7 atm [Run 14]

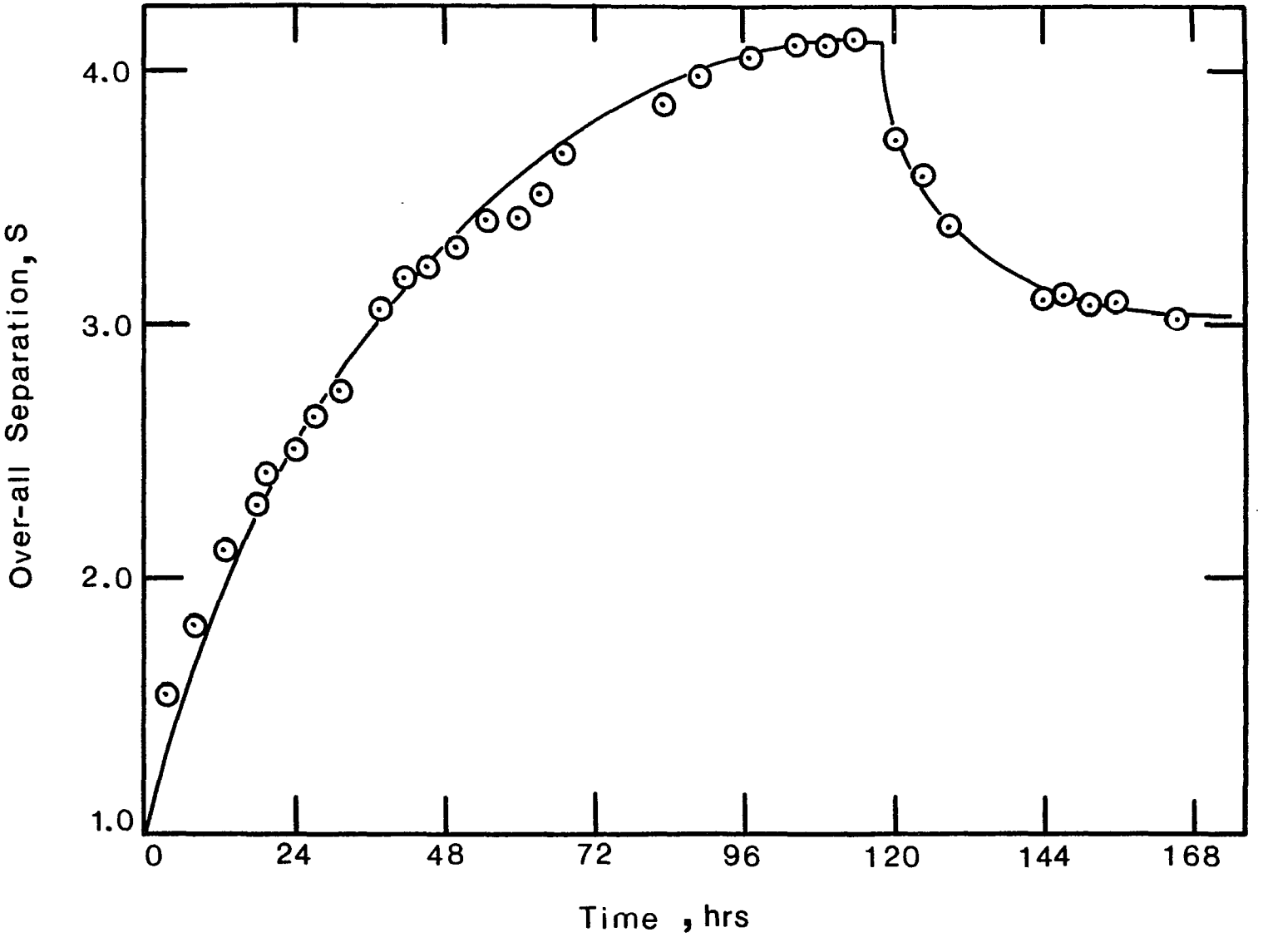

Figure 35: Overall Separation as a Function of Time: T = 14.5°C, P = 3.4 atm [Run 15]

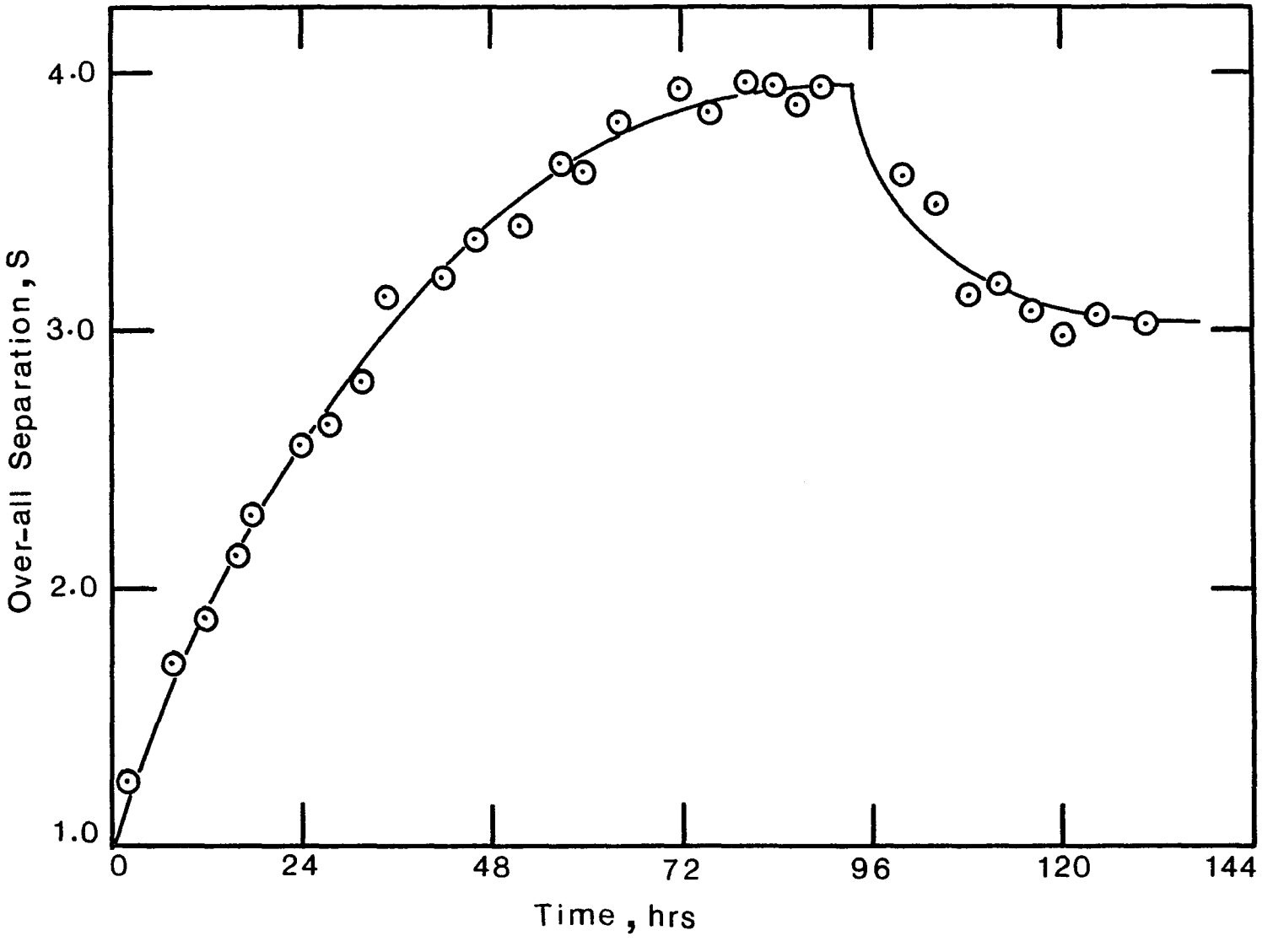

Figure 36: Overall Separation as a Function of Time: T = 15.0°C, P = 4.1 atm [Run 16]

Table V. Summary of Runs with Isotope Exchange Column[a]

Run No.	T °C	P_t atm	x[b]	d gms/ml	λ ml/min	L mmoles N/min	L/A mmoles N/min·cm^2	P, mmoles N/min	P/L, %	S_o	S_P	α	n	HETP, cm
12A	+20.0	1.5	.871	1.4380	0.840	27.5	14.6	.199	.72	2.19	1.71	1.009	87.5	0.57
12B	+20.0	2.0	.785	1.4320	0.773	26.0	13.8	.223	.86	2.64	2.12	1.020	49.0	1.02
10A	+15.5	1.0	.929	1.4508	0.785	25.4	13.5	.318	1.25	1.49	1.29	1.006	66.7	0.75
10B	+15.5	1.5	.818	1.4404	0.819	27.4	14.5	.251	.92	2.06	1.69	1.012	60.6	0.83
10C	+15.5	2.0	.739	1.4331	0.894	30.6	16.2	.251	.82	2.45	2.06	1.021	43.1	1.16
14	+15.0	2.7	.661	1.4260	0.552	19.4	10.3	.161	.83	3.90	2.83	1.030	46.0	1.09
15	+14.5	3.4	.612	1.4213	0.695	24.8	13.1	.179	.72	4.15	3.07	1.032	45.2	1.11
16	+15.0	4.1	.586	1.4187	0.913	32.9	17.4	.207	.63	3.98	3.05	1.030	46.7	1.07
7B	+14.0	1.0	.908	1.4514	0.565	18.4	9.8	.104	1.08	1.82	1.64	1.010	60.2	0.83
5	+5.0	1.0	.786	1.4472	0.730	24.8	35.0	.152	.61	7.04	3.40	1.020	98.6	1.01
8	-4.0	1.0	.677	1.4379	0.671	23.6	12.5			4.87		1.029	55.4	0.90
9	-4.0	1.0	.677	1.4379	0.976	34.4	18.2	.167	.49	4.40	3.40	1.029	51.8	0.97
11	-4.0	1.6	.591	1.4209	0.863	31.1	16.5	.173	.56	3.90	3.05	1.028	49.3	1.01
7A	-9.0	1.0	.627	1.4389	0.664	23.9	12.7	.102	.43	5.70	4.30	1.036	49.2	1.02

[a]All runs except Run No. 5 were carried out using an exchange column (50 cm long x 1.55 cm I.D.) packed with Podbielniak SS Helipack No. 3013. For Run 5 a narrower and longer exchange column (100 cm long x .95 cm I.D.) was used. The table headings are T = temperature, P_t = total pressure, x = mole fraction of +4 nitrogen in liquid phase, d = density of the N_2O_3/N_2O_4 liquid mixture, λ = liquid flow rate, L = interstage flow rate, L/A = linear flow rate, A = cross-sectional area of exchange column, P = product withdrawal rate, S_o = overall separation at total reflux, S_P = overall separation at the product withdrawal rate P, α = effective unit stage separation factor, n = number of theoretical plates, HETP = height equivalent of a theoretical plate.

[b]Calculated from Eq. (23) (Ref. 27).

Table VI. Summary of Results of Gas and Liquid Chemical Phase Composition[a]

Run No.	K_1 atm	K_2 atm	P_{NO} atm	P_{NO_2} atm	$P_{N_2O_3}$ atm	$P_{N_2O_4}$ atm	y_{NO}	y_{NO_2}	$y_{N_2O_3}$	$y_{N_2O_4}$	x	y
12B	.0876	.894	1.432	0.153	0.244	0.266	0.550	0.059	0.188	0.204	0.77	0.36
10A	.0541	.538	0.282	0.165	0.086	0.502	0.174	0.102	0.106	0.618	0.91	0.77
10B	.0570	.604	0.778	0.149	0.192	0.388	0.373	0.071	0.184	0.372	0.80	0.53
10C	.0573	.665	1.360	0.125	0.255	0.271	0.536	0.049	0.201	0.214	0.73	0.36
14	.0595	.772	2.186	0.092	0.261	0.143	0.708	0.030	0.169	0.093	0.66	0.21
15	.0572	.784	2.914	0.078	0.292	0.107	0.769	0.021	0.154	0.057	0.61	0.15
16	.0586	.814	3.579	0.073	0.321	0.091	0.800	0.016	0.143	0.041	0.58	0.13
5	.0250	.413	0.647	0.066	0.103	0.173	0.511	0.052	0.163	0.274	0.79	0.41
9	.0106	.264	0.846	0.025	0.080	0.059	0.736	0.022	0.140	0.103	0.67	0.19
11	.0107	.261	1.370	0.028	0.144	0.071	0.750	0.015	0.158	0.077	0.59	0.17

[a] P_t is total pressure; K_1 and K_2 are the dissociation constants for N_2O_4 and N_2O_3, respectively; P_{NO}, P_{NO_2}, $P_{N_2O_3}$ and $P_{N_2O_4}$ are the partial pressures of the corresponding components; y_{NO}, y_{NO_2}, $y_{N_2O_3}$ and $y_{N_2O_4}$ are the mole fractions of nitrogen in the respective components of the gas phase; x and y are the mole fractions of +4 nitrogen in the liquid and gas phases, respectively.

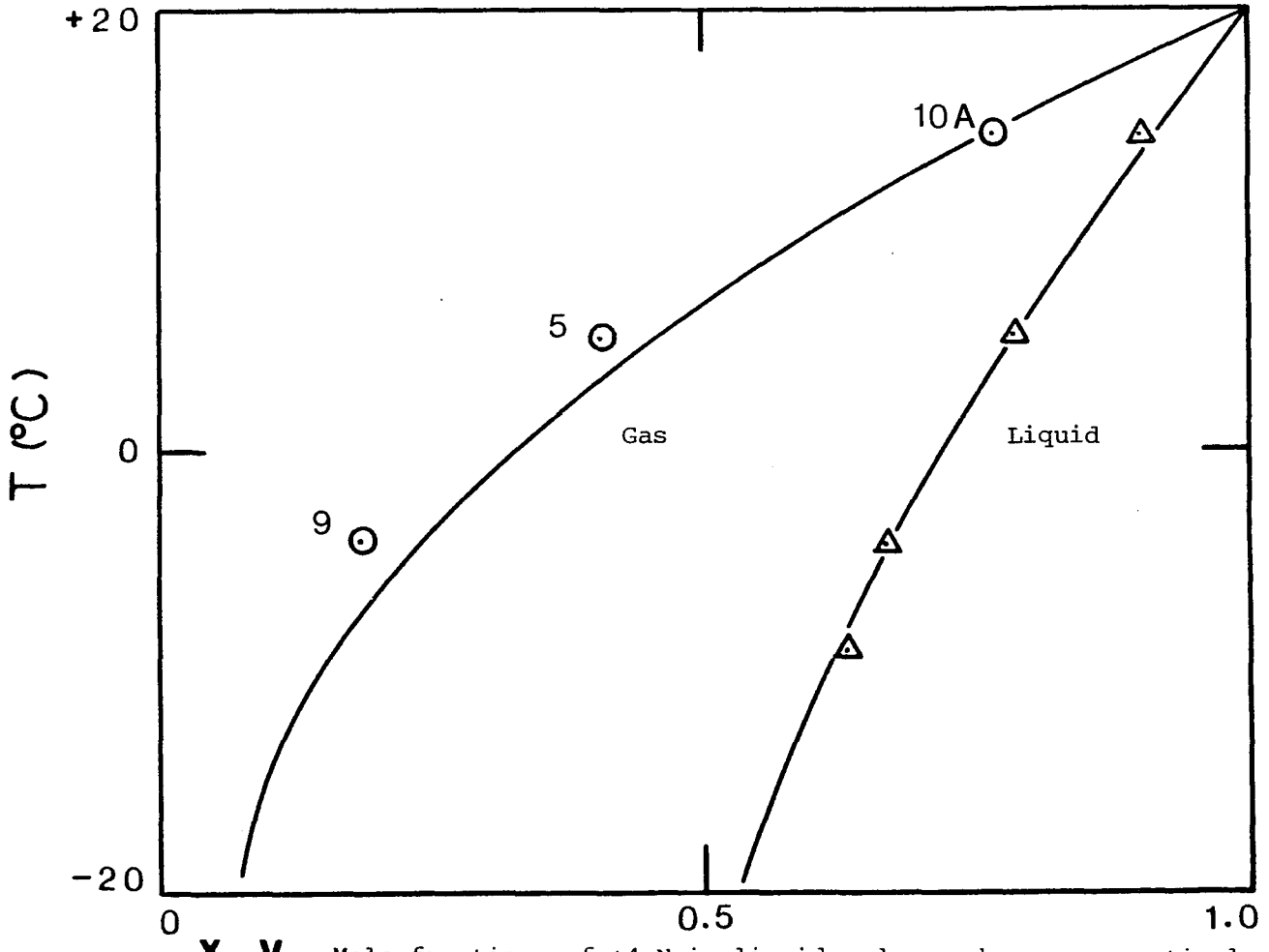

Figure 37: System $NO-NO_2$; (N_2O_4) at 1 atm pressure. (Alphanumerics represent run numbers).

⊙ Gas Phase Composition - Obtained from Spectrophotometric Measurements.

△ Liquid Phase Composition - Calculated from Eq. (23), Ref. 27.

Solid Curves - Extrapolated, Ref. 25.

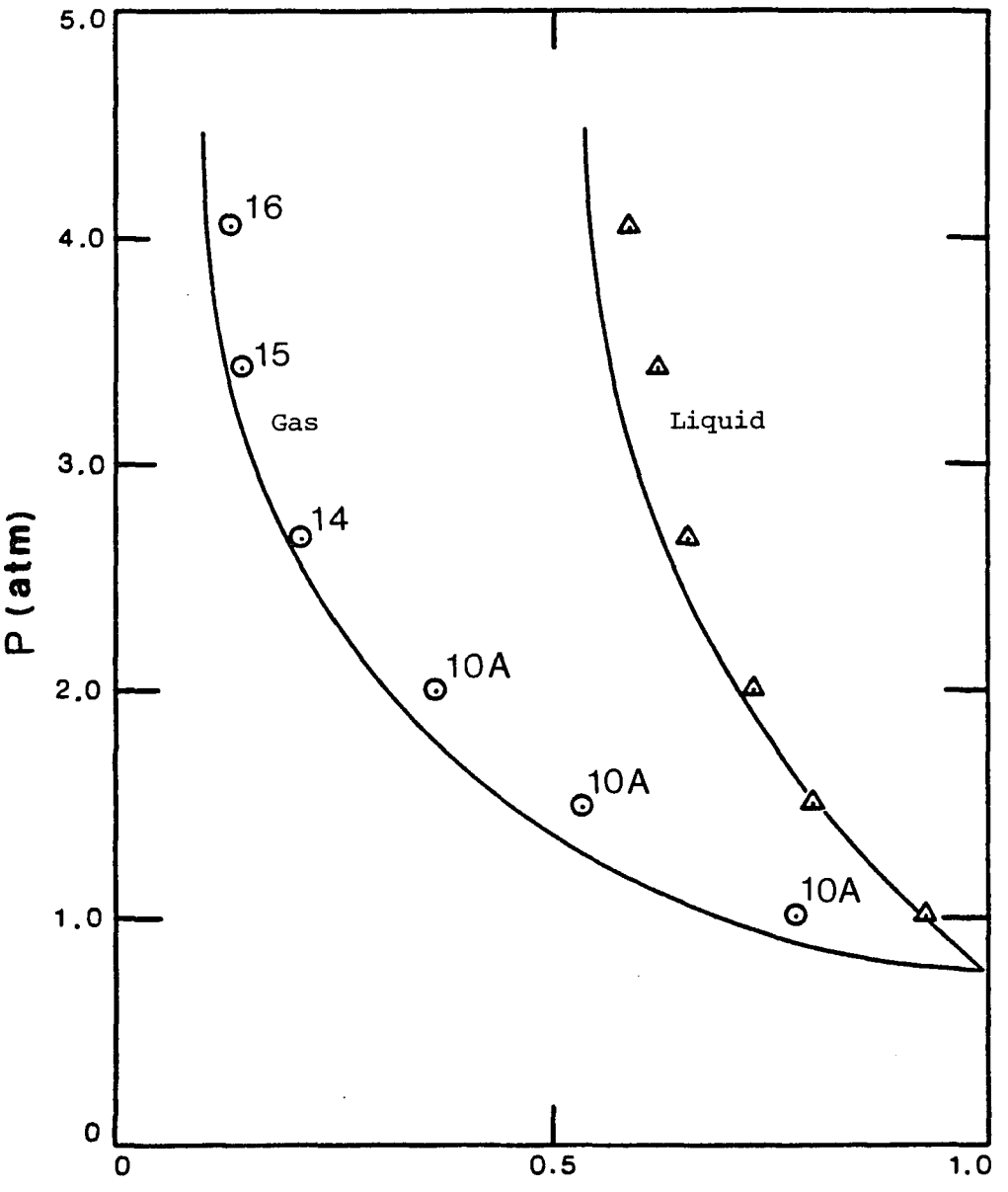

x, y - Mole Fraction of +4 Nitrogen in Liquid and Gas Phases, respectively.

Figure 38: System NO-NO_2; (N_2O_4) at temperatures near 15°C.

(Alphanumerics represent run numbers).

⊙ Gas Phase Composition - Obtained from Spectrophotometric Measurements.

△ Liquid Phase Composition - Calculated from Eq. (23), Ref. 27.

Solid Curve, Extrapolated Ref. 25.

VII. DISCUSSION

This chapter is comprised of two parts. Section VIIA deals with a discussion of the effects of various parameters on the results of the exchange column experiments and includes a section on the design of a multiunit cascade for the production of 99% N-15 which is based on the results of the present study. Section VIIB contains details of a vibrational analysis performed on the N_2O_3 and N_2O_4 molecules which is used in conjunction with the phase composition studies for the theoretical evaluation of the single stage separation factor. A comparison of experimental and theoretical α which leads to a discussion on the frequency assignments and molecular and intermolecular interactions is dealt with in Section VIIC of this Chapter.

VIIA. Parameters Which Influence the Performance of an Isotope Fractionating System

VIIA-1. Effect of Temperature

In the simplest isotope exchange system which consists of a one-component gas phase and a one-component liquid phase, both α and HETP increase with decreasing temperature if other factors such as the inter-stage flow rate and the column packing are unchanged. The separation factor increases with decreasing T simply because the isotope effect is a quantum mechanical one, which usually becomes more pronounced by lowering T. The HETP increases with decreasing temperature because both the reaction and diffusion rates decrease with T.

In the case of the present N_2O_3 system, changing the temperature also affects the phase compositions and, in particular, the composition of the gas phase. At atmospheric pressure, decreasing the temperature results in a reduction in the ratio of +4 to +2 nitrogen in the gas

phase relative to the liquid (Table VI and Figure 37). This phenomenon, in turn, causes the effective single stage separation factor to increase because the reduced partition function ratio (Eq. (5)) is smaller for NO (+2 nitrogen) than for any other oxides of nitrogen.[10] The quantitative relationships between α and T found in the present column exchange experiments as well as Monse's column and single stage results[5] are shown in Figure 39. The present results fall between the single stage equilibration data and the column experiment data, but the temperature dependence of our results is greater than theirs.

A plot of HETP vs T at P=1 atm and a liquid interstage flow rate of approximately 13 mmoles $N/cm^2 \cdot min$ is offered in Figure 40. The results indicate that the overall exchange rate increases with T as expected.

Although the increase in both α and HETP with decreasing T (Figures 39 and 40) has an opposing effect on the fractionation of isotopes, the overall separation at steady state under total reflux for runs at 1 atm increases with decreasing temperature (Table V). Apparently, the increase in α more than compensates for any decrease in the overall exchange rate.

VIIA-2. Effect of Pressure

In the N_2O_3 exchange system, a decrease in the +4 to +2 ratio of the gas phase compared to that of the liquid at near-ambient temperatures can be implemented by increasing the partial pressure of nitric oxide,[9,10] and this effect is in fact observed in the present experiments (Table VI and Figure 38). Accordingly, the single stage separation factor increases. Figure 41 offers a quantitative

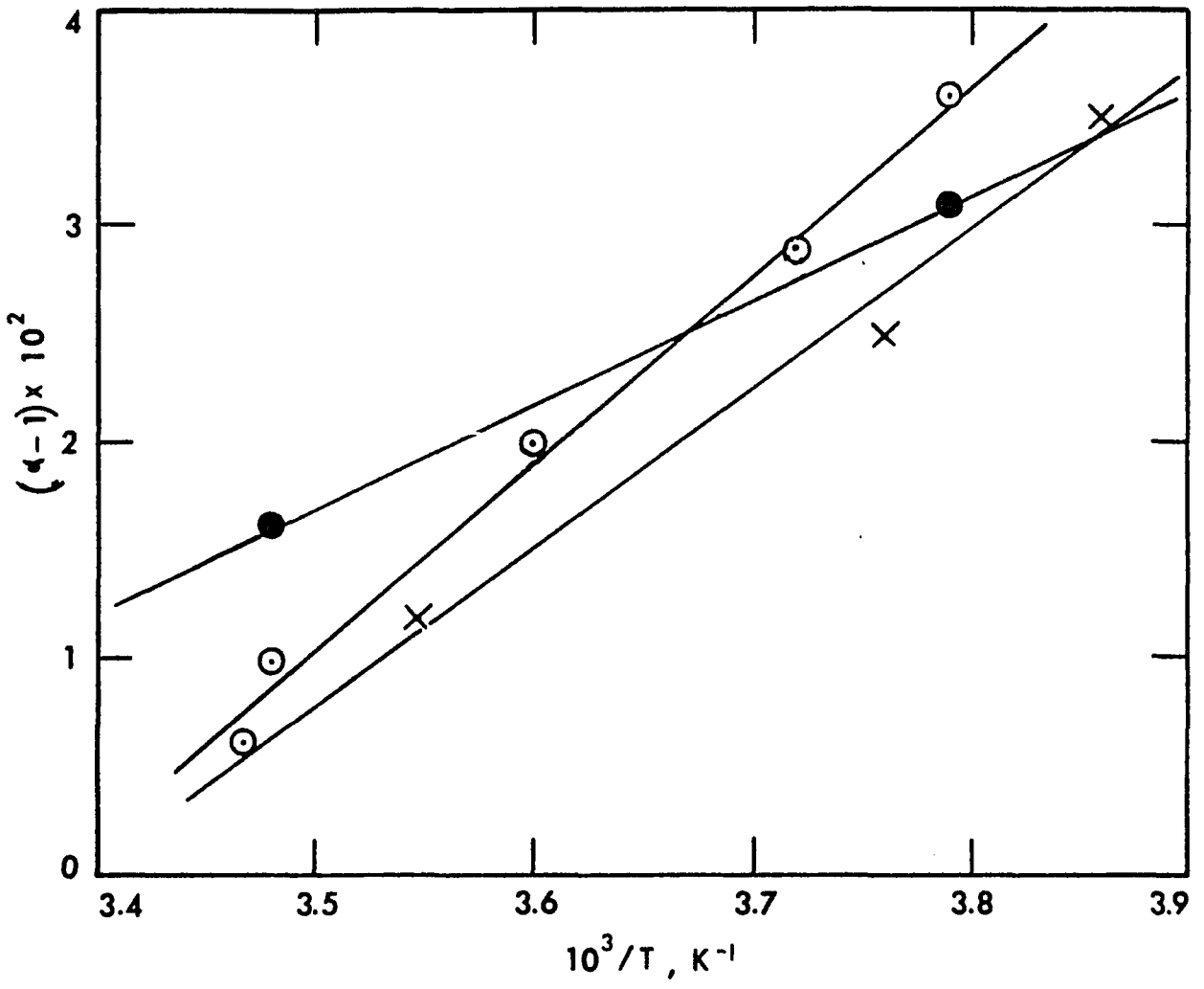

Figure 39: Single Stage Separation Factor vs 1/T, K^{-1}at Atmospheric Pressure

⊙ Present Results

✕ Monse et al., Single Stage Equilibration Data (Ref. 5)

● Monse et al., Column Experiments (Ref. 5)

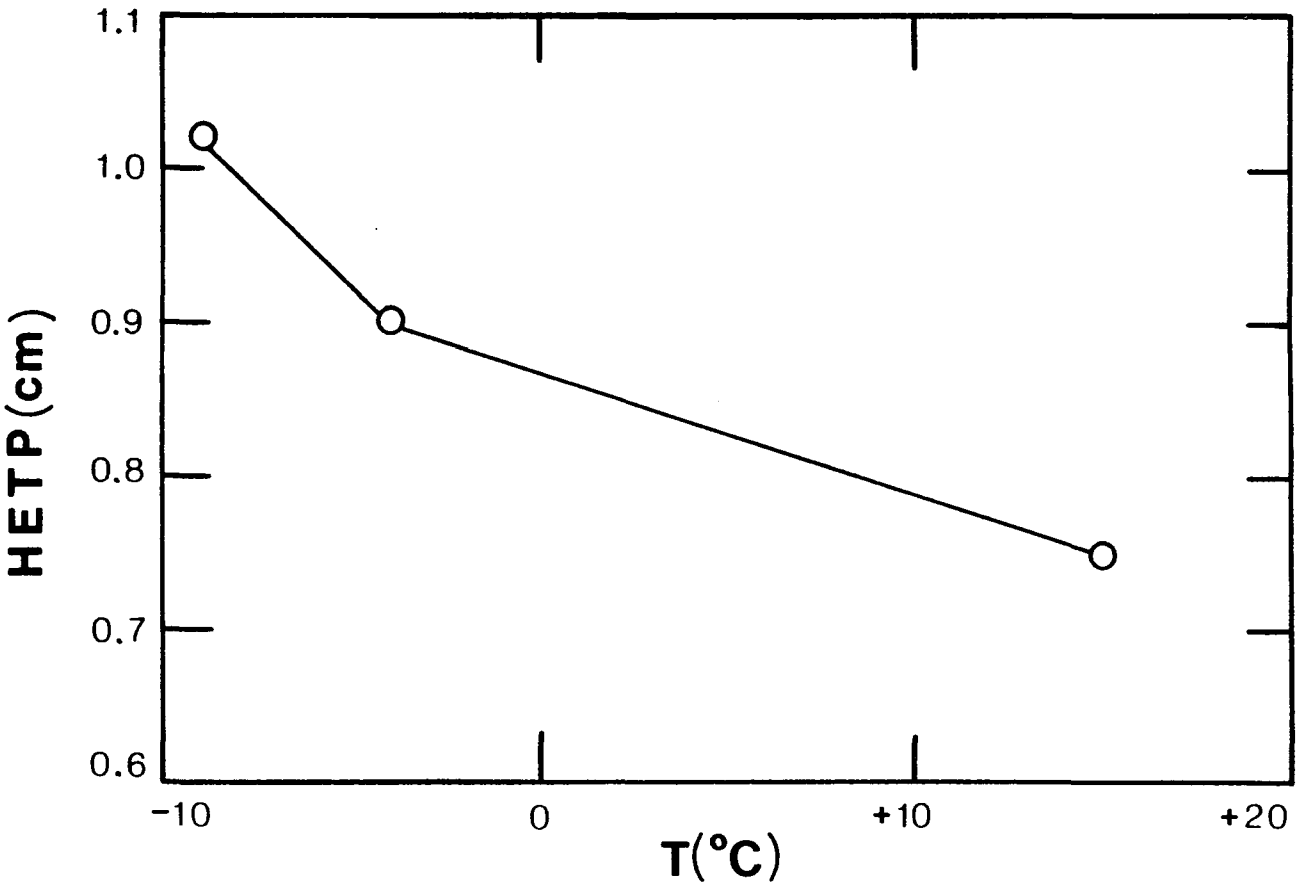

Figure 40. HETP as a function of Temperature at One Atm (L∿13 mmoles N/min)

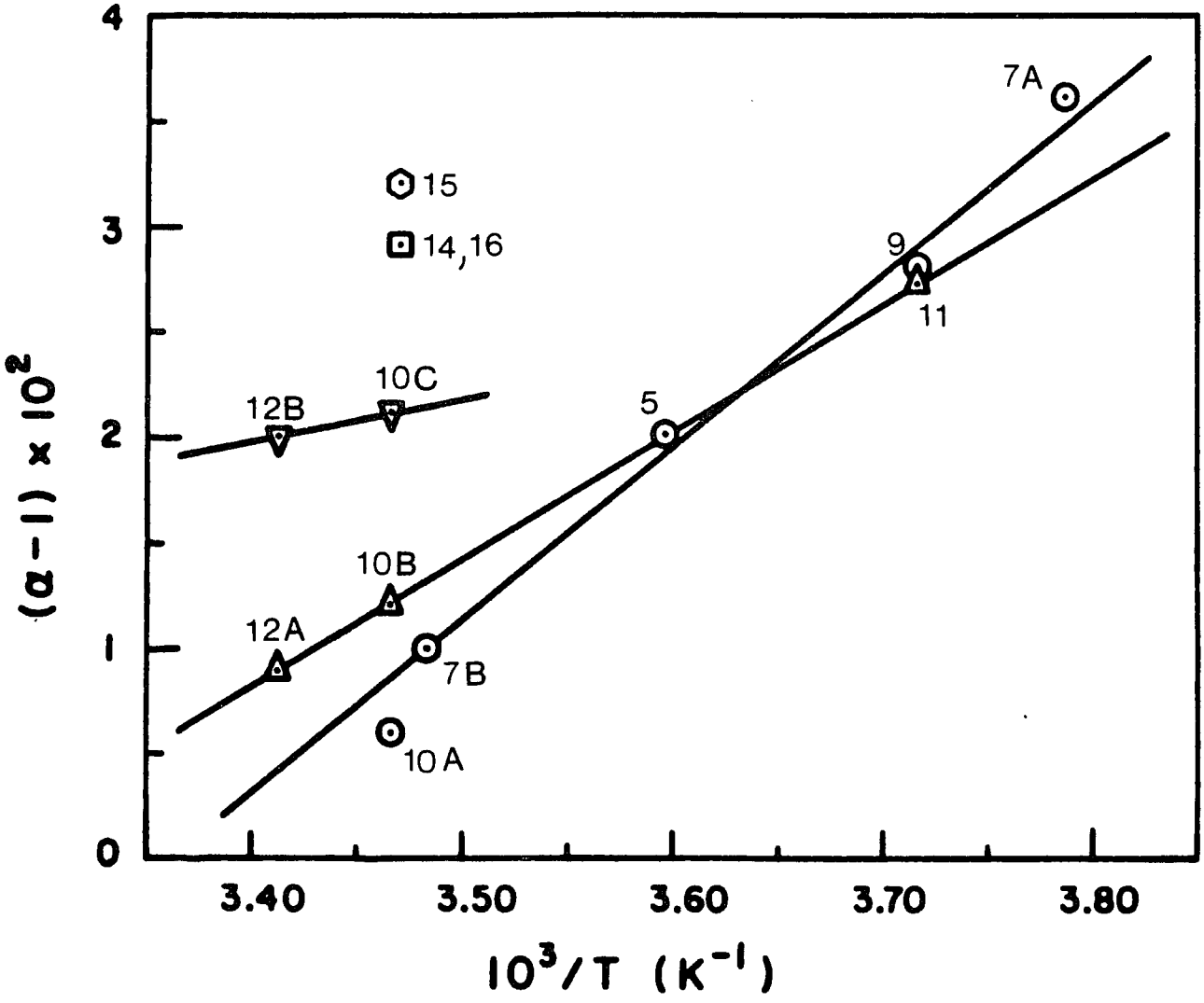

Figure 41: Effective Separation Factor vs 1/T, K^{-1}.

Runs Performed at:

- ⊙ Atmospheric Pressure
- △ 1.5 atm
- ▽ 2.0 atm
- ⊡ 2.7 and 4.1 atm
- ⬡ 3.4 atm

comparison of α as a function of 1/T at several pressures. The results point out the increase in α with increasing pressure, with values near-ambient temperatures approaching those obtained at -4.0°C and -9.0°C.

Figure 42 shows α as a function of +4 nitrogen in the gas phase, regardless of the temperature and pressure imposed on the system. The high correlation of the experimental points seems to indicate that within the T and P range studied, the increase in the separation factor is mainly due to changes in the phase composition, rather than any variations in the quantum mechanical distribution of isotopes amongst the exchanging chemical species, which is itself a function of temperature.

The height of an equivalent theoretical plate is plotted vs pressure at several temperatures in Figure 43. The results show that for runs performed at 15°C, HETP levels off beyond 3 atm after an initial steep rise. This effect is paralleled by changes in the chemical phase compositions (Figure 38). The mole fraction of +4 nitrogen in the gas phase, for example, decreases from 0.77 at 1 atm and 15°C to 0.13 at 4.1 atm (an 83% change), with the largest decrease occurring below 3 atm (75% out of a total 83%). For Runs 9 and 11 (T=-4.0°C, L$\sim$17 mmoles $N/cm^2 \cdot min$) varying the pressure did not seem to induce a significant change in HETP. This is in accordance with the small decrease in y (only 10%) relative to an 83% total change which was possible by manipulation of T and P in our experiments.

Figure 44 shows HETP as a function of mole fraction of +4 nitrogen in the gas phase. The downward trend in HETP, and hence a more efficient overall rate of exchange, can be attributed to the catalytic effect of the tetravalent nitrogen, which undoubtedly acts as a key

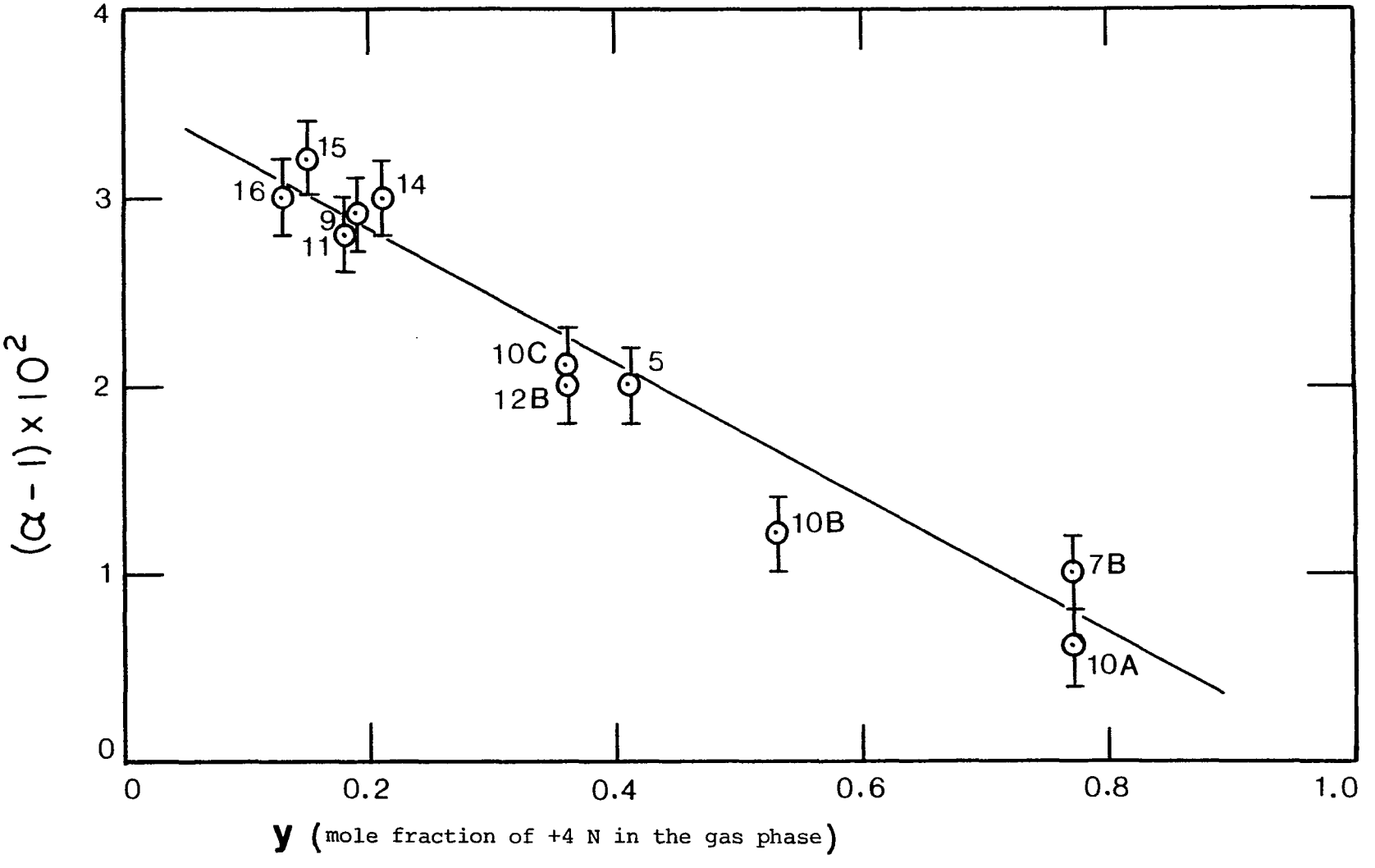

Figure 42. Effective Separation Factor, α, as a Function of Gas Phase Composition [Runs 7A and 12Anot included]

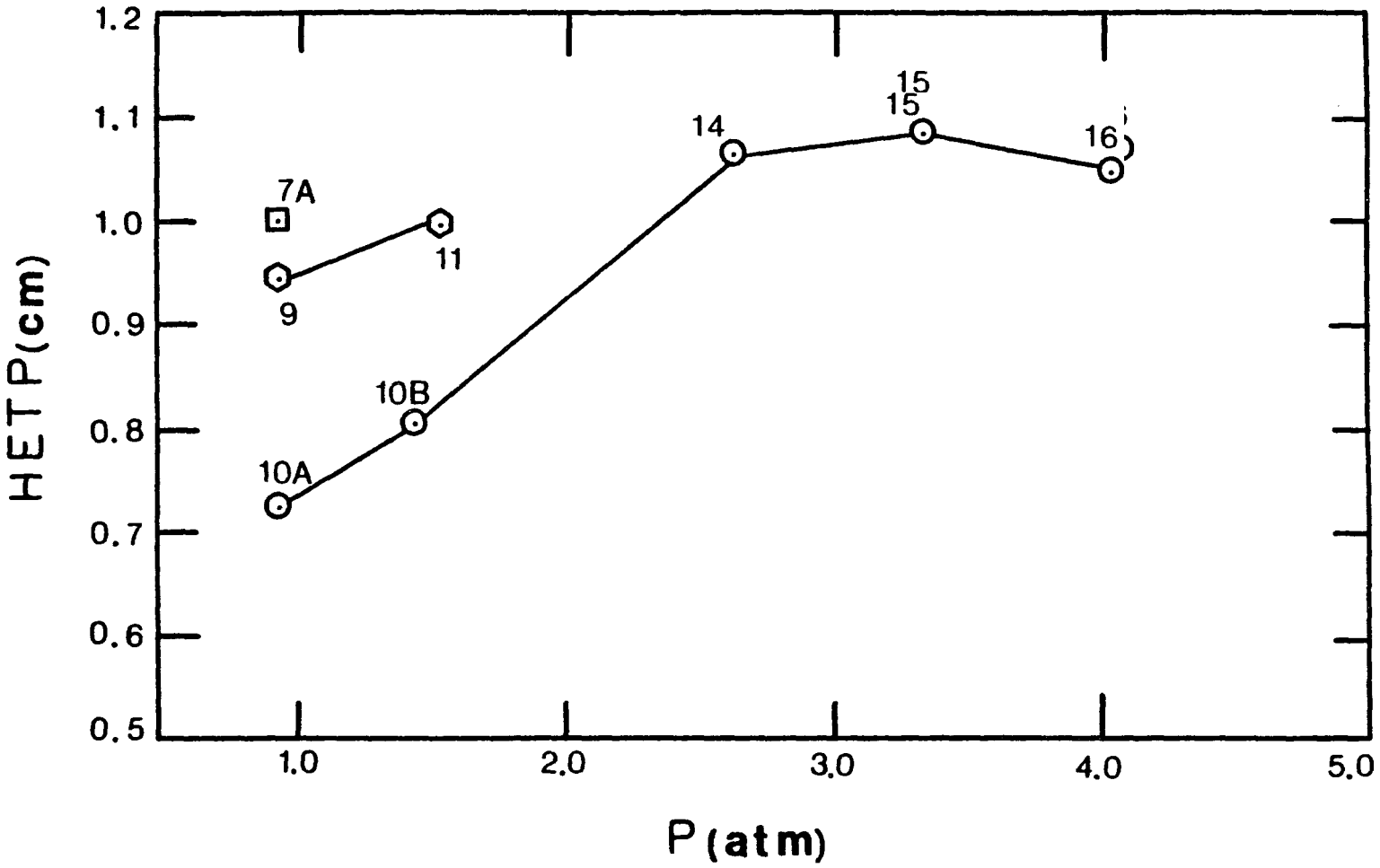

Figure 43: HETP as a Function of Pressure.

⊡ T = -9°C, Run 7A, L = 12.7 mmoles N/min·cm^2

⬡ T = -4°C, Runs 9, 11, L ∿ 17 mmoles N/min·cm^2

⊙ T = +15°C, Runs 10A, 10B, 14, 15, 16, L ranges from 10.3 to 17.4 mmoles N/min·cm^2

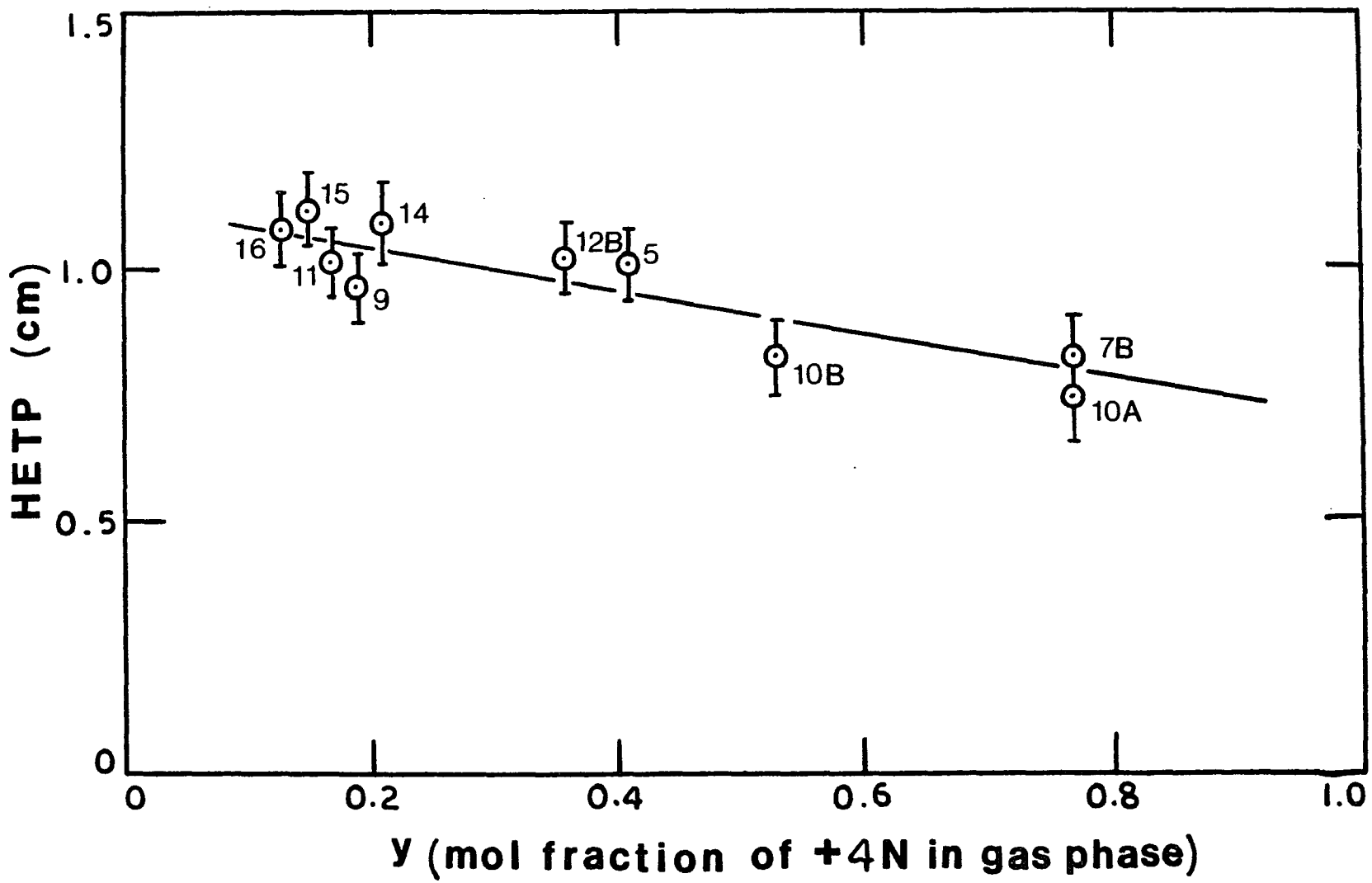

Figure 44: HETP as a Function of Gas Phase Composition

intermediate in the exchange process.[29]

Although an increase in pressure causes both an increase in α and HETP (Figs. 41 and 43), the resulting S_o is enhanced (Table V) so long as there are accompanying significant changes in the chemical phase compositions. As was the case with temperature, the larger α more than compensates for a lowering of the exchange rate. In fact the increase in S_o with P near ambient T results in a marked improvement on the fractionating power of the N_2O_3 system at those temperatures, i.e., +15°C and +20°C, as will be shown in Section VIIA-5.

VIIA-3. Effect of Flow Rate

In the ideal situation, HETP should be proportional to the interstage flow rate L and inversely proportional to the overall rate of isotope exchange, the latter consisting of the reaction rate and diffusion rate.[11] If this overall rate of exchange does not change, a plot of HETP vs L should be a straight line. However, within the flow rate range employed, HETP did not vary significantly for runs having about the same phase composition. For example, for Runs 14, 15, and 16, increasing the flow rate from 10.3 to 17.4 mmoles N/cm^2·min did not induce a corresponding increase in HETP (Fig. 43). The absence of influence of L on HETP, which has also been reported by other authors,[5] is neither due to changes in T nor to changes in the phase composition, and suggests that the exchange rate is increasing with L. This, in turn, implies that the process is diffusion controlled under the experimental conditions utilized in the present study. Another possibility is that, the linear liquid flow rates being so small (e.g., less than 0.5 cm/min; cf. Table V), significant back-mixing is playing a role in

the exchange column. In any event, what this result shows is that we can increase the flow rate considerably (hence increasing the throughput) without having to pay the price of a higher HETP.

VIII-4. Approach to Steady State

An important property of a system for separating isotopes is the rate of approach to equilibrium. In this type of experiment, it is desirable to minimize the initial start-up time before the product can be withdrawn to reduce the waste in time, chemicals and energy consumption. A comparison of the experimental behavior of the system with that predicted from theory can be employed to check or determine some of the important cascade constants influencing the approach to steady state, such as α, n, and the holdups of material in the exchange column and product refluxer. The measurement of the holdup is usually difficult to determine experimentally[50] and it was therefore evaluated by direct comparison with theory.

For a two phase countercurrent exchange system such as the one employed in the present experiment, the fundamental partial differential equation is obtained from consideration of the material balance and expresses the increase in the mole fraction of the desired isotope as a function of time of operation of a fractionating column at a given location along the column:[11]

$$\lambda_o \partial N/\partial t = \partial^2 N/\partial n^2 - (\alpha - 1)(1 + \psi)\ \partial N/\partial n\ , \qquad (39)$$

where N is the mole fraction of the desired isotope in the n_{th} stage at time t; λ_o is the processing time per stage, and is given by the holdup of the column per stage, H_s (mmoles N) divided by the liquid flow rate

L, and ψ is given by $P/L(\alpha-1)$. Cohen[11] solved the differential equation under the following conditions: 1) The value of α is close to unity, 2) The mole fraction of N-15 in the product is always small compared to 1, i.e. $Np<<1$, 3) The column is operated at total reflux, with the feed end being maintained at a constant mole fraction N_f of the desired isotope by supplying fresh material continuously.

For the boundary conditions mentioned above, the solution to Eq. (39) at $t>>\lambda_o n^2/10$ is of the form:

$$S_t = S_o - A(S_o-1)\exp(-Bt/\lambda_o n^2) \quad , \tag{40}$$

where S_t and S_o are the overall separations at time t and at equilibrium, respectively, when no product is withdrawn, and n is the number of stages in the fractionating column. The constants A and B are tabulated functions of $(\alpha-1)n$ and $K'/\lambda_o n$, where K' is the holdup, H_r, at the product end divided by L. Thus, $K'/\lambda_o n$ is the ratio of holdup at the product end of the column, H_r, to the total holdup in the column, H_c. This ratio is the quantity to be determined.

Equation (40) can be written as a linear function of time;

$$\ell n[(S_o-S_t)/(S_o-1)] = \ell nA - Bt/\lambda_o n^2 \quad , \tag{41}$$

where ℓnA is the intercept and $B/\lambda_o n^2$ is the slope. Such a plot is shown for Run 9 in Figure 45, where the holdup in the column is given by:

$$H_c = B \cdot L/n|\text{slope}| \quad . \tag{42}$$

Tables for the values of the functions A and B are given by Cohen[11] and were more finely mapped and extended to include larger values for

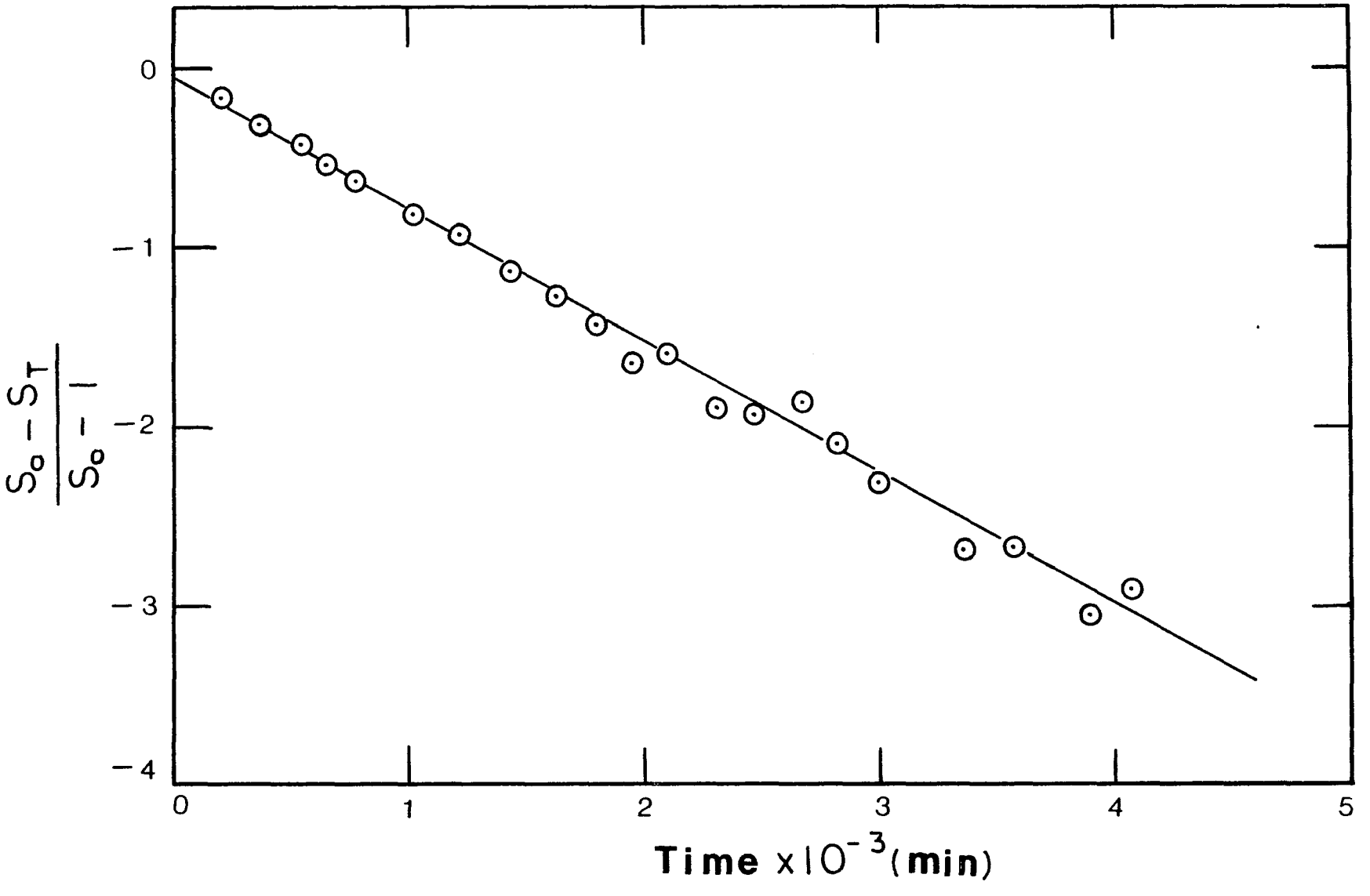

Figure 45. Determination of Hold-up in Exchange System for Run 9

$(\alpha-1)n$ by Wieck and Ishida.[72-73] B was obtained from the aforementioned tabulations for a given positive $(\alpha-1)n$ (an already known quantity) and for A, which was obtained as the intercept of Figure 45. A positive $(\alpha-1)n$ is used because the equations for determining the rate of approach to steady state are not symmetrical about $(\alpha-1)n=0$, and it is incorrect to analyze a stripper section, i.e., the column for which $(\alpha-1)n<0$, as if it were a rectifier, i.e., the column for which $(\alpha-1)n>0$.[11,73]

A comparison of the experimental results with the theoretical curves shown in Figure 46 indicates that $K'/\lambda_o n$ is 0.1. The above calculations were performed on the results of several other experiments, and Table VII contains a summary of column holdup measurements.

The approach to steady state with this column is fairly rapid because the ratio of the holdups is relatively small. The larger the ratio, the longer it will take the column to reach equilibrium. This is due to the fact that, for a large holdup in the refluxer, a large inventory of the desired isotope must be built at the product end. Without a constant mole fraction of the desired component at both ends of the column, steady state cannot be achieved. When the desired isotope, which is the minor component, enriches in the liquid phase, the material holdup in the refluxer is necessarily large. If the desired component enriches in the gas phase (inverse isotope effect) the holdup could be made very small, and the column would require a much shorter start-up period.

The approach to steady state for Run 5, which was performed with the narrower and longer column (0.95 cm I.D., 100 cm in length) was slower than expected because of the larger number of plates.

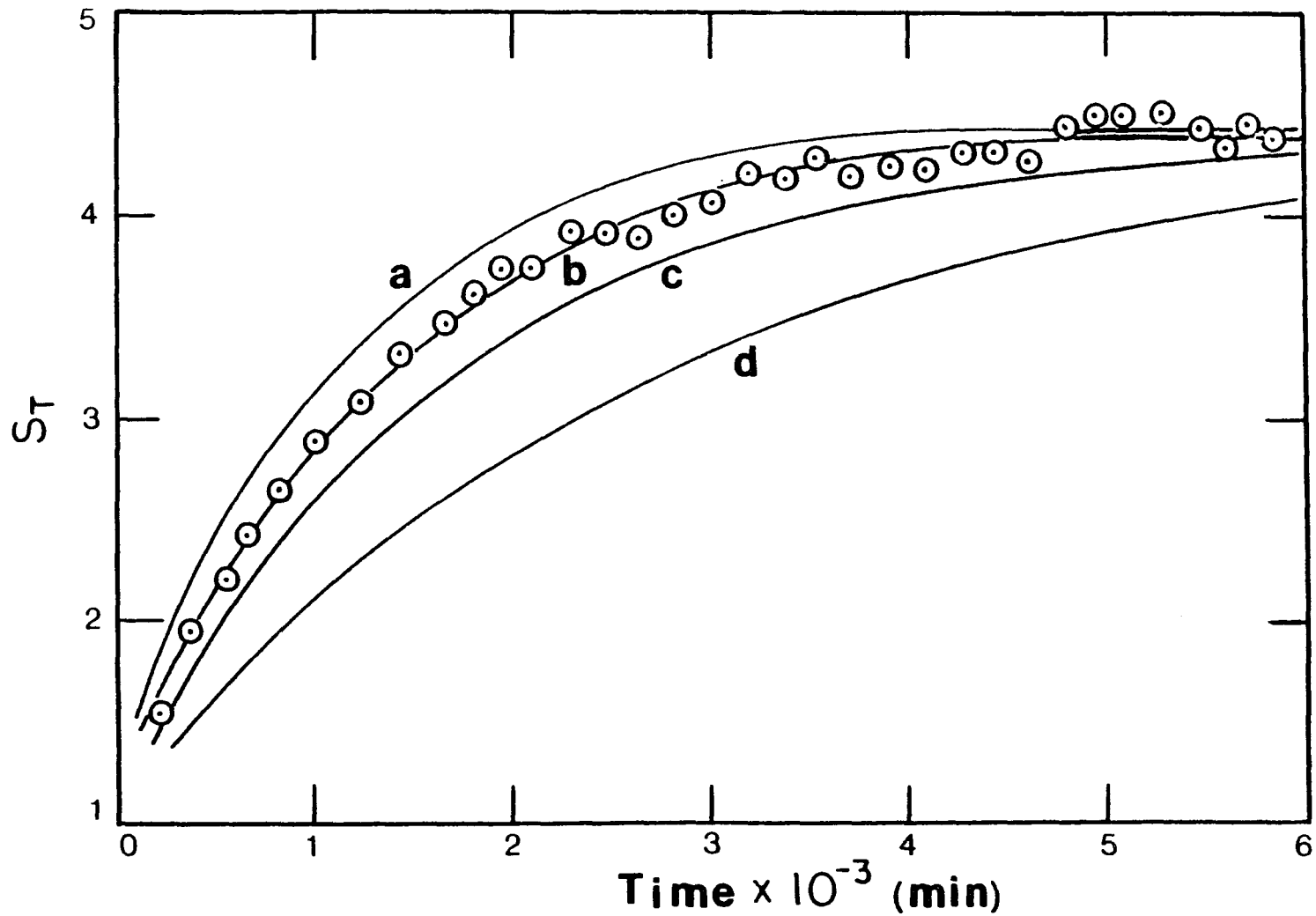

Figure 46. Effect of Hold-up in the Exchange System on the Approach to Steady State for Run 9.

a) $K'/\lambda_o n = 0$, b) $K'/\lambda_o n = 0.1$, c) $K'/\lambda_o n = 0.2$, d) $K'/\lambda_o n = 0.5$

Table VII. Summary of Column Hold-up Measurements

Run	T	P	α	n	L	H_r	H_c	$K'/\lambda_o n$
	°C	atm			mmoles N /min	mmoles N		
9	-4	1.0	1.029	51.8	34.4	87	870	0.10
11	-4	1.6	1.028	49.3	31.1	180	710	0.25
12A	+20	1.5	1.009	87.5	27.5	26	510	0.05
14	+15	2.7	1.030	46.0	19.4	49	930	0.05
15	+15	3.4	1.032	45.2	24.8	77	1,600	0.05
16	+15	4.1	1.030	46.7	32.9	260	1,300	0.20

Unfortunately, even the experiments with the shorter column having a larger I.D. were rather long because after an initial steep rise, the approach to equilibrium is very slow. This is compounded by the uncertainty in the overall separation caused mostly by experimental fluctuations in L, which are of the order of 5%. Hence the determination of the equilibrium values for S_o and S_p required a large number of points, even after the experimental steady state had been reached for quite some time.

VIIA-5. Comparison of the N_2O_3 Process Under Different Experimental Conditions

Chemical exchange of N-15 between NO and N_2O_3 has been proven to be a particularly efficient and economical process for concentrating nitrogen isotopes because of the favorable separation factor, the rapid exchange rate, and the inexpensive chemicals used for refluxing at both ends of the system.[5] It therefore seems worthwhile to compare the characteristics of this process in the light of the new experimental data.

Significant comparative data on the N_2O_3 process for different experimental conditions are summarized in Table VIII. For comparison purposes, the operating requirements for production of 1 gm per day of 99% N-15 were calculated. A square cascade consisting of a single exchange column packed with stainless steel helices (Helipack) was assumed. The term square cascade is used to describe a number of stages connected in series for which the liquid and gaseous flow rates (L and ℓ) do not vary with stage number. The minimum number of stages, $n_{(min)}$, and the liquid flow rate, $L_{(min)}$, were calculated from the

Table VIII. Comparison of Operating Conditions as Bases for Producing 1g/day of 99% N-15: S_0=27,020

		7A	10A	15	16	12B
1	Operating temp., °C	-9	+15	+15	+15	+20
2	Operating press, atm	1.0	1.0	3.4	4.1	2.0
3	α_{eff}	1.036	1.006	1.032	1.030	1.020
4	Min. no. of stages, n_{min}	289	1,706	324	345	515
5	Min. liq. interstage flow, L_{min} (mmoles N/min)	361	2,105	405	431	640
6	Min. reflux ratio, $(L/P)_{min}$	7,805	45,500	8,747	9,312	13,832
7	Interstage flow per unit area (mmole N/cm^2·min)	12.7	13.5	13.1	17.4	13.8
8	Liquid flow rate (ml/cm^2·min)	0.35	0.42	0.37	0.48	0.42
9	HETP (cm)	1.02	0.75	1.11	1.07	1.07
10	Min. length of column (cm)	295	1,280	360	369	525
11	Min. area of column (cm^2)	28.4	157.0	30.9	24.8	46.0
12	Min. volume of column (cm^3)	8.4×10^3	2.0×10^5	1.1×10^4	9.2×10^3	2.4×10^4

experimental α, HETP, and flow per unit areas for the required product flow P, using the following equations:[5]

$$n_{(min)} = \ell n\ S_o/(\alpha-1) \ , \tag{43}$$

and

$$(L/P)_{min} = \{N_p[1+(\alpha-1)(1-N_f)]-N_f\}/[(\alpha-1)N_f(1-N_f)] \ , \tag{44}$$

where N_p is the mole fraction of N-15 in the product, i.e., 0.99, and N_f is the mole fraction in the feed material, 0.00365.

Equations (43) and (44) show that both the cross-sectional area and length are dependent on $(\alpha-1)$, so that everything else being equal (HETP, L, etc.) the volume of column required for a given task of isotope separation varies as $1/(\alpha-1)^2$. Table VIII illustrates that a twentyfold reduction in the volume of column is achieved by increasing the pressure from 1 to 4 atm at 15°C. Also, these calculations show that the volume of column at -9°C and atmospheric pressure is approximately the same as that obtained at +15°C and 4 atm. The obvious advantage of the high pressure operation is the elimination of the refrigeration to keep the system at -9°C.

The calculations shown in Table VIII should be used only for comparison purposes. Any actual system designed for production of N-15 would require about 1.5 times the minimum calculated value of the number of stages to compensate for the fact that the maximum transport of the desired product is wanted, which would be obtained only with an infinite number of plates.[51] Also, it is an engineering practice to use about 20-40% larger flow rate than the calculated minimum value to provide for losses, fluctuations, etc.

VIIA-6. Design of a Multiunit Cascade for Fractionation of 99 Atom % N-15

As discussed earlier, a square cascade consisting of a single exchange column was used as a basis for comparison (Table VIII) because of its simplicity, and since the relative magnitude of the parameters discussed would not change. In practice, however, a single long column is never used since equilibrium would be approached very slowly.[52-53] A stepped down cascade consisting of two or three columns which have correspondingly smaller cross-sectional areas is used to attain the desired separation faster.

Such compound columns offer other advantages, such as not being too long and still have the required number of plates for producing the desired product. Channeling (the tendency of the liquid to concentrate at some area of the column cross section while leaving the remaining area unwetted), large pressure drops, and temperature gradients (if thermostatting is needed) are frequent problems associated with long columns. The result is usually a lowering of efficiency for the operation of the cascade. The effect of losses of enriched nitrogen in the product refluxer is also considerably reduced if a two or three section cascade is used rather than a single column.[29]

The characteristics of a two column cascade for the production of 1 gm/day of 99 atom % of N-15 based on the data obtained for Run 16 are given in Table IX. If 99% N-15 is to be obtained from 0.365% natural abundance level, an overall separation of 27,020 is required. This corresponds to 345 theoretical plates under total reflux. For a practical system when product is withdrawn, 1.5 times the theoretical plates are usually provided, which translates to 518 plates being

Table IX. Summary of Parameters for a Two Column Cascade to Produce 1 gm/day of 99% N-15 Based on Data Obtained in Run 16

Column #	I.D., (cm)	A (cm^2)	Height (cm)	S_o	No. of Stages	Mole Fraction of N-15 N_f	Mole Fraction of N-15 N_p	L mmoles N/min	L/A mmoles N/min·cm^2
1	5.62	24.8	250	98	155	0.00365	0.264	431	17.4
2	0.66	0.34	306	275	190	0.264	0.99	5.94	17.4

needed for this system. For the sake of simplicity, the HETP for the following calculations will be assumed to be 1.07x1.5 = 1.61 cm.

A column 5.62cm I.D. x 250 cm long fitted with SS Helipack 3013 was selected for column 1 of the cascade for which the feed material contains natural abundance N-15. The cross-sectional area is 24.8 cm^2, so that a liquid flow of 0.48 $ml/cm^2 \cdot min$ yields a total flow of 11.9 ml/min, corresponding to 431 mmoles N/min. With this flow rate, a maximum transport, PN_p, of 1 gm/day of 99% N-15 is possible. The number of plates in this column is 250/1.61 = 155 stages, yielding an overall separation of 98 and N_p = 26.4%. In column 2, for the same transport (1 gm/day of 99% N-15), a feed material containing 26.4% N-15, and S_o=275 (n=190 plates for a column 306 cm long) the liquid flow is 5.94 mmoles N/min.

In actual production, column one would be operated first under total reflux until the separation vs time curve begins to flatten out. Product withdrawal would then be started since it is not profitable to wait for equilibrium or to produce near the maximum separation (the product flow in that case would have to be very little). The nonproductive time of waiting for equilibrium would thus be reduced, and a respectable yield is produced since the column is at low operating efficiency.

The benefit of not having to refrigerate a system such as the one just described becomes extremely apparent. Except for an initial investment in the materials needed to build an isotope separation plant in which a multicolumn cascade is employed, the elimination of compressors for cooling the entire column system is a distinct advantage.

VII-B. Vibrational Analysis of Oxides of Nitrogen

Although the vibrational spectra of oxides of nitrogen have been studied by several authors, there have been many uncertainties in the values and assignments of the vibrational frequencies for N_2O_3 and N_2O_4 molecules which only recently were partially resolved. The fundamentals of gaseous NO and NO_2 have been reported sometime ago,[54-55] and more recent studies[56-57] are in very good agreement with the earlier ones. A force field calculation based on the experimental data of Shaw[54] and Arakawa et al.[55] has been performed by Monse et al.,[58] and their results were used for the present computation of α from the reduced partition function ratios (Eq. (13)). However, since a valence force field study based on the more recent experimental studies of liquid/solid and gaseous N_2O_3 and N_2O_4 has not been done, and some questions still remain on the assignments and magnitude of the frequencies, a vibrational analysis of these two species was undertaken. Results for N_2O_3 will be presented first, and calculations for N_2O_4 will be discussed in the later section.

VIIB-1. Dinitrogen Trioxide

(i) Frequency Assignments

In the past three decades many authors have studied the vibrational spectra of N_2O_3, including Hisatsune and coworkers[59-62] who have given a reasonably complete assignment for their observed frequencies. However, difficulties in their work arose due to the fact that N_2O_3 is in equilibrium with the other oxides of nitrogen which interfere with its infrared spectrum. It has also been suggested[14] that trace amounts of water, resulting in the formation of HNO_2 which has intense absorptions in the

region of interest, might have interfered with Hisatsune's spectral analysis. Fortunately more recent studies in the gas[14] and liquid phase,[12] and in a nitrogen matrix[13] have provided a more complete set of frequencies, including isotopic shifts due to single and double isotope substitution at the nitrogen positions. Frequencies from the nitrogen matrix study were treated as gas phase data since interactions in the matrix are assumed to be negligible.

The observed fundamentals of asymmetric N_2O_3, whose structure is shown in Figure 47, are summarized in Table X. An unstable isomer (symmetric N_2O_3) has been observed spectroscopically at cryogenic temperatures in a matrix environment.[13] Since symmetric N_2O_3 has not been observed within the temperature range imposed in the present study, its concentration is assumed to be negligible. The first four in-plane frequencies in Table X (ν_1-ν_4), leave little doubt as to the proper assignment because they are similar in value to the individual NO and NO_2 molecules. This phenomenon is explainable in terms of the extraordinarily long N-N bond (1.864 Å),[63] which causes only a weak coupling between NO and NO_2.

The in-plane frequency ν_5, has been assigned by Bibart and Ewing[14] to be the nitro rocking mode, and has been observed by Varetti et al.[13] and Hisatsune et al.[62] The next two bands (ν_6 and ν_7), and the torsional mode (ν_9) have recently been observed by Bradley et al.[12] in the liquid phase at -35°C, and correspond to 260, 160, and 76 cm^{-1}, respectively. However, the N-N stretch frequency, ν_7, has been assigned by Hisatsune et al.[62] to be a weak band at 313 cm^{-1}, with a strong absorption in the 627 cm^{-1} region being attributed to the nitro out-of-plane wag ν_8. Bibart and Ewing have suggested a value of 337 cm^{-1} for

Table X. Summary of Experimental Fundamental Frequencies of N_2O_3[a]

Description	Gas[b]	Liquid[c]	N_2 Matrix[d]				Solid[e]	
	$^{14}NO-$ $^{14}NO_2$	$^{14}NO-$ $^{14}NO_2$	$^{14}NO-$ $^{14}NO_2$	$^{15}NO-$ $^{14}NO_2$	$^{14}NO-$ $^{15}NO_2$	$^{15}NO-$ $^{15}NO_2$	$^{14}NO-$ $^{14}NO_2$	$^{15}NO-$ $^{15}NO_2$
ν_1 Nitroso Str.	1832	-	1839.7	1807.4	1840.3	1807.3	1863	1830
ν_2 Asym. Nitro Str.	1652	-	1630.4	1630.4	1594.8	1594.6	1589	1546
ν_3 Sym. Nitro Str.	1305	-	1302.5	1302.5	1287.8	1286.8	1297	1277
ν_4 Nitro Scissors	773	-	775.7	775.1	765.2	764.9	783	771
ν_5 Nitro Rock	414	-	420.4	418.8	-	409.5	407	397
ν_6[f] Nitroso Rock	(241)[+]	260	-	-	-	-	253	-
ν_7[f] NN Stretch	-	160	-	-	-	-	313	308
ν_8 Nitro Out-of-Plane Wag	337	-	-	-	-	-	627	614
ν_9 Torsion	(63)[‡]	76	-	-	-	-	-	-

[a]All frequencies in cm^{-1}.

[b]From Bibart and Ewing.[14]

[c]From Bradley et al.[12]

[d]From Varetti and Pimentel.[13]

[e]From Hisatsune et al.[62]

[f]Assignment reversed in Ref. 14.

( )[+]Calculated from overtone and combination bands.

( )[‡]Calculated from third law entropy considerations.

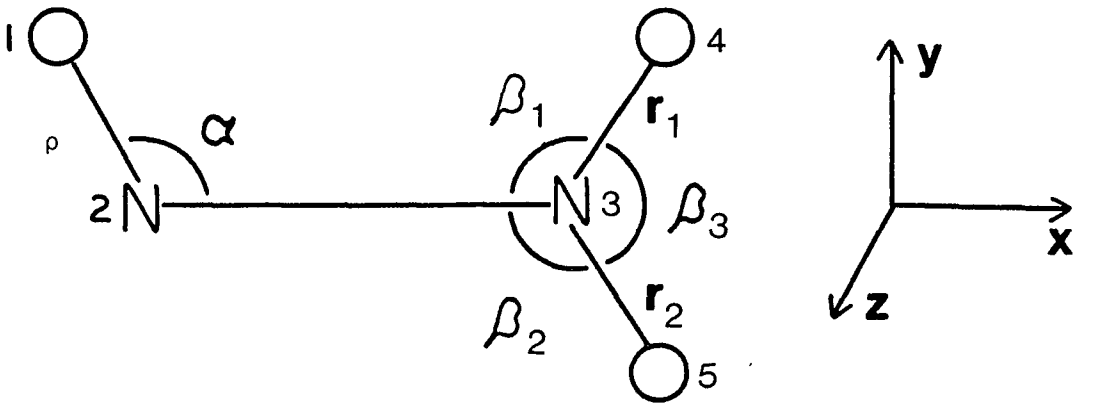

ρ^{o} (1-2)[a] = 1.142 Å , ∢ (1-2-3) = 105.1°

R^{o} (2-3) = 1.864 Å , ∢ (2-3-4) = 112.7°

r_1^{o} (3-4) = 1.202 Å , ∢ (2-3-5) = 117.5°

r_2^{o} (3-5) = 1.217 Å , ∢ (4-3-5) = 129.8°

$m_{^{14}N}$ = 14.003070 amu $\qquad$ $m_{^{15}N}$ = 15.000110 amu

$m_{^{16}O}$ = 15.994910 amu

Figure 47: Structure,[63] Atomic Masses, and Numbering of Atoms for N_2O_3

[a]The superscript o is to differentiate internal coordinates (i.e., ρ) from equilibrium bond lengths (ρ^{o}). The numbers in parenthesis identify the atoms being involved.

the out-of-plane mode since the weak features they observed in the 600-700 cm^{-1} region do not correspond to the correct band shape. Bradley et al. found only weak bands in the 300 cm^{-1} area and indicated that these may be overtones of the 160 cm^{-1} band they observe, concluding that the 627 cm^{-1} frequency of Hisatsune et al. is due to the ν_8 fundamental. However, the spectroscopic evidence does not seem conclusive, and there is still some question as to which of the two values suggested for ν_8, 337 or 627 cm^{-1}, is correct. In fact a recent review by Laane and Olshen[15] prefers the former assignment arguing that the latter may very well be its overtone.

In the present work both values for this controversial frequency are considered in the force field calculations, and two $\underset{\sim}{F}$-matrices (F_1 and F_2) differing from each other only in the out-of-plane block (ν_8 and ν_9) were constructed for condensed and gaseous N_2O_3.

(ii) Normal Coordinate Analysis

The procedure for calculating the frequencies associated with the normal modes of vibration involves the solution of the secular equation based on Wilson's $\underset{\sim}{FG}$-matrix method:[19]

$$|\underset{\sim}{FG} - \lambda \underset{\sim}{I}| = \underset{\sim}{0} , \tag{45}$$

where

$$\lambda = 4\pi^2\nu^2 , \tag{46}$$

and $\underset{\sim}{I}$ is the identity matrix. A modified version of the Schachtschneider-Snyder program[64] was used to solve the vibrational secular problem. The G-matrices were obtained from the equilibrium geometry of N_2O_3 (Figure 47). The internal coordinate definition

employed for the calculations, shown in Table XI, is based on the one reported by Hisatsune.[60] Internal coordinates are more convenient and more meaningful to the chemist because they describe the motion of atoms in terms of changes in interatomic distances and angles between bonds. The simplicity and usefulness of the symmetry coordinates, which are linear combinations of the internal ones, does not apply here because of the low order of symmetry of N_2O_3 (C_s).

(iii) Construction of the $\underset{\sim}{F}$-Matrices

Hisatsune et al.[60] and more recently Bradley et al.[12] have constructed $\underset{\sim}{F}$-matrices based on the Urey-Bradley potential field, which takes into account interactions present between non-bonded atoms. The valence force field obtained by transforming these UBFF was used as a starting point of the present further refinement.

To avoid the usual problems of falling into local minima, divergence, and oscillations associated with computerized iterative algorithms, a more deliberate procedure was used for reproducing the fundamental frequencies in which a table of first derivatives of every normal frequency with respect to every $\underset{\sim}{F}$-matrix element was constructed and examined to decide on the next move in improving the overall agreement. Typically, $\partial\omega_k/\partial f_{ij}$ was calculated by solving the secular problem twice, i.e., once by using a basis $\underset{\sim}{F}$-matrix and then by using a modified $\underset{\sim}{F}$-matrix in which the value of f_{ij} is reduced by 1% of its original value. The reduced f_{ij} was used at all equivalent positions in the $\underset{\sim}{F}$-matrix. The difference in the corresponding values of ω_k is divided by 0.01 f_{ij} to approximate $\partial\omega_k/\partial f_{ij}$. A first derivative table for the in-plane and out-of-plane force constants is summarized in Table XII. The squared-off areas show the frequency most effected by the 1% change of the appropriate element.

Table XI. Internal Coordinate Definition for N_2O_3[a]

No.	Symbol	Description
1	ρ	NO bond stretch (1-2)[b]
2	R	NN bond stretch (2-3)
3	r_1	NO bond stretch (3-4)
4	r_2	NO bond stretch (3-5)
5	$\alpha\rho^o$	ONN angle bend (1-2-3), weighted by ρ^o = 1.142 Å
6	$\beta_1 r_1^o$	NNO angle bend (2-3-4), weighted by r_1^o = 1.202 Å
7	$\beta_2 r_1^o$	NNO angle bend (2-3-5), weighted by r_1^o = 1.202 Å
8	$\beta_3 r_1^o$	ONO angle bend (4-3-5), weighted by r_1^o = 1.202 Å
9[c]	θr_1^o	NNO_2 out-of-phone wag (2-3-5-4), weighted by r_1^o = 1.202 Å
10[c]	$\tau\rho^o$	ONNO Wilson Torsion (1-2-3-4), weighted by ρ^o = 1.142 Å

[a]Stretching and bending coordinates in mdyn/Å, weighting of angle coordinates is in accordance with Hisatsune et al. (Ref. 60).

[b]The number in parenthesis following each coordinate definition identify the atoms being involved (see Fig. 47).

[c]The order in which the atoms appear in the definition of the out-of-plane wag and torsion specifies the phases of these displacement coordinates relative to the others, which is in accordance with the input format of the Schachtschneider-Snyder[64] G-matrix program.

Table XII. Differential Effects of a 1% Decrease of the Force Constants on the Fundamental Frequencies of N_2O_3[a]

	$\underset{\sim}{F}$-matrix Element	Initial Value	Isotopic[b] Molecule	ν_1	ν_2	ν_3	ν_4	ν_5	ν_6	ν_7	ν_8	ν_9
In-plane	f_ρ	14.74	14-14	[62.8	0.3	0.0	0.0	0.1	0.0	0.0		
			15-15	61.7]	0.3	0.0	0.0	0.1	0.0	0.0		
	f_R	0.233	14-14	1.1	0.0	16.0	30.3	[66.5	41.2	166.1]		
			15-15	1.0	0.0	14.0	29.3	61.2]	44.8	167.4]		
	f_r	10.09	14-14	0.2	[46.3	28.9]	0.4	0.3	0.1	0.0		
			15-15	0.1	45.3]	28.9]	0.3	0.3	0.1	0.0		
	f_α	0.653	14-14	8.4	10.3	0.1	0.5	[356.5]	17.8	35.2		
			15-15	7.7	9.7	0.1	0.5	349.2]	20.0	33.5		
	f_{β_1}	0.432	14-14	8.3	25.1	12.9	[62.3	41.4	134.7]	9.1		
			15-15	7.5	23.6	11.2	62.7]	42.3	133.3]	8.4		
	f_{β_3}	1.547	14-14	0.0	0.0	[56.7	272.1]	1.3	0.5	1.5		
			15-15	0.0	0.0	49.2]	273.2]	1.1	0.4	1.5		
	f_{rr}	1.599	14-14	-0.3	[-92.9	57.0]	0.7	-0.4	-0.3	0.0		
			15-15	-0.3	-91.0]	56.4]	0.5	-0.3	-0.2	0.0		
	$f_{r\beta_3}$	0.673	14-14	0.0	0.2	[-75.3	18.5]	-1.1	0.4	-0.3		
			15-15	0.0	0.2	-69.9]	15.6]	-1.0	0.3	-0.2		
Out-of-plane	f_θ	0.25	14-14								[1270.1]	1.7
			15-15								1236.2]	1.9
	f_τ	0.0027	14-14								272.5	[2026.6]
			15-15								263.7	1994.4]

[a] In-plane and out-of-plane frequencies were treated separately. All $\underset{\sim}{F}$-matrix elements in units of mdyn/Å; see Table XI for appropriate weighting factor of the bending force constants.

[b] The two numbers designate the isotopic mass numbers of the two nitrogens in N_2O_3.

The final F-matrices which reproduced what was felt to be the most reliable set of experimental frequencies for condensed and gaseous N_2O_3 are summarized in Table XIII and the calculated frequencies are presented in Table XIV. No external modes were considered because of the low symmetry (C_s) and the lack of information on the external frequencies: An introduction of external modes would add three coordinates to seven in-plane internal coordinates, and three to only two out-of-plane internal coordinates. Besides, the interactions with the external modes were not needed since the agreement between the calculated and experimental frequencies of the condensed internal motions is reasonably good. However, a different situation was found for N_2O_4, and it will be discussed in detail in the next section.

VIIB-2. Dinitrogen Tetroxide

The infrared and Raman spectra of $^{14}N_2O_4$ and $^{15}N_2O_4$ have been the subject of numerous investigations in the gas phase,[16,17] liquid/solid phases,[17,18,62] and in matrix environments.[65] Electron diffraction studies of the gas phase[66] show the structure to be planar D_{2h} geometry with an unusually long N-N bond (1.782 Å). A low barrier to internal rotation is indicated by the infrared studies.[17] The same geometry has been found in X-ray diffraction studies,[67] where the length of the N-N bond was found to increase 0.01 Å per 100° of temperature rise.

The existence of unstable isomers of N_2O_4 was first shown by Fately et al.[65] using the matrix isolation method to stabilize the

Table XIII. F-Matrices for N_2O_3[a,b]

Element	Gas	Liquid
In-Plane		
f_ρ	14.7385	15.1295
f_R	0.336	0.343
f_{r_1}	10.065	9.795
f_{r_2}	10.065	9.795
f_α	0.473	0.436
f_{β_1}	0.321	0.300
f_{β_2}	0.321	0.300
f_{β_3}	1.048	1.084
$f_{r_1r_2}$	1.588	1.758
$f_{r_1\beta_3}$	0.559	0.559
$f_{r_2\beta_3}$	0.559	0.559
Out-of-Plane		
f_θ	0.2728 (0.076)	0.2711 (0.0740)
f_τ	0.0123 (0.0128)	0.0180 (0.0191)

[a] All elements in units of mdyn/Å; bending force constants are weighted so that every coordinate has dimensions of length (see Table XI for definitions).

[b] The $\underset{\sim}{F}$-matrices for N_2O_3 were fitted to the following observed fundamentals. F_2 out-of-plane elements are shown in parenthesis.

Gas phase, $\underset{\sim}{F}_1$: Varetti and Pimentel for ν_1-ν_5, Bradley et al. for ν_6 and ν_7, Hisatsune et al. for ν_8, Bibart and Ewing for ν_9.

Table XIII. (cont.)

$\underset{\sim}{F}_2$: Same as $\underset{\sim}{F}_1$ except for ν_8 which is from Bibart and Ewing (337 cm^{-1}).

Condensed Phase, $\underset{\sim}{F}_1$: Hisatsune et al. for ν_1-ν_6, Bradley et al. for ν_7 and ν_9, ν_8 = 627 cm^{-1}.

$\underset{\sim}{F}_2$: Same as $\underset{\sim}{F}_1$ condensed except for ν_8 = 337 cm^{-1}.

Table XIV. Summary of Observed Fundamentals[a] and Calculated Frequencies[b] of N_2O_3

Description	Gas	N_2 Matrix								Liquid	Solid			
	$^{14}N_2O_3$	$^{14}NO^{14}NO_2$		$^{15}NO^{14}NO_2$		$^{14}NO^{15}NO_2$		$^{15}NO^{15}NO_2$		$^{14}N_2O_3$	$^{14}N_2O_3$		$^{15}N_2O_3$	
	B-E	V-P	Calc'd	V-P	Calc'd	V-P	Calc'd	V-P	Calc'd	BSSV	HDW	Calc'd	HDW	Calc'd
ν_1 nitroso stretch	1832	1839.7	1839.7	1807.4	1806.4	1840.3	1839.5	1807.3	1806.2	-	1863	1862.9	1830	1829.1
ν_2 asym. nitro str.	1652	1630.4	1630.5	1630.4	1630.4	1594.8	1593.9	1594.6	1593.8	-	1589	1587.5	1546	1551.8
ν_3 sym. nitro str.	1305	1302.5	1302.4	1302.5	1302.4	1287.8	1287.3	1286.8	1287.3	-	1297	1298.3	1277	1283.1
ν_4 nitro scissors	773	775.7	775.4	775.1	775.4	765.2	765.7	764.9	765.6	-	783	782.9	771	773.1
ν_5 nitro rock	414	420.4	420.4	418.8	411.7	-	420.0	409.5	411.3	-	407	406.8	397	397.9
ν_6 nitroso rock	241	-	260.2	-	258.6	-	259.3	-	257.7	260	253	253.1	-	250.7
ν_7 N-N stretch	-	-	159.9	-	159.1	-	159.4	-	158.6	160	313[c]	159.4	308[c]	158.1
ν_8 nitro wag(O-P)[d]	337	-	627.0 (337.0)	-	626.1 (336.5)	-	611.0 (328.5)	-	610.1 (327.9)	-	627	627.0 (337.0)	614	610.1 (327.9)
ν_9 torsion(O-P)	63	-	63.0 (63.1)	-	62.1 (62.2)	-	63.0 (63.1)	-	62.1 (62.2)	76	-	76.0 (76.0)		74.8 (74.8)

[a](B-E) = Bibart and Ewing,[14] (V-P) = Varetti and Pimental,[13] (BSSV) = Bradley, Sidall, Strauss, and Varetti,[12] (HDW) = Hisatsune, Devlin, and Wada.[62]

[b]Calculated results are present work's. The values without parentheses are from F_{21} matrices and those with parenthesis are from F_{22}-matrices (cf: Table XIII).

[c]Not used for the fitting.

[d](O-P) = Out-of-plane modes.

various forms of this molecule. The existence of these isomers was later confirmed by Hisatsune et al.[62] in the infrared study of solid N_2O_4 at liquid nitrogen temperatures. However, even at such low temperatures only very small concentrations were detected, and the amounts near ambient temperature, where the unstable forms have not been observed, are considered to be negligible.

(i) Frequency Assignments

According to a group theoretical analysis of the N_2O_4 molecule in its stable form, (D_{2h} symmetry), the irreducible representations are as follows:

$$\Gamma(\text{internal}) = 3A_g+A_u+2B_{1g}+B_{1u}+B_{2g}+2B_{2u}+2B_{3u} , \quad (47)$$

$$\Gamma(\text{rotational}) = B_{1g}+B_{2g}+B_{3g} , \quad (48)$$

$$\Gamma(\text{translational}) = B_{1u}+B_{2u}+B_{3u} . \quad (49)$$

The gerade species are Raman active, and the ungerade species are infrared active, except for species A_u which is inactive. A summary of the vibrational frequencies reported in various studies is listed in Table XV. It should be noted that a major discrepancy occurs for the NO_2 rock (ν_{10}), where the values assigned by Bibart et al.[16] and Andrews et al.[18] are quite different from those of Begun and Fletcher.[17] This point will be discussed in more detail in the next section, after the force field calculations. A trend which emerges when comparing values reported by Begun and Fletcher for the gas and liquid phases is a red shift of the frequencies upon condensation. The construction of two separate $\underset{\sim}{F}$-matrices for the gas and liquid phases seems appropriate

Table XV. Summary of Observed Fundamental Frequencies for N_2O_4[a]

ν (cm)	Gas Phase $^{14}N_2O_4$	Gas Phase $^{15}N_2O_4$	Liquid Phase $^{14}N_2O_4$	Liquid Phase $^{15}N_2O_4$	Solid Phase $^{14}N_2O_4$	Solid Phase $^{15}N_2O_4$
ν_1 (A_g) NO stretch			1379.6	1360.2	1383.2 (1381)	1362.8
ν_2 (A_g) NO_2 deform.			808	797	811 (808)	800
ν_3 (A_g) NN stretch			266.0	263.9	274.8 (281)	272.8
ν_4 (A_u) torsion (OPLA)	[79]‡		-	-	-	-
ν_5 (B_{1g}) NO stretch			1711.6	1672.2	1723.5 (1727)	1683.3
ν_6 (B_{1g}) NO_2 rock			482	478	491 (496)	487
ν_7 (B_{1u}) NO_2 wag (OPLA)	∿429 [425]	∿420	423	416	(439)	
ν_8 (B_{2g}) NO_2 wag (OPLA)			672	654	(677)	
ν_9 (B_{2u}) NO stretch	1748 [1758]	1707	1733	1703	(1737)	
ν_{10} (B_{2u}) NO_2 rock	381 [∿270]+	377			(265)	
ν_{11} (B_{3u}) NO stretch	1262 [1264]	1251	1257	1248	(1249)	
ν_{12} (B_{3u}) NO_2 deform.	750 [751]	739	743	735	(742)	

[a] All frequencies in cm^{-1}.

Values w/o ( ) or [ ] are Begun and Fletcher's, Ref. 17 (1960).

Values in ( ) are Andrews and Anderson's, Ref. 18 (1981).

Values in [ ] are Bibart and Ewing's, Ref. 16 (1974).

[ ]+ Calculated from overtone and combination bands.

[ ]‡ Calculated from third law entropy calculations.

since a reasonable amount of experimental spectroscopic data is available for both phases, including isotopic shifts due to isotope substitution at the nitrogen positions.

(ii) Normal Coordinate Analysis

A normal coordinate analysis was performed recently by Six et al.[68] for dinitrogen tetroxide. However their work was not useful for our present calculations because of several reasons: 1) The wrong geometry was employed for N_2O_4, where the N-O bond distance was mistakingly reported to be 1.88 Å. This is longer than the 1.782 Å of the N-N bond, which is considered unusually long. The generally accepted distance for this bond is 1.190 Å as reported by McClelland et al.,[66] and to the best of our knowledge the wrong value originated from a misprint in the paper by Begun and Fletcher[17] who were reporting electron diffraction data of Smith and Hedberg.[69] The actual value reported by Smith et al. was 1.18 Å, which is in reasonable agreement with the later determination.[66] 2) The normal coordinate analysis of Six et al. was based on a combination of gas and liquid frequencies reported by Begun and Fletcher, and 3) Only the in-plane frequencies were considered in their force field calculations.

The geometry of N_2O_4 with a definition of the internal coordinates are presented in Figure 48 and Table XVI. Because of the high symmetry of N_2O_4 it was found more convenient to work with symmetry coordinates, which are presented in Table XVII. The definitions of the symmetry and internal coordinates for the in-plane frequencies are those of Six et al. The in-plane and out-of-plane modes were treated separately.

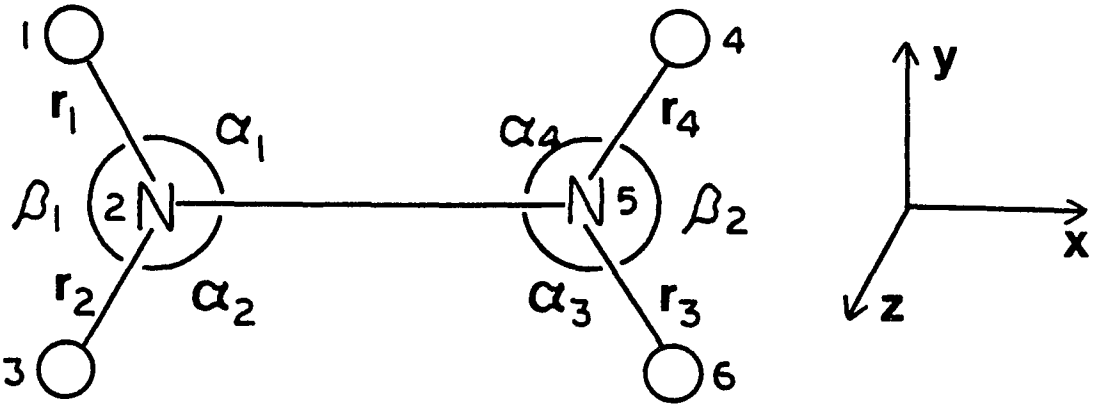

r_1^{o} (1-2)[a] = 1.190 Å

R^{o} (2-5)[a] = 1.782 Å

∢ (1-2-3) = 135.4°

∢ (1-2-5) = 112.3°

m_{14_N} = 14.003070 amu

m_{15_N} = 15.000110 amu

m_{16_N} = 15.994910 amu

Figure 48: Structure[66] and Numbering of Atoms for N_2O_4.

[a]See footnote of Figure 47.

Table XVI. Internal Coordinate Definition for N_2O_4[a]

	No.	Symbol	Description
In-plane	1	R	N-N bond stretch (2-5)[b]
	2	r_1	N-O bond stretch (2-1)
	3	r_2	N-O bond stretch (2-3)
	4	r_3	N-O bond stretch (5-6)
	5	r_4	N-O bond stretch (5-4)
	6	$\alpha_1 r_1^o$	ONN angle bend (1-2-5)
	7	$\alpha_2 r_1^o$	ONN angle bend (3-2-5)
	8	$\alpha_3 r_1^o$	NNO angle bend (2-5-6)
	9	$\alpha_4 r_1^o$	NNO angle bend (2-5-4)
	10	$\beta_1 r_1^o$	ONO angle bend (1-2-3)
	11	$\beta_2 r_1^o$	ONO angle bend (4-5-6)
Out-of-plane	12[c]	τr_1^o	O_2NNO_2 Crawford Torsion (2-5-1-4-3-6)
	13[c]	$\theta_1 r_1^o$	NNO_2 out-of-plane wag, (5-2-3-1)
	14[c]	$\theta_2 r_1^o$	NNO_2 out-of-plane wag, (2-5-4-6)

[a]Stretching coordinates is mdyn/Å, angle coordinates weighted by r_1^o (N-O distance). Definition of internal coordinates from Ref. 68. See also Fig. 48 for structure.

[b,c]See notes on Table XI.

Table XVII. Symmetry Coordinates Definition for Gaseous N_2O_4[a]

In-plane	$S_{1R}^{A_g} = R$
	$S_{2r}^{A_g} = 1/2\ (r_1+r_2+r_3+r_4)$
	$S_{3\alpha}^{A_g} = 1/2\ (\alpha_1+\alpha_2+\alpha_3+\alpha_4)$
	$S_{3\beta}^{A_g} = 1/\sqrt{2}\ (\beta_1+\beta_2)$
	$S_{4r}^{B_{1g}} = 1/2\ (r_1-r_2+r_3-r_4)$
	$S_{5\alpha}^{B_{1g}} = 1/2\ (\alpha_1-\alpha_2+\alpha_3-\alpha_4)$
	$S_{6r}^{B_{2u}} = 1/2\ (r_1-r_2-r_3+r_4)$
	$S_{7\alpha}^{B_{2u}} = 1/2\ (\alpha_1-\alpha_2-\alpha_3+\alpha_4)$
	$S_{8r}^{B_{3u}} = 1/2\ (r_1+r_2-r_3-r_4)$
	$S_{9\alpha}^{B_{3u}} = 1/2\ (\alpha_1+\alpha_2-\alpha_3-\alpha_4)$
	$S_{9\beta}^{B_{3u}} = 1/\sqrt{2}\ (\beta_1-\beta_2)$
	with redundancies
	$\sqrt{2}\ S_{3\alpha}^{A_g} + S_{3\beta}^{A_g} = 0$
	$\sqrt{2}\ S_{9\alpha}^{B_{3u}} + S_{9\beta}^{B_{3u}} = 0$
Out-of-plane	$S_{1O}^{A_u} = \tau$
	$S_{11\theta}^{B_{1u}} = 1/\sqrt{2}\ (\theta_1+\theta_2)$
	$S_{12\theta}^{B_{2g}} = 1/\sqrt{2}\ (\theta_1-\theta_2)$

[a]See footnote a in Table XVI.

(iii) Potential Energy Matrices

The internal coordinate $\underset{\sim}{F}$-matrix for gaseous N_2O_4 is tabulated in Table XVIII. In order to symmetrize the potential energy matrices, the following operation is applied:

$$\underset{\sim}{F}_s = \underset{\sim}{T}\underset{\sim}{F}_r\underset{\sim}{T}^T \quad , \tag{50}$$

where $\underset{\sim}{F}_r$ and $\underset{\sim}{F}_s$ are the internal coordinate and symmetrized $\underset{\sim}{F}$-matrices, respectively, and $\underset{\sim}{T}$ is the transformation matrix, shown in Table XIX. The two redundancies which exist in the A_g and B_{3u} blocks are eliminated by substituting the redundancy conditions:

$$\sqrt{2}S_{3\alpha}^{A_g} + S_{3\beta}^{A_g} = 0 \quad , \tag{51}$$

and

$$\sqrt{2}S_{9\alpha}^{B_{3u}} + S_{9\beta}^{B_{3u}} = 0 \quad , \tag{52}$$

in the algebraic expression for the potential energy:

$$2V = \sum_{i,J} f_{ij}S_iS_j \quad , \tag{53}$$

where f_{ij} and S_i, S_j are the force constants and symmetrized coordinates, respectively. The force constant matrix for gaseous N_2O_4 is reported in Table XX after removal of the redundancies.

In the case of the liquid $\underset{\sim}{F}$-matrix, the external motions, i.e. translational and rotational, are taken into account (Table XXI). The fitting of the gas and liquid $\underset{\sim}{F}$-matrices was performed with the derivative method discussed earlier. As a starting point, the values of the force constants for the NO_2 part of N_2O_3 were employed, and it was found that some degree of transferability existed.

Table XVIII. Gaseous $\underset{\sim}{F}$-matrices for Dinitrogen Tetroxide[a]

In-plane

	R	r_1	r_2	r_3	r_4	α_1	α_2	α_3	α_4	β_1	β_2
R	f_R	f_{Rr}	f_{Rr}	f_{Rr}	f_{Rr}	$f_{R\alpha}$	$f_{R\alpha}$	$f_{R\alpha}$	$f_{R\alpha}$	$f_{R\beta}$	$f_{R\beta}$
r_1		f_r	f_{rr}	-	-	$f_{r\alpha}$	$f_{r\alpha}'$	-	-	$f_{r\beta}$	-
α_1						f_α	$f_{\alpha\alpha}$	-	-	$f_{\alpha\beta}$	-
β_1										f_β	-

Out-of-plane

	τ	θ_1	θ_2
τ	f_τ	-	-
θ_1		f_θ	$f_{\theta\theta}$

[a] An $\underset{\sim}{F}$-matrix element with one subscript is a diagonal element, and one with two subscripts is an off-diagonal element. When two off-diagonal elements are listed for a similar interaction, i.e. $f_{r\alpha}$ $f_{r\alpha}'$, the one without the prime refers to the interaction between two coordinates which share a common N-O bond.

Table XIX. Transformation Matrices for Gaseous N_2O_4

In-plane

	R	r_1	r_2	r_3	r_4	α_1	α_2	α_3	α_4	β_1	β_2
$S_{1R}^{A_g}$	1										
$S_{2r}^{A_g}$		1/2	1/2	1/2	1/2						
$S_{3\alpha}^{A_g}$						1/2	1/2	1/2	1/2		
$S_{3\beta}^{A_g}$										$1/\sqrt{2}$	$1/\sqrt{2}$
$S_{4r}^{B_{1g}}$		1/2	-1/2	1/2	-1/2						
$S_{5\alpha}^{B_{1g}}$						1/2	-1/2	1/2	-1/2		
$S_{6r}^{B_{2u}}$		1/2	-1/2	-1/2	1/2						
$S_{7\alpha}^{B_{2u}}$						1/2	-1/2	-1/2	1/2		
$S_{8r}^{B_{3u}}$		1/2	1/2	-1/2	-1/2						
$S_{9\alpha}^{B_{3u}}$						1/2	1/2	-1/2	-1/2		
$S_{9\beta}^{B_{3u}}$										$1/\sqrt{2}$	$-1/\sqrt{2}$

Out-of-plane

	τ	θ_1	θ_2
$S_{10\tau}^{A_u}$	1		
$S_{11\theta}^{B_{1u}}$		$1/\sqrt{2}$	$1/\sqrt{2}$
$S_{12\theta}^{B_{2g}}$		$1/\sqrt{2}$	$-1/\sqrt{2}$

Table XX. Symmetrized $\underset{\sim}{F}$-matrices for Gaseous N_2O_4[a]

In plane

A_g	$F_{11} = f_R$	$F_{12} = 2f_{Rr}$
	$F_{22} = f_r + f_{rr}$	$F_{13} = 2(f_{R\alpha} - f_{R\beta})$
	$F_{33} = f_\alpha + f_{\alpha\alpha} + 2f_\beta - 4f_{\alpha\beta}$	$F_{23} = f_{r\alpha} + f_{r\alpha}' - 2f_{r\beta}$
B_{1g} and B_{2u}	$F_{11} = f_r - f_{rr}$	$F_{12} = f_{r\alpha} - f_{r\alpha}'$
	$F_{22} = f_\alpha - f_{\alpha\alpha}$	
B_{3u}	$F_{11} = f_r + f_{rr}$	$F_{12} = f_{r\alpha} + f_{r\alpha}' - 2f_{r\beta}$
	$F_{22} = f_\alpha + f_{\alpha\alpha} + 2f_\beta - 4f_{\alpha\beta}$	

Out-of-plane

A_u	$F_1 = f_\tau$
B_{1u}	$F_1 = f_\theta + f_{\theta\theta}$
B_{2g}	$F_1 = f_\theta - f_{\theta\theta}$

[a]For a definition of internal coordinates and weighting factors, see Table XVI.

Table XXI. Symmetrized $\underset{\sim}{F}$-matrices for Liquid N_2O_4[a]

In plane

A_g

$F_{11} = f_R$ $\quad F_{12} = 2f_{Rr}$

$F_{22} = f_r + f_{rr}$ $\quad f_{13} = 2(f_{R\alpha} - f_{R\beta})$

$f_{33} = f_\alpha + f_{\alpha\alpha} + 2f_\beta - 4f_{\alpha\beta}$ $\quad f_{23} = f_{r\alpha} + f_{r\alpha}' - 2f_{r\beta}$

B_{1g}

$F_{11} = f_r - f_{rr}$ $\quad F_{12} = f_{r\alpha} - f_{r\alpha}'$

$F_{22} = f_\alpha - f_{\alpha\alpha}$ $\quad F_{13} = 2f_{rR_z}$

$F_{33} = R_z$ $\quad F_{23} = 2f_{\alpha R_z}$

B_{2u}

$F_{11} = f_r - f_{rr}$ $\quad F_{12} = f_{r\alpha} - f_{r\alpha}'$

$F_{22} = f_\alpha - f_{\alpha\alpha}$ $\quad F_{13} = 2f_{rT_y}$

$F_{33} = T_y$ $\quad F_{23} = 2f_{\alpha T_y}$

B_{3u}

$F_{11} = f_r + f_{rr}$ $\quad F_{12} = f_{r\alpha} + f_{r\alpha}' - 2f_{r\beta}$

$F_{22} = f_\alpha + f_{\alpha\alpha} + 2f_\beta - 4f_{\alpha\beta}$ $\quad F_{13} = 2f_{rT_x}$

$F_{33} = T_x$ $\quad F_{23} = 2(f_{\alpha T_x} - f_{\beta T_x})$

Out-of-plane

A_u $\quad F_1 = f_\tau$

B_{1u} $\quad F_{11} = f_\theta + f_{\theta\theta}$ $\quad F_{22} = T_z$ $\quad F_{12} = \sqrt{2}\, f_{\theta T_z}$

B_{2g} $\quad F_{11} = f_\theta - f_{\theta\theta}$ $\quad F_{22} = R_y$ $\quad F_{12} = \sqrt{2}\, f_{\theta R_y}$

Table XXI. (cont.)

[a] T_x, T_y, T_z and R_x, R_y, R_z are the translational and rotational force constants, respectively. All $\underset{\sim}{F}$-matrix elements are in units of mdyn/Å except for the rotational force constants, which are in units of mdyn Å. For a definition of the internal coordinates and weighting factor, see Table XVI.

In the liquid state, the symmetry-allowed interactions between the internal and external motions remove some of the constraints existing for the gas phase. For example, even though the algebraic expression for the liquid F_{11} elements of the B_{1g} and B_{2u} blocks are the same (Table XXI), the numerical values do not necessarily have to be equal (which is the case for the gas). This is clearly shown in Table XXII, where the values for the liquid and gaseous $\underset{\sim}{F}$-matrix elements are listed. The experimental data used to fit the $\underset{\sim}{F}$-matrices is tabulated along with the calculated frequencies in Table XXIII.

Our vibrational assignment is in agreement with that of Bibart et al.[16] and Begun et al.,[17] and our calculations confirm a value of about 270 cm^{-1} for ν_{10}, as suggested by the recent experimental studies.[16] The reversal of the assignment of ν_1 (A_g) and ν_2 (A_g) reported by Six et al., with ν_{10} (B_{2u}) having a value of 203 cm^{-1} is probably due to the mistaken geometry reported by these authors.

The liquid force field displays large internal-external interaction force constants, which were found necessary in order to obtain a better match between the calculated and experimental values by reducing the isotope shift. The phenomenon of red shifting of the frequencies upon condensation (which is accompanied with a decrease in the isotopic shift as well) is due to an increase in the intermolecular forces, and is the cause for the decrease in the strength of the bonds in the molecule.

Specifically of interest is the NO stretching fundamental, ν_9, of the B_{2u} block, which has an isotopic shift of 41 cm^{-1} in the gas phase, and 30 cm^{-1} in the liquid. Large fundamentals which are usually associated with large isotope shifts in the vibrational modes that directly involve the motion of the isotopically substituted atoms will contribute

Table XXII. Final Results for the Symmetrized Gas and Liquid Force Fields of N_2O_4[a]

	Type	F-matrix Elements	
		Gas	Liquid
In-plane	A_g	$F_{11} = 1.3980$	$F_{11} = 1.3980$
		$F_{12} = -0.9300$	$F_{12} = -0.9300$
		$F_{13} = 0.0850$	$F_{13} = 0.0850$
		$F_{22} = 11.9230$	$F_{22} = 11.9230$
		$F_{23} = -1.1760$	$F_{23} = -1.1760$
		$F_{33} = 2.1470$	$F_{33} = 2.1470$
	B_{1g}	$F_{11} = 10.0480$	$F_{11} = 10.0480$
		$F_{12} = 0.6900$	$F_{12} = 0.7000$
		$F_{22} = 0.6500$	$F_{22} = 0.6700$
			$F_{33} = 0.1000$
	B_{2u}	$F_{11} = 10.0480$	$F_{11} = 10.1970$
		$F_{12} = 0.6900$	$F_{12} = 1.4000$
		$F_{22} = 0.6500$	$F_{13} = 2.0000$
			$F_{22} = 0.7470$
			$F_{23} = 0.2050$
			$F_{33} = 0.8000$
	B_{3u}	$F_{11} = 11.9230$	$F_{11} = 11.8330$
		$F_{12} = -1.1760$	$F_{12} = -1.1760$
		$F_{22} = 2.1470$	$F_{13} = -1.2000$
			$F_{22} = 2.0890$
			$F_{23} = -0.8000$
			$F_{33} = 0.8000$

Table XXII. (cont.)

	Type	F-matrix Elements	
		Gas	Liquid
Out-of-plane	A_u	$F_1 = 0.02615$	$F_1 = 0.02615$
	B_{1u}	$F_1 = 0.1523$	$F_{11} = 0.14580$
			$F_{12} = -0.1800$
			$F_{22} = 0.6000$
	B_{2g}	$F_1 = 0.1982$	$F_{11} = 0.1978$
			$F_{12} = -0.0800$
			$F_{22} = 0.4000$

[a]See footnotes of Table XXI.

Table XXIII. Comparison of Experimental and Calculated Frequencies for Gaseous and Liquid N_2O_4[a]

	Liquid[b]		Gas[b]	
ν (cm^{-1})	$^{14}N_2O_4$	$^{15}N_2O_4$	$^{14}N_2O_4$	$^{15}N_2O_4$
ν_1	1379.6 (1380.7)	1360.2 (1359.7)	- (1380.7)	- (1359.7)
ν_2	808 (805.7)	797 (796.1)	- (806.7)	- (796.1)
ν_3	266.0 (266.0)	263.9 (264.4)	- (266.0)	- (264.4)
ν_4	79‡ (78.9)	79‡ (78.9)	79‡ (78.9)	79‡ (78.9)
ν_5	1711.6 (1712.0)	1672.2 (1673.3)	- (1711.5)	- (1672.9)
ν_6	482 (481.9)	478 (478.2)	- (474.8)	- (471.1)
ν_7	423 (423.5)	416 (415.6)	429 (429.5)	420 (419.4)
ν_8	672 (672.1)	654 (653.7)	- (672.4)	- (653.4)
ν_9	1733 (1733.3)	1703 (1699.0)	1748 (1747.5)	1707 (1709.3)
ν_{10}	265[c] (264.5)	- (264.0)	270+ (270.9)	- (270.5)
ν_{11}	1257 (1257.7)	1248 (1248.2)	1262 (1262.1)	1251 (1251.2)
ν_{12}	743 (743.9)	735 (734.7)	750 (750.2)	739 (739.1)
T_x	(67.5)	(66.5)		
T_y	(85.7)	84.6		
T_z	(67.8)	(67.0)		
R_y	(82.3)	(81.4)		
R_z	(28.1)	(28.0)		

Table XXIII. (cont.)

[a]Values of present force field calculations in parenthesis.

[b]Experimental values from Ref. 17.

[c]Experimental values from Ref. 18.

[+]Calculated from third law entropy, Ref. 16.

[‡]Calculated from combination and overtone bands, Ref. 16.

significantly to the reduced partition function ratios that are used to evaluate α. This can easily be seen from the simplified expressions for the partition function ratios shown in Eqs. (7)-(9).

One of the possible methods to reduce the isotope shift of ν_9 from 41 to 30 cm^{-1} was by introducing a large internal-external force constant, F_{13}, which in the B_{2u} block corresponds to an interaction between the translational motion in the positive y direction (which is perpendicular to the N-N bond in the plane of the molecule) with the N-O stretching mode, ν_9. (For a definition of the axis see Figure 48). The introduction of the potential terms associated with translational and rotational coordinates leave the internal vibrations of the basis molecule (in this case $^{14}N_2O_4$) unchanged. However, the internal vibrations of $^{15}N_2O_4$ are perturbed by the internal-external interactions as a consequence of the fact that the center of gravity shifts and the moments of inertia change.

F_{13} is positive, indicating that the potential energy of the molecule increases as it translates in the positive y direction while the N-O stretch occurs. This means that it is energetically less likely for these two motions to be in phase. All other internal-external interaction force constants are small, except for the relatively large negative F_{13} value of the B_{3u} block. In this case interaction between the N-O stretch (ν_{11}) and the translation in the x direction is negative, or energetically more likely to be coupled.

VIIC. Correlation of Spectroscopic Data with the Experimental Single Stage Separation Factor

The single stage separation factor was evaluated from the known chemical compositions of the two phases (Table VI) and the frequencies generated from the force field calculations (Table XXIV) using Eq. (13). Since the ^{15}N concentrations were low throughout the present experiment, the highest being only seven times the natural abundance of 0.37%, only single isotope substitutions need be considered for N_2O_3 and N_2O_4. The assumption of the isotope rule of the geometric mean[74,75] is sufficient for calculation of the reduced partition function ratio (RPFR) of mono-substituted dinitrogen tetroxide because of the equivalence of the two nitrogens in N_2O_4.

The situation is different for N_2O_3. However, several sample calculations based on frequencies generated by the $\underset{\sim}{F}_1$-matrix of the gas phase (Table XIII) showed that values of the properly weighted average and the geometric mean of $(s/s')f$ to be used for N_2O_3 in Eq. (13) were not significantly different (1.1071 and 1.1060, respectively). In view of this finding, the geometric mean for the RPFR of the N_2O_3 terms were used in both gaseous and condensed phases.

A comparison of calculated and experimental α is presented in Table XXV. In Figure 49, the effective separation factor, α, is plotted as a function of P at 15°C. This figure shows that the present calculations are definite improvement over the ones obtained from the $\underset{\sim}{F}$-matrices of Monse.[58,70-71] The difference is due to the fact that (1) Bradley's 160 cm^{-1} assignment for ν_7 of N_2O_3 was not available to Monse, and (2) sufficient spectroscopic data did not exist at the time of Monse's work to warrant construction of separate $\underset{\sim}{F}$-matrices for the

Table XXIV. Calculated Fundamental Frequencies of Oxides of Nitrogen[a]

^{14}NO gas	^{15}NO gas	$^{14}NO_2$ gas	$^{15}NO_2$ gas	$^{14}N_2O_3$ gas	$^{15}N_2O_3$ gas	$^{14}N_2O_3$ liq.	$^{15}N_2O_3$ liq.	$^{14}N_2O_4$ gas	$^{15}N_2O_4$ gas	$^{14}N_2O_4$ liq.	$^{15}N_2O_4$ liq.
1876.3	1842.7	1617.2	1581.4	1839.7	1806.2	1862.9	1829.1	1380.7	1359.7	1380.7	1359.7
		1318.4	1306.0	1630.5	1593.8	1587.5	1551.8	806.7	796.1	806.7	796.1
		750.3	739.8	1302.4	1287.3	1298.3	1283.1	266.0	264.4	266.0	264.4
				775.4	765.6	782.9	773.1	78.9	78.9	78.9	78.9
				420.4	411.3	406.8	397.9	1711.5	1672.9	1712.0	1673.3
				260.2	257.7	253.1	250.7	474.8	471.1	481.9	478.2
				159.9	158.6	159.4	158.1	429.5	419.4	423.5	415.6
				627.0 (337.0)	610.1 (327.9)	627.0 (337.0)	610.1 327.9)	672.4	653.4	672.1	653.7
				63.0 (63.1)	62.1 (62.2)	76.0 (76.0)	74.8 (74.8)	1747.5	1709.3	1733.3	1699.0
								270.9	270.5	264.5	264.0
								1262.1	1251.2	1257.7	1248.2
								750.2	739.1	743.9	734.7
										67.5	66.5
										85.7	84.6
										67.8	67.0
										82.3	81.4
										28.1	28.0

[a] All frequencies in cm^{-1}. Frequencies of NO and NO_2 taken from Ref. 58.

[b] Frequencies of N_2O_3 without parenthesis were reproduced with F_{ν_1}-matrices while those with parenthesis are from F_{ν_2}-matrices (Table XIII).

Table XXV. Comparison of the Single Stage Separation Factor Obtained from Exchange Column Experiments with Calculated Values

Run No.	T(°C)	P(atm)	α_{exp}	α_{cal}
12B	20.0	2.0	1.020	1.026
10A	15.5	1.0	1.006	1.006
10B	15.5	1.5	1.012	1.016
10C	15.5	2.0	1.021	1.023
14	15.0	2.7	1.030	1.030
15	14.5	3.4	1.032	1.031
16	15.0	4.1	1.030	1.031
7B	14.0	1.0	1.010	1.006
5	5.0	1.0	1.020	1.025
8	-4.0	1.0	1.029	1.035
9	-4.0	1.6	1.028	1.032

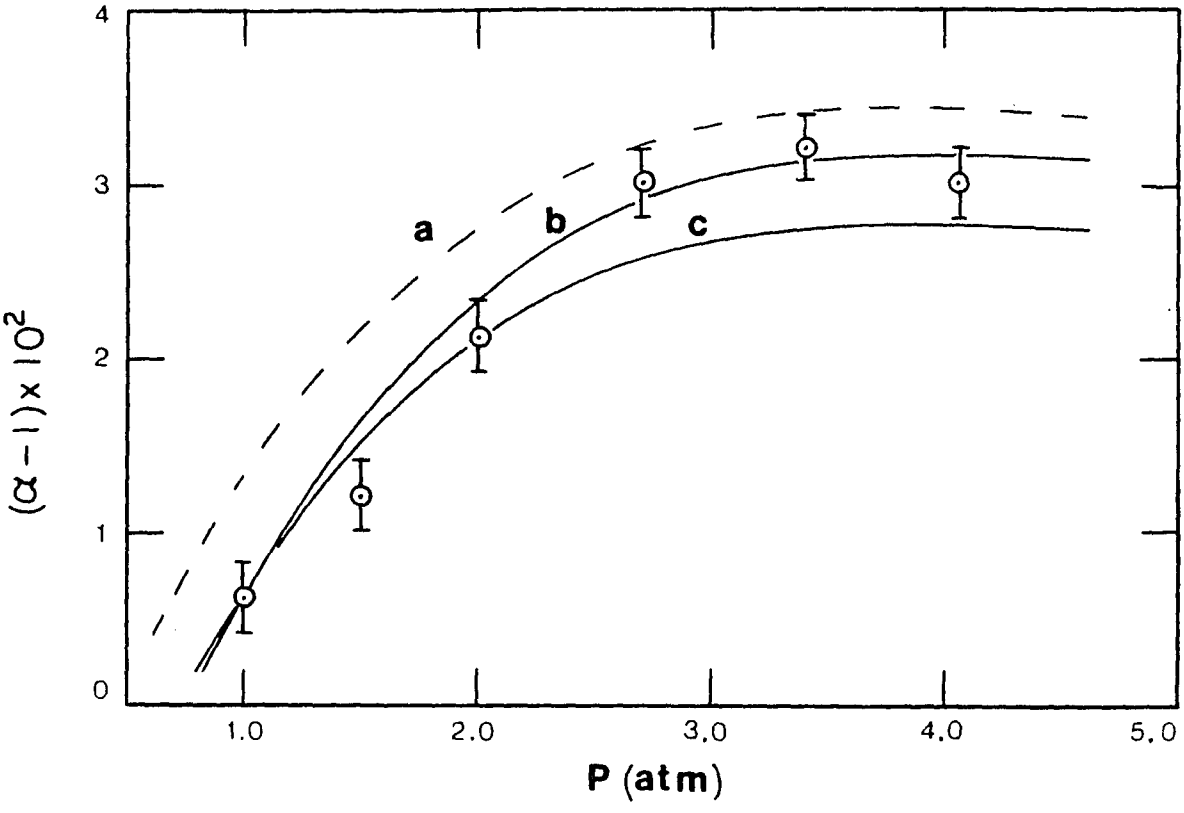

Figure 49. Comparison of Effective Separation Factor of Column Experiments with Calculated Values

a - Computed from force field calculations of Monse et al.[58,70-71]

b - Computed from present force field calculations using $F_{1,gas}$ and $F_{1,cond.}$ of N_2O_3 (Table XIII)

c - Computed from present force field calculations using $F_{2,gas}$ and $F_{2,cond.}$

different phases of N_2O_3 and N_2O_4.

Figure 49 further shows that the combination, $F_{\tilde{\nu}1,gas} + F_{\tilde{\nu}1,cond.}$, for N_2O_3 yields a distinctly better agreement with the observed α_{eff} than the combination, $F_{\tilde{\nu}2,gas} + F_{\tilde{\nu}2,cond.}$. Thus, the present experimental results favor the ν_8 assignment of Hisatsune[62] and Bradley and coworkers[12] over that of Bibart and Ewing.[14]

The mole fraction of +4 nitrogen in the liquid can be obtained directly from the experimental single stage factor. These results are plotted against pressure at 15°C in Figure 50, with the extrapolated data of Beattie and Vosper,[27] and Purcell and Cheeseman.[25] Except for the datum at 1.5 atm, the agreement between our experimentally derived values and the extrapolation of Beattie and Vosper is excellent, especially when one considers the fact that these authors data covered a pressure range well below one atmosphere.

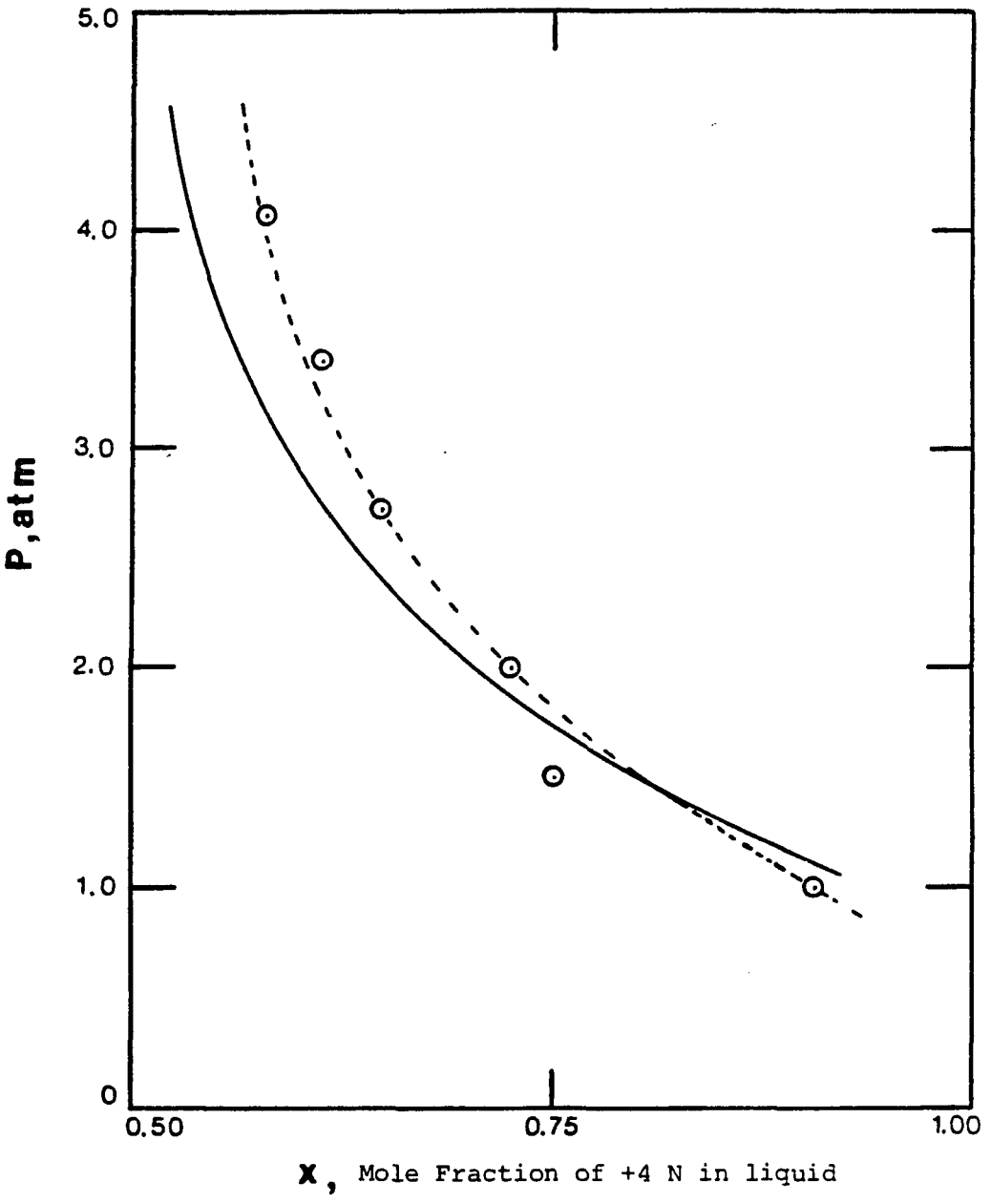

Figure 50: Vapor Pressure of NO-NO_2 Mixture as a Function of Mole Fraction x.

⊙ Calculated from Experimental Single Stage Separation Factor.

---· = Extrapolated, Ref. 27.

—— = Extrapolated, Ref. 25.

VIII. SUMMARY

An all stainless steel isotope exchange system that withstands elevated pressures and can be operated for several days using two types of automatic level controls was designed and fabricated. This system was used to study N-15 production by means of a countercurrent isotope exchange between a gas phase, which is a mixture of NO_x, and a liquid phase composed mainly of N_2O_3 and N_2O_4, in a randomly packed column at various pressures, temperatures, and flow rates.

Results show that near ambient temperatures, the effective single stage separation factor, α_{eff}, increases with partial pressure of nitric oxide. At 15°C, α_{eff} increases from 1.006 at atmospheric pressure, to 1.030 at 4 atm. This is in accordance with model calculations for predicting α using an experimental chemical phase composition study and a normal coordinate analysis based on recent spectroscopic data for N_2O_3 and N_2O_4.

HETP studies indicate that the phase changes upon lowering the temperature or increasing the pressure adversely affects the overall exchange rate of the nitrogen isotopes across the liquid-vapor interphase. However, comparative data on the N_2O_3 exchange system suggests a twenty-fold decrease in the volume of column needed to accomplish a given isotope separation task when pressure is increased from 1 to 4 atm at 15°C. This is a direct consequence of the increase in α with pressure. Furthermore, the results indicate that the size of the column at elevated pressures (4 atm and 15°C) is comparable to that of much lower temperatures (1 atm and -9°C), thereby eliminating the need for refrigeration. The parameters for a laboratory scale two column cascade to produce 1 gm/day of 99% N-15 at 15°C and 4 atm were

estimated.

The experimental results on α_{eff} for the $^{15}N/^{14}N$ isotope fractionation in conjunction with the normal coordinate analyses support the following conclusions. (1) Using separate $\underset{\sim}{F}$-matrices for the different phases of N_2O_3 and N_2O_4 yields a better agreement with the observed α_{eff}. (2) For N_2O_4, this work supports the assignment of Begun and Fletcher's,[17] with the exception of ν_{10} for which the agreement is better with the assignment of Bibart and Ewing[16] and Andrews and Anderson.[18] (3) For N_2O_3, the present study supports the assignments by Hisatsune et al.[62] and Bradley et al.,[12] with the exception of ν_7, for which a better agreement is obtained when Bradley's 160 cm^{-1} is used.

IX. FURTHER STUDIES

The study of the N_2O_3 isotope exchange system showed several interesting results. One is that the single stage separation factor, α, increases with increasing mole fraction of divalent nitrogen in the gas and liquid. However, beyond 3 atm and at 15°C, the phase compositions are no longer altered significantly, hence causing a levelling off effect for the separation factor. The other is the strong internal-external interactions present in the condensed phase of N_2O_4 which indicate that the liquid molecules are not in an isotropic environment.

Further studies on this exchange system would be to investigate the effect of increasing the flow rate on the overall separation while keeping the temperature and pressure constant at 15°C and 4 atm. If the linear flow rates during the experiments were too small and back-mixing was a significatnt factor, then increasing the flow rate would have little or no effect on HETP, causing the efficiency of the exchange system to be increased. It would also be interesting to determine under what conditions HETP becomes a linear function of the liquid flow rate.

Another aspect would be to investigate more thoroughly the nature of the intermolecular forces of the condensed state. A molecular orbital study of bimolecular, termolecular, and higher conglomerates of dinitrogen tetroxide and perhaps mixtures of N_2O_3 and N_2O_4 would indicate more definitely the nature of the interactions present in the liquid nitrogen oxide mixtures.

X. REFERENCES

1. V.J. Tennery, E.S. Bomar, W.D. Bond, S.W. Kaye, L.E. Morse, and J.E. Till, ERDA Report, ORNL/TM-5538 (1975).

2. V.J. Tennery, ERDA Report, ORNL/TM-5621 (1976).

3. W. Spindel and T.I. Taylor, J. Chem. Phys. 24, 626 (1956); Trans. NY Acad. Sci. 19, 3 (1956).

4. K. Klusius, K. Schleich, and M. Vecchi, Hel. Chim. Acta 44, 343 (1961).

5. E.U. Monse, W. Spindel, L.N. Kauder, and T.I. Taylor, J. Chem. Phys. 32, 1557 (1960); E.U. Monse, T.I. Taylor, and W. Spindel, J. Phys. Chem. 65, 1625 (1961).

6. G. Jansco and W.A. VanHook, Chem. Reviews 74, 689 (1974).

7. A.J. Vosper, J. Chem. Soc. (A), 1589 (1971).

8. F.H. Verhoeck and F. Daniels, J. Chem. Soc. 1250 (1931).

9. E.U. Monse, L.N. Kauder, and W. Spindel, Z. Naturforschg. 18a, 235 (1963).

10. T. Ishida and W. Spindel, J. Chem. Eng. Data 15, 107 (1970).

11. K. Cohen, J. Chem. Phys. 8, 588 (1940); "The Theory of Isotope Separation", McGraw-Hill Book Co. Inc., NY (1951).

12. G.M. Bradley, W. Sidall, H. Strauss, and E.L. Varetti, J. Phys. Chem. 79, 1949 (1975).

13. E.L. Varetti and G.C. Pimentel, J. Chem. Phys. 55, 3813 (1971).

14. C.H. Bibart and G.E. Ewing, Ibid. 61, 1293 (1974).

15. J. Laane and J. Olshen, Prog. Inorg. Chem. 27, 465 (1980).

16. C.H. Bibart and G.E. Ewing, J. Chem. Phys. 61, 1284 (1974).

17. G.M. Begun and W.H. Fletcher, J. Mol. Spectroscopy 4, 388 (1960).

18. B. Andrews and A. Anderson, J. Chem. Phys. 74, 3 (1981).

19. E.B. Wilson, J.C. Decius, and P.C. Cross, "Molecular Vibrations", McGraw-Hill, NY (1955).

20. H.C. Urey and D. Rittenberg, J. Chem. Phys. 1, 137 (1933).

21. H.C. Urey and L.G. Greiff, J. Am. Chem. Soc. 57, 321 (1935).

22. J. Bigeleisen and M.G. Mayer, J. Chem. Phys. 15, 261 (1947).

23. H. London, "Separation of Isotopes", Ed. H. London, George Newes Limited, London (1961).

24. M. Benedict and T.H. Pigford, "Nuclear Chemical Engineering", McGraw-Hill, NY (1957).

25. R.H. Purcell and G.H. Cheesman, J. Chem. Soc. 826 (1932).

26. G. Baume and M. Robert, Compt. rend. 169, 970 (1919).

27. I.R. Beattie and A.J. Vosper, J. Chem. Soc. 2106 (1961).

28. I.R. Beattie, Prog. Inorg. Chem. 5, 1 (1963).

29. T.I. Taylor and W. Spindel, "Proceedings of the Amsterdam Symposium on Isotope Separation", 158 (1957).

30. M.G. Fontana and N.D. Greene, "Corrosion Engineering", McGraw-Hill Co., NY (1928).

31. R.A. Friedel, A.G. Sharkey, Jr., J.L. Shultz, and C.R. Humbert, Anal. Chem. 25, 1314 (1953).

32. G. Norwitz, Anal. Chem. 34, 227 (1962).

33. T.I. Taylor, Annual Progress Report to US Atomic Energy Commission, AT (30-1) 755, (1957).

34. C.C. Addison and B.C. Smith, J. Chem. Soc. 3664 (1958).

35. A. Geuther, Annalen 245, 96 (1888).

36. P. Pascal and M. Garnier, Bull. Soc. Chim. France 25, 309 (1919).

37. A.W. Shaw and A.J. Vosper, J. Chem. Soc. (A), 2708 (1971).

38. C.M. Steese and A.G. Whittaker, J. Chem. Phys. 24, 776 (1956).

39. A.G. Whittaker, Ibid. 24, 780 (1956).

40. H. Wieland, Ber. 54, B, 1776 (1921).

41. C.C. Addison and J. Lewis, J. Chem. Soc. 4079 (1952).

42. F.A. Jenkins, H.A. Barten, and R.S. Mulliken, Phys. Rev. 30, 150 (1927).

43. T.C. Hall, Jr. and F.E. Blacet, J. Chem. Phys. 20, 1745 (1952).

44. J. Mason, J. Chem. Soc. 1288 (1959).

45. J.K. Dixon, J. Chem. Phys. 8, 157 (1940).

46. H.H. Holmes and F. Daniels, J. Am. Chem. Soc. 56, 630 (1934).

47. M. Bodenstein and F. Böes, Zeits. f. Physik. Chemie 100, 75 (1922).

48. W.F. Giauque and J.D. Kemp, J. Chem. Phys. 6, 40 (1938).

49. I.R. Beattie and S.W. Bell, J. Chem. Soc. 1681 (1957).

50. S.C. Saxena and T.I. Taylor, J. Phys. Chem. 66, 1480 (1963).

51. M.R. Ghate and T.I. Taylor, Separation Science 10 (5), 547 (1975).

52. A.F. Reid and H.C. Urey, J. Chem. Phys. 11, 403 (1943).

53. I. Dostrovski, J. Gillis, D.R. Llewellyn, and B.R. Vromen, J. Chem. Soc. 3517 (1952).

54. J.H. Shaw, J. Chem. Phys. 24, 399 (1956).

55. E.T. Arakawa and A.H. Nielsen, J. Mol. Spectroscopy 2, 413 (1958).

56. D.B. Keck and C.D. Hause, Ibid. 26, 163 (1968).

57. J.L. Hardwick and J.C. Brand, Can. J. Phys. 54, 80 (1976).

58. E.U. Monse, W. Spindel, and M.J. Stern, Advanc. Chem. Ser. No. 89, 148 (1969).

59. I.C. Hisatsune and J.P. Devlin, Spectrochimica Acta 16, 401 (1960).

60. J.P. Devlin and I.C. Hisatsune, Ibid. 17, 218 (1961).

61. I.C. Hisatsune, J.P. Devlin, and Y. Wada, Ibid. 18, 1641 (1962).

62. I.C. Hisatsune, J.P. Devlin, and Y. Wada, J. Chem. Phys. 33, 714 (1960).

63. A.H. Brittain, A.P. Cox, and R.L. Kuczkowsky, Trans. Faraday Soc. 65, 1963 (1969).

64. J.H. Schachtschneider and R.G. Snyder, Spectrochim. Acta 19, 117 (1963).

65. W.G. Fateley, H.A. Bent, and B. Crawford, Jr., J. Chem. Phys. 31, 204 (1959).

66. B.W. McClelland, G. Gundersen, and K. Hedberg, J. Chem. Phys. 56, 4541 (1972).

67. B.S. Cartwright and J.H. Robertson, Chem. Commun. 3, 82 (1966).

68. P. Six, G. Chauvet, B. Taravel, and V. Lorenzelli, Physica C, 244 (1978).

69. D.W. Smith and K. Hedberg, J. Chem. Phys. 25, 1282 (1956).

70. E.U. Monse, L.N. Kauder, and W. Spindel, Ibid. 41, 3898 (1964).

71. E.U. Monse, Ibid. 33, 312 (1960).

72. H. Wieck, M.A. Thesis, Brooklyn College (1975).

73. H. Wieck and T. Ishida, Separation Science, 12(6), 587 (1977).

74. J. Bigeleisen, J. Chem. Phys. 23, 2264 (1955).

75. T. Ishida and J. Bigeleisen, Ibid. 64, 4475 (1976).